ESPOO 2007 VTT PUBLICATIONS 639

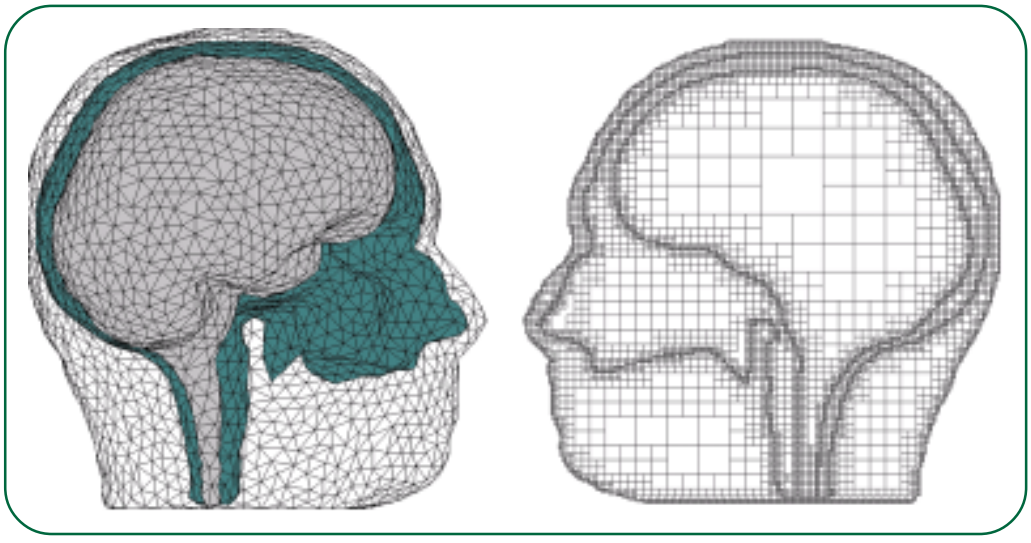

Petri Kotiluoto

Adaptive tree multigrids and simplified spherical harmonics approximation in deterministic neutral and charged particle transport

VTT PUBLICATIONS 639

Adaptive tree multigrids and simplified spherical harmonics approximation in deterministic neutral and charged particle transport

Petri Kotiluoto

ACADEMIC DISSERTATION

To be presented, with the permission of the Faculty of Science of the University of Helsinki, for public criticism in Auditorium D101 of the Department of Physical Sciences (Physicum), Gustaf Hällströmin katu 2, on June 9th, 2007, at 12 o'clock noon.

ISBN 978-951-38-7016-4 (soft back ed.)
ISSN 1235-0621 (soft back ed.)

ISBN 978-951-38-7017-1 (URL: http://www.vtt.fi/publications/index.jsp)
ISSN 1455-0849 (URL: http://www.vtt.fi/publications/index.jsp)

JULKAISIJA – UTGIVARE – PUBLISHER

VTT, Vuorimiehentie 3, PL 1000, 02044 VTT
puh. vaihde 020 722 111, faksi 020 722 4374

VTT, Bergsmansvägen 3, PB 1000, 02044 VTT
tel. växel 020 722 111, fax 020 722 4374

VTT Technical Research Centre of Finland, Vuorimiehentie 3, P.O. Box 1000, FI-02044 VTT, Finland
phone internat. +358 20 722 111, fax + 358 20 722 4374

VTT, Otakaari 3 A, PL 1000, 02044 VTT
puh. vaihde 020 722 111, faksi 020 722 6390

VTT, Otsvängen 3 A, PB 1000, 02044 VTT
tel. växel 020 722 111, fax 020 722 6390

VTT Technical Research Centre of Finland, Otakaari 3 A, P.O. Box 1000, FI-02044 VTT, Finland
phone internat. +358 20 722 111, fax +358 20 722 6390

Technical editing Anni Kääriäinen

Edita Prima Oy, Helsinki 2007

Kotiluoto, Petri. Adaptive tree multigrids and simplified spherical harmonics approximation in deterministic neutral and charged particle transport. Espoo 2007. VTT Publications 639. 106 p. + app. 46 p.

Keywords MultiTrans, particle transport, tree multigrid, simplified spherical harmonics, boron neutron capture therapy, BNCT, radiotherapy, reactor physics, radiation transport

Abstract

A new deterministic three-dimensional neutral and charged particle transport code, MultiTrans, has been developed. In the novel approach, the adaptive tree multigrid technique is used in conjunction with simplified spherical harmonics approximation of the Boltzmann transport equation.

The development of the new radiation transport code started in the framework of the Finnish boron neutron capture therapy (BNCT) project. Since the application of the MultiTrans code to BNCT dose planning problems, the testing and development of the MultiTrans code has continued in conventional radiotherapy and reactor physics applications.

In this thesis, an overview of different numerical radiation transport methods is first given. Special features of the simplified spherical harmonics method and the adaptive tree multigrid technique are then reviewed. The usefulness of the new MultiTrans code has been indicated by verifying and validating the code performance for different types of neutral and charged particle transport problems, reported in separate publications.

Preface

The work presented in this thesis has been carried out at VTT Technical Research Centre of Finland. I wish to thank both VTT and the University of Helsinki, particularly Professor Juhani Keinonen, Head of the Department of Physical Sciences, for greatly supporting my studies.

I wish to express my gratitude to my instructors, Professor Emeritus Pekka Hiismäki, D.Tech., and Docent Sauli Savolainen, Ph.D. It was Professor Hiismäki who came up with the idea that the tree multigrid technique could be used to solve radiation transport problems. I have always admired his creativity and innovativeness, which I have found unique. Docent Savolainen has been the leader of the academic medical physics research on boron neutron capture therapy (BNCT) in Finland, and I deeply appreciate his enthusiasm and commitment to the education of new scientists. His supervision of students and postgraduates has been goal-oriented, with individual encouragement and guidance to scientific work and publishing.

I am grateful to Pawel Simbierowicz, M.Sc., who introduced me to the technical details of the tree multigrid technique and to the existing software at VTT. I found his help very necessary in the beginning of my study.

I wish to thank my colleagues, Iiro Auterinen, M.Sc.Tech., and Tom Serén, Lic.Tech., from VTT for their valuable support during all these years. Their expertise in BNCT and dosimetry has been inspiring. I also pay tribute to Markku Anttila, M.Sc.Tech., Randolph Höglund, Lic.Tech., and Frej Wasastjerna, Lic.Tech., for their deep knowledge on reactor physics. I am thankful to all my colleagues at VTT for creating both an educative and lively working atmosphere. I also wish to thank all my leaders at VTT who have trusted me and supported my work through the years in changing organisations.

I am greatly indebted to Professor Tapio Ala-Nissilä, Ph.D., and Docent Simo Hyödynmaa, Ph.D., for their professional reviews of the manuscript and constructive comments that have markedly improved this thesis.

I warmly acknowledge the co-authors of Publication V, Joakim Pyyry, M.Sc.Tech, and Hannu Helminen, M.Sc.Tech, from Varian Medical Systems Finland Oy.

Antti Kosunen, Ph.D., from STUK, the Radiation and Nuclear Safety Authority, had an active role in the managing committee of the R&D project, and has been interested in my work and supporting it in many ways ever since, for which I am thankful. Such an interest has been very consoling and has given me strength to continue my scientific efforts.

I am also grateful that I have had the opportunity to work in an encouraging multidisciplinary working environment such as the BNCT project. I have had delightful discussions with my colleagues, Tiina Seppälä, Ph.D., and Hanna Koivunoro, M.Sc., on many things. These informal discussions I have always found inspiring as they have filled the scientific discipline with creative joy. I wish to equally thank Mika Kortesniemi, Ph.D., Carita Aschan, Ph.D., Jouni Uusi-Simola, M.Sc., Johanna Karila, M.Sc., and all the other physicists, doctors and nurses who have been involved in BNCT.

Tekes, the Finnish Funding Agency for Technology and Innovation, VTT Technical Research Centre of Finland, Varian Medical Systems Finland Oy, Academy of Finland, and the State Nuclear Waste Management Fund are gratefully acknowledged for their financial support.

I thank my parents and my brother for the interest they have shown to my work.

Special thanks belong to my dear wife Ulla and to our children, for keeping my thoughts often enough outside the thesis. They have brought the joy of life and the necessary counterbalance to the scientific work.

Espoo, March 26, 2007

Petri Kotiluoto

List of publications

This thesis consists of an introduction to the computational radiation transport methods and a review of the main results reported in the following publications:

I Kotiluoto, P., "Fast tree multigrid transport application for the simplified P_3 approximation", *Nuclear Science and Engineering* **138** (2001), pp. 269–278.

II Kotiluoto, P., Hiismäki, P. and Savolainen, S., "Application of the new MultiTrans SP_3 radiation transport code in BNCT dose planning", *Medical Physics* **28** (2001), pp. 1905–1910.

III Kotiluoto, P., "Application of the new MultiTrans SP_3 radiation transport code in criticality problems and potential use in dosimetry", in J. Wagemans, H. A. Abderrahim, P. D'hondt and C. De Raedt (Eds.), *Reactor Dosimetry in the 21st Century* (World Scientific, Singapore, 2003), pp. 580–587.

IV Kotiluoto, P., "Verification of MultiTrans calculations by the VENUS-3 benchmark experiment", *Journal of ASTM International* **3** Issue 3 (2006), 6 p.

V Kotiluoto, P., Pyyry, J. and Helminen, H., "MultiTrans SP_3 code in coupled photon-electron transport problems", *Radiation Physics and Chemistry* **76** (2007), pp. 9–14.

Publication I introduces a new deterministic 3D radiation transport method that the author has developed, using adaptive tree structured meshing and multigrid acceleration for the solution of the simplified spherical harmonics SP_3 transport approximation.

In Publication II the new method is applied to a BNCT dose-planning problem, with a comparison to experimental and computational data to verify and validate the accuracy.

Implementation of a multiplication eigenvalue search algorithm needed for the solution of reactor physics criticality problems has been made to the code by the author and reported in a peer-reviewed proceedings article of the 11th International Symposium on Reactor Dosimetry held in Brussels in 2002 and published in the book *Reactor Dosimetry in the 21st Century*, Publication III. Numerical results were obtained for a light-water reactor and for a fast breeder reactor benchmark.

In Publication IV the author has tested the applicability of the new code to reactor dosimetry problems by calculating the light-water reactor pressure vessel steel benchmark experiment VENUS-3 of the OECD Nuclear Energy Agency.

In Publication V the new code has been applied to coupled photon-electron transport problems encountered in conventional radiotherapy treatment planning. Comparison calculations have been made for both homogeneous and heterogeneous dose-planning problems.

The author has had the major role in conducting the code development work and other studies reported in the preceding publications. He has also been the principal author of all the above publications.

Contents

Symbols and abbreviations

$\Phi(\vec{r},E)$	Scalar flux
$\Psi(\vec{r},E,\vec{\Omega})$	Angular flux
$\vec{r}$	Position vector
E	Energy
$\vec{\Omega}$	Direction vector
∇	Nabla operator
$\sigma^T(\vec{r},E,\vec{\Omega})$	Total cross section
$\sigma^S(\vec{r},E,E',\vec{\Omega},\vec{\Omega}')$	Scattering cross section
$Q(\vec{r},E,\vec{\Omega})$	Source term
$\chi(\vec{r},E)$	Fission spectrum
$\nu(\vec{r},E)$	Number of neutrons emitted per fission
$\sigma^f(\vec{r},E)$	Fission cross section
k_{eff}	Multiplication eigenvalue
β	Fraction of fission neutrons born delayed
l	Index for Legendre order
L	Maximum Legendre order in the Legendre expansion *or* tree multigrid subdivision level
μ_0	Incident angle
$P_l(\mu_0)$	Legendre polynomial
g	Energy group index
G	Maximum energy group number
$\Psi^g(\vec{r},\vec{\Omega})$	Group angular flux
$\sigma_t^g(\vec{r})$	Group total cross section
$\sigma_{s,l}^{g'\to g}(\vec{r})$	Group-to-group scattering cross section
$Q^g(\vec{r},\vec{\Omega})$	Group source term
$S^g(\vec{r},\vec{\Omega})$	Effective group source term
$S_{fiss}(\vec{r})$	Fission source
$\chi^g(\vec{r})$	Group value for the fission spectrum
m	Index used for discrete direction *or* for indexing spherical harmonics

M	Maximum number of discrete directions
$\{\hat{\Omega}_m\}$	Set of discrete directions
$\{w_m\}$	Set of quadrature weights
μ_m	Direction cosine
η_m	Direction cosine
ξ_m	Direction cosine
$\{\alpha_m\}$	General direction cosine set
C	Constant
i	Spatial index
j	Spatial index
k	Spatial index
$\sigma^T_{i,j,k,g}$	Total group cross section in discrete ordinates formalism
$N_{i,j,k,m,g}$	Angular flux in discrete ordinates formalism
$S_{i,j,k,m,g}$	Source term in discrete ordinates formalism
$V_{i,j,k}$	Cell volume
$A_{i+\frac{1}{2},j,k}$	Cell face area
$A_{i-\frac{1}{2},j,k}$	Cell face area
$B_{i,j+\frac{1}{2},k}$	Cell face area
$B_{i,j-\frac{1}{2},k}$	Cell face area
$C_{i,j,k+\frac{1}{2}}$	Cell face area
$C_{i,j,k-\frac{1}{2}}$	Cell face area
θ	Polar angle
φ	Azimuthal angle
$P_l^m(\cos\theta)$	Associated Legendre polynomial
$\psi_{l,m}(\vec{r},E)$	Angular flux expansion coefficient in spherical harmonics
$\gamma_{l,m}(\vec{r},E)$	Angular flux expansion coefficient in spherical harmonics
$q_{l,m}(\vec{r},E)$	Source expansion coefficient in spherical harmonics
$s_{l,m}(\vec{r},E)$	Source expansion coefficient in spherical harmonics
σ^g_{al}	Group transport cross section

H_E	Sobolev space
$\psi(\vec{r},\vec{\Omega})$	Arbitrary angular flux belonging to Sobolev space
(f,g)	Inner product
$\langle f,g\rangle$	Inner product at boundary
$K\circ$	Collision operator
S^h	Finite element subspace
$\psi_i^h(\vec{r},\vec{\Omega})$	Local basis function
A	Matrix
$\vec{\Psi}$	Flux solution vector
$\vec{S}$	Source vector
x	Spatial co-ordinate
μ	Angular direction cosine
$\psi_i(x)$	Spatial one dimensional basis function
$\psi_j(\mu)$	Angular one dimensional basis function
$\psi_n(x,\mu)$	Direct product of spatial and angular basis functions
s	Distance
ζ	Random number
$u_{i,j,k}^L$	Cell in octree
X_{min}	Minimum x co-ordinate of the root cell
Y_{min}	Minimum y co-ordinate of the root cell
Z_{min}	Minimum z co-ordinate of the root cell
x_{min}	Minimum x co-ordinate of an octree cell
y_{min}	Minimum y co-ordinate of an octree cell
z_{min}	Minimum z co-ordinate of an octree cell
x_{max}	Maximum x co-ordinate of an octree cell
y_{max}	Maximum y co-ordinate of an octree cell
z_{max}	Maximum z co-ordinate of an octree cell
Δ	Side length of the root cell
$\Delta_{\min}$	Minimum cell side length of an octree
$\vec{u}$	Column vector
h	Mesh size
S_h	Discretised source vector
$\tilde{u}_h$	Approximate solution of the discretised system

u_h	Exact solution of the discretised system
v_h	Error of the solution
$\tilde{v}_h$	Approximate error of the solution
r_h	Residual
H	Mesh size on a coarser grid
$\Re$	Restriction operator
$\wp$	Prolongation operator
γ	Number of two-grid iterations
$\Psi(x,\theta)$	Angular flux in slab geometry
$\delta_{l,l'}$	Kronecker delta
$\Phi_l(x)$	One-dimensional angular flux expansion coefficient in Legendre order l
$\Phi_l(\vec{r})$	Three-dimensional angular flux expansion coefficient in Legendre order l
$q_l(x)$	One-dimensional source expansion coefficient in Legendre order l
$q_l(\vec{r})$	Three-dimensional source expansion coefficient in Legendre order l
$\hat{\Phi}_0(\vec{r})$	Variable defined relative to scalar flux and second moment term of the angular flux
$D_0^{i,g}$	A diffusion coefficient
$D_2^{i,g}$	A diffusion coefficient
$Q_l^{i,g}(\vec{r})$	Order l moment terms of the source
$S_l^{i,g}(\vec{r})$	Order l moment terms of the effective group source
$S^{i,g}(\vec{r})$	Scalar effective group source
$\hat{S}_1^{i,g}(\vec{r})$	A modified group source term
$\hat{S}_3^{i,g}(\vec{r})$	A modified group source term
$\vec{n}$	Normal vector of a surface
$\Psi^{(u)}(\vec{r},E,\vec{\Omega})$	Uncollided angular flux
$\psi_{lm}^{(u),g}$	Uncollided angular flux spherical harmonics expansion coefficient

$\gamma_{lm}^{(u),g}$	Uncollided angular flux spherical harmonics expansion coefficient
$\Phi_l^{(u),g}(\vec{r})$	Uncollided angular flux Legendre expansion coefficient
$\delta(\vec{\Omega}-\vec{\Omega}_r)$	Delta function in angle
$\vec{r}_s$	Source point
$\beta(\vec{r},\vec{r}_s)$	Number of mean-free-paths
$\overline{\sigma}_t^g$	Average total group cross section along the path
dΓ	Cell surface element
$S_f^{(n)}(\vec{r})$	Fission source after *n* iterations
$k^{(n)}$	Multiplication eigenvalue after *n* iterations
ε_1	Variable used for criticality convergence criterion
ε_2	Variable used for fission source convergence criterion
1D	One-dimensional
2D	Two-dimensional
3D	Three-dimensional
BFP	Boltzmann-Fokker-Planck
BNCT	Boron neutron capture therapy
BNCT_rtpe	A Monte Carlo simulation code, predecessor of SERA
BUGLE	Coupled neutron and gamma-ray cross section library
CAD	Computer-aided design
CEPXS	A multigroup coupled electron-photon cross section generating code
c.p.e.	Charged particle equilibrium
CSD	Continuous slowing down
CSDA	Continuous slowing down approximation
CT	Computed tomography
DORT	A two-dimensional discrete ordinates (deterministic) transport code
EGS	“Electron Gamma Shower”, a Monte Carlo simulation system
EGS4	A Monte Carlo code from the EGS system
EGSnrc	A Monte Carlo code from the EGS system
EMERALD	Past project of the SAFIR research programme at VTT
ENDF	Evaluated nuclear data file
FBR	Fast breeder reactor

FEM	Finite element method
FiR 1	Nuclear research reactor located in Otaniemi, Espoo
Fluental™	Neutron moderator material developed at VTT
GEANT4	A toolkit for the simulation of the passage of particles through matter
ICRU	International Commission on Radiation Units and Measurements
IMRT	Intensity modulated radiotherapy
INL	Idaho National Laboratory
IRDF	International reactor dosimetry file
KUCA	Kioto University Critical Assembly
LET	Linear energy transfer
LWR	Light-water reactor
MCNP	General Monte Carlo N-Particle Transport Code
Mesh2d	An adaptive two-dimensional unstructured mesh generator
MIT	Massachusetts Institute of Technology
MOX	Mixed-oxide
MRI	Magnetic resonance imaging
MSU	Montana State University
MultiTrans	A three-dimensional simplified spherical harmonics (deterministic) transport code
NCT_Plan	A Monte Carlo simulation code based on MCNP
NEA	Nuclear Energy Agency
NMF	Nuclear metrology file
OECD	Organisation for Economic Co-operation and Development
P_1	Spherical harmonics approximation of Legendre order one, congruent with diffusion theory approximation
P_3	Spherical harmonics approximation of Legendre order three
PMMA	Polymethyl-methacrylate
P_N	Spherical harmonics approximation of Legendre order N
PSG	“Probabilistic Scattering Game”, a Monte Carlo transport code developed at VTT
PTV	Planning target volume
PWR	Pressurised water reactor
SAFIR	Finnish Research Programme on Nuclear Power Plant Safety

SAND-II	A fine multigroup structure of neutron cross sections
SERA	A simulation environment for radiotherapy applications
S_N	Discrete ordinates approximation
SP_1	Simplified spherical harmonics approximation of Legendre order one, congruent with diffusion theory approximation
SP_3	Simplified spherical harmonics approximation of Legendre order three
SP_N	Simplified spherical harmonics approximation of Legendre order N
SS_N	Simplified discrete ordinates approximation
STL	Stereolitography file format
Tekes	Finnish Funding Agency for Technology and Innovation
TLD	Thermoluminescent dosimeter
TORT	A three-dimensional discrete ordinates (deterministic) transport code
TPS	Treatment planning system
TRIGA	"Training, Research, Isotopes, General Atomics", a research reactor type
VENUS	"Vulcain Experimental Nuclear Study", zero power critical reactor located in Mol, Belgium
VENUS-2	VENUS reactor with mixed-oxide fuel, a NEA benchmark
VENUS-3	VENUS reactor fuelled with partial length shielded assemblies, a NEA benchmark
VTT	Technical Research Centre of Finland
X333	A utility program for multigroup data condensation

1. Introduction

Ionising radiation is radiation in which an individual particle carries enough energy to ionise an atom or molecule by completely removing an electron from its orbit. Ionising radiation can cause DNA damage and mutations, and is therefore potentially dangerous to human health.

There are both natural and artificial radiation sources, which are identical in their nature and their effect. Despite the potential dangers, sometimes the benefits in the utilisation of radiation sources outweigh the drawbacks. Ionising radiation can be used, for instance, in medicine to kill cancerous cells. Nuclear fission is used as an efficient source of power production to benefit all mankind, but as a harmful by-product also direct ionising radiation as well as long-term radioactive waste is produced.

In many areas dealing with ionising radiation, it is important to be able to calculate the particle transport through matter. In radiotherapy applications it is required to estimate the radiation dose to the patient in order to ensure the safety and success of the therapy. In reactor physics one is interested in criticality safety, radiation shielding issues, activity inventories, and radiation damage induced to materials and components important for safety.

Neutral and charged particle transport – referred hereinafter less strictly also as *radiation transport* – is a complicated problem especially in 3D, and generally requires the use of sophisticated computer codes. A variety of such computer codes exists, based on the development work of many person-years. These codes are used, for instance, in radiotherapy treatment planning and nuclear engineering, where the computational accuracy can be vital for safety. Therefore, many of these codes are carefully validated and verified for the purpose they are intended.

Why should a new radiation transport code be developed, especially if it requires many years of development and validation work? Much of the answer depends on how well the current codes perform in different applications, and whether there are some new techniques that might supplement the computational radiation transport field. Naturally, the research and development process itself

has an educational aspect, and can give a much deeper insight into the already existing codes and their usage.

The transport solution method described in this thesis is based on the tree multigrid technique, not utilised before in radiation transport.

The development of the new radiation transport code started in the framework of the Finnish boron neutron capture therapy (BNCT) project. Patients suffering, e.g. from malignant brain tumours or head and neck cancer, are treated with epithermal neutrons obtained from FiR 1 TRIGA research reactor [1–5]. The radiation damage is chemically intensified in tumour cells by a boron carrier agent that accumulates into cancer tissue. The incident epithermal neutrons slow down to thermal energy range ($E < 0.5$ eV) in tissue, and have a high probability to be captured by the ^{10}B isotope, producing short, cell range high-LET radiation (α-particle and ^{7}Li recoil nucleus, see Figure 1) [6]. In addition to the chemical targeting of the dose, it is important to direct the epithermal beam (usually two fields have been used from two different directions) in an optimal way to produce a good thermal neutron field in the planning target volume (PTV) and to minimise the radiation risk to sensitive organs. To make an anatomical model of the patient with PTV, tomographic data of the patient is required. In BNCT, treatment plans are made individually for each patient based on computed tomography (CT) or magnetic resonance imaging (MRI), and detailed radiation transport modelling [7–10].

For treatment planning in Finland, the SERA code and its previous version BNCT_rtpe have been used [8, 9]. Both codes are based on the Monte Carlo method, and they have been developed by Idaho National Laboratory (INL) and Montana State University (MSU).

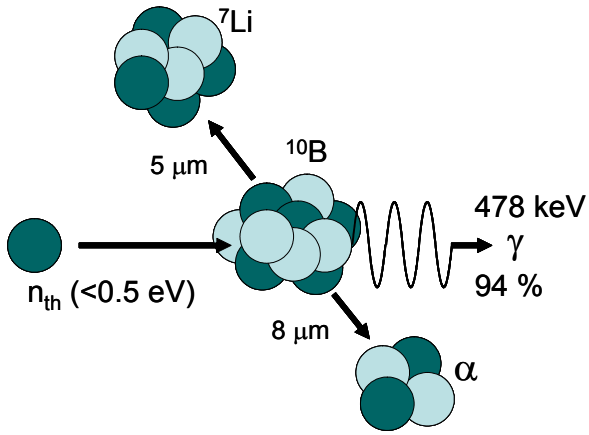

Figure 1. Nuclear reaction utilised in BNCT. A ^{10}B nucleus absorbs a thermal neutron and promptly emits a ^{4}He (alpha) particle. Together with the recoil ^{7}Li nucleus, the resulting particles have a combined average kinetic energy of 2.33 MeV and limited path lengths in tissue (5–9 μm) similar to cell dimensions [6].

The BNCT_rtpe code that was initially used in BNCT treatment planning was rather time consuming: each field calculation took about 7 hours, and the whole optimisation procedure for two field irradiation setup for each patient took about one week [11]. Since then (BNCT trials in Finland started May 1999) the SERA code has experienced a speed up due to some BNCT-specific algorithm changes and the general performance improvement of computers. To be more detailed, the SERA code uses integer arithmetic in the particle tracking method through uniform volume elements (univels), which has accelerated the transport calculations notably [9]. However, at that time when the first clinical protocols in Finland were about to start, there seemed to be an urgent need for a fast deterministic radiation transport code that could be used in BNCT to shorten the production time of treatment plans.

There was some previous in-house experience (by Pawel Simbierowicz, a former research scientist at VTT) in solving elliptic differential equations (for instance diffusion equations) by using the novel tree multigrid technique [12, 13, 14]. It was soon realised that this technique might also be used for radiation transport problems.

During 1998–2001 a research and development project financed by VTT and Tekes, the Finnish Funding Agency for Technology and Innovation, was conducted. The aim of the project was to demonstrate the applicability of the tree multigrid technique to radiation transport modelling, especially in varying phantom geometries used in BNCT dosimetry.

Radiation transport theory for neutral and charged particles [15, 16, 17] is discussed later in this thesis, but it is worth noting that, in practice, the basic transport equation is too ill-formed for a direct numerical deterministic solution and needs to be approximated. Therefore, full spherical harmonics approximation (P_N) was first studied [18, 19], but the resulting equations were still found to be very complicated in 3D, and a simpler but somewhat more restricted, simplified spherical harmonics approximation (SP_3) was adopted instead [20–25].

For treatment planning purposes, an algorithm for construction of the computation grid (tree multigrid) directly from segmented CT images was implemented.

As a result of the project, a new code called MultiTrans was developed, capable of solving 3D radiation transport problems with the efficient tree multigrid technique, as reported in Publications I and II. The application of the new code to BNCT dose planning was also studied further in the BNCT dosimetry project co-ordinated by the University of Helsinki and funded by the Finnish Academy.

It should be noted that 5 % accuracy of the patient dose is recommended by ICRU for external radiotherapy [26]. This is because the therapeutic window for the patient dose is usually quite narrow: often the adverse effects start to appear in the healthy tissue before the complete tumour control (Figure 2). Thus, the accuracy requirement for any new dose planning code is very strict, and careful verification of the code performance is needed.

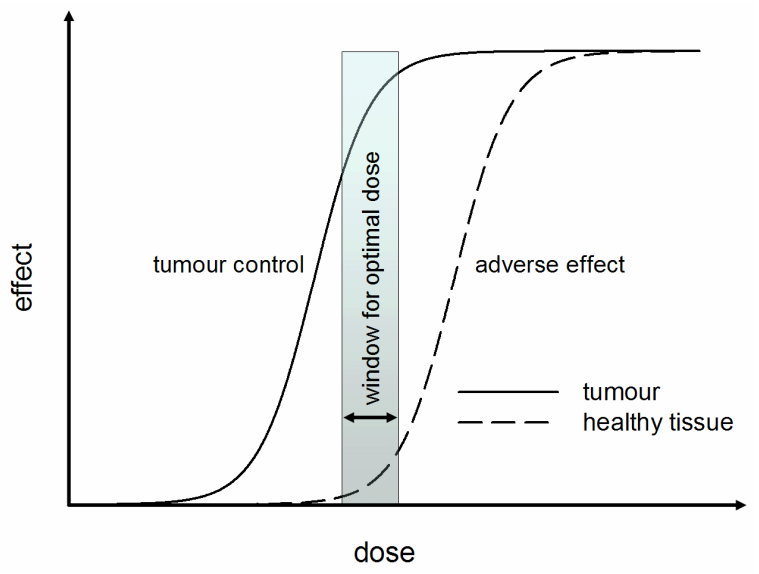

Figure 2. An example of the effect of radiotherapy on the tumour and healthy tissue. The effect (cell kill) is a sigmoidal function of radiation dose. For a therapeutic dose, there is often only a narrow window before adverse effects in healthy tissue start to appear (this figure is freely modified from the book by Perez and Brady [27]).

Obviously, MultiTrans as a 3D radiation transport code is not restricted to any specific BNCT problem, but is far more generic in nature. Algorithms for generating a 3D octree grid from stereolitography (STL) files already existed. These STL files can be exported from practically all computer-aided design (CAD) systems. The ability to generate octree grids directly from CAD models offers a flexible state-of-the-art interface for construction and upgrading of the calculation geometry.

Since the first application of the MultiTrans code to a BNCT dosimetry planning problem, the applicability of the MultiTrans code in coupled photon-electron transport problems encountered in conventional radiation therapy planning was studied (Publication V). This work was financed by Varian Medical Systems Finland Oy.

Lately, the MultiTrans code has also been applied to reactor physics problems, where the radiation transport codes are most commonly used. This has been

done within the EMERALD project of SAFIR, the Finnish Research Programme on Nuclear Power Plant Safety. For instance, a multiplication eigenvalue search algorithm has been implemented (Publication III). It should be noted that the accuracy requirement of computer codes is high in reactor physics as well. Some well-known 3D neutron transport benchmarks have therefore been conducted, such as the VENUS-3 reactor dosimetry benchmark (Publication IV).

This thesis first provides the reader with a short introduction to the computational methods of radiation transport. After that, the basis of the new MultiTrans code – the tree multigrid technique and the simplified spherical harmonics approximation – are reviewed. The objective is to give a somewhat more general overview of radiation transport, in order to be able to piece together the special features of the new method. Finally, the applications of the new radiation transport code to various transport problems are reviewed, and both the benefits and the drawbacks of the new method are discussed.

2. Aims of the study

The study aimed to develop and test a new 3D deterministic radiation transport code. The specific aims were:

1. To study radiation transport theory in order to find a suitable deterministic 3D transport approximation to be used in conjunction with the tree multigrid technique. (Theoretical overview presented in this thesis)

2. To apply the tree multigrid technique for the first time in 3D neutron transport modelling. (Publication I)

3. To test the applicability of the new code in BNCT neutron and photon dose-planning problems. (Publication II)

4. To extend the applicability of the new code to rector physics problems with multiplicative systems. (Publication III)

5. To verify the accuracy of the code in reactor physics problems by calculating dosimetric responses for a real nuclear reactor. (Publication IV)

6. To extend the applicability of the new code to coupled photon-electron transport problems and to test the code in conventional radiotherapy dose planning. (Publication V)

3. Overview of radiation transport theory

The term "transport theory" is commonly used to refer to the mathematical description of the transport of particles through a host medium [15]. Transport theory arises in a wide variety of disciplines. The foundation of transport theory lies in the kinetic theory of gases developed by Austrian physicist Ludwig Boltzmann (1844–1906). In fact, there are at least three equations named after Boltzmann: a famous equation for entropy, an equation concerning particles in a gravitational field, and an equation for particle transport. The latter one is often called the Boltzmann transport equation.

When time-dependence is suppressed, the Boltzmann transport equation for neutral particles – such as neutrons and photons – has a static form

$$\nabla \cdot \vec{\Omega}\Psi(\vec{r}, E, \vec{\Omega}) + \sigma^T(\vec{r}, E, \vec{\Omega})\Psi(\vec{r}, E, \vec{\Omega}) =$$

$$Q(\vec{r}, E, \vec{\Omega}) + \iint \sigma^S(\vec{r}, E, E', \vec{\Omega}, \vec{\Omega}')\Psi(\vec{r}, E', \vec{\Omega}')d\vec{\Omega}'dE' \quad , \qquad (3.1)$$

where $\Psi(\vec{r}, E, \vec{\Omega})$ is angular flux (function of position $\vec{r}$, energy E and angle $\vec{\Omega}$), $\sigma^T(\vec{r}, E, \vec{\Omega})$ is total cross section, $\sigma^S(\vec{r}, E, E', \vec{\Omega}, \vec{\Omega}')$ is scattering cross section, and $Q(\vec{r}, E, \vec{\Omega})$ is a source term. The direction vector $\vec{\Omega}$ is illustrated in Figure 3 in the Cartesian co-ordinate system. The fundamental equation (3.1) can also be seen as an expression of the equation of continuity:

$$\text{losses + leakage = production.} \qquad (3.2)$$

The Boltzmann equation is an integro-differential equation, which means that the integral scattering source term on the right-hand side depends on the solution itself. It is said that, in this form, the Boltzmann equation is almost impossible to handle [28]. Exact analytical solutions exist only for some very special cases, such as for point, line or plane source in an infinite homogeneous medium or for the so-called Milne problem (for an infinite homogeneous half-space) [16]. The complexity of the equation usually forces one to implement numerical (i.e., computer-based) methods of solution. For this purpose it is practically necessary to do mathematical approximations, which are always compromises between physical accuracy and feasibility.

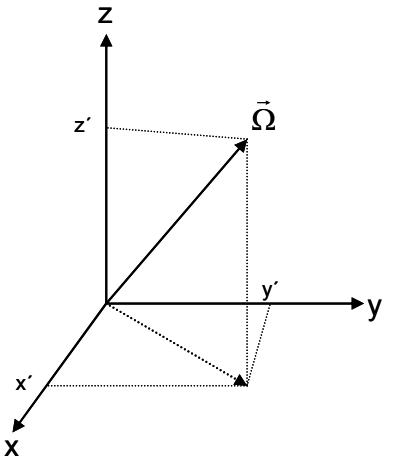

Figure 3. Direction vector $\vec{\Omega}$ illustrated in Cartesian co-ordinate system.

Numerical methods in radiation transport can be divided into deterministic and stochastic methods. In the deterministic methods, the radiation transport of neutral particles is described by solving the Boltzmann equation numerically. In stochastic methods, i.e. the Monte Carlo method, individual particle trajectories are followed through the geometry, until particle escape or absorption. The latter method does not use the Boltzmann equation at all: instead it uses simple probabilistic laws for each emission, scattering and absorption event that the particles undergo in their history. Thus, the stochastic nature, the random walk in which particles stream in reality, is imitated by statistical computer simulation. As the Boltzmann equation represents the collective behaviour of the particles, simulating a large number of particle trajectories will lead to statistical flux density that will be the solution of the Boltzmann equation within the obtained statistical uncertainty.

Neutrons and photons deposit their energy into matter indirectly through creation of secondary charged particles. The Boltzmann equation (3.1) holds for neutral particles. If charged particles are concerned, the situation is more complicated. Charged particles, such as electrons, interact with the matter through the long-range Coulomb force. Charged particle transport is in general described by the Boltzmann-Fokker-Planck (BFP) equation.

Electrons are often those secondary particles which actually deposit the energy into material, e.g. induce the primary dose to the tissue in radiotherapy. If a

sufficient local secondary charged particle equilibrium (c.p.e.) condition exists, one can use mass-energy absorption coefficients (for photons) or kerma factors (for neutrons) to directly convert the calculated fluence rate to dose rate [29]. In other words, under the c.p.e. condition, the dose is equal to collision kerma (kinetic energy released in material subtracted by bremsstrahlung fraction). However, if the c.p.e. condition is not met, the transport of electrons might have a vital effect on the dose distribution, e.g. in a case with strong tissue heterogeneities [30, 31].

One approximative form of the BFP-equation is the Boltzmann-CSD (continuous-slowing-down) equation. It is possible to include the CSD-term into electron "pseudo" cross sections and the Boltzmann equation for neutral particles can be applied for electrons as well [32]. The deterministic solution of the electron transport can then be based on essentially the same concepts as the neutral particle transport.

Also statistical simulation can be used to solve the charged particle transport. It should be noted that the stochastic Monte Carlo method is often very time consuming. The reason is that in order to get results – fluence or dose values for instance – with sufficiently low statistical uncertainty, usually a huge number of particle tracks have to be simulated. Especially the tracking of electrons is tedious, as the long-range Coulomb force results in a large number of scattering events.

Whereas electron transport is sometimes important in radiotherapy, in reactor physics one is often dealing with fissionable material. This leads to a new class of problems, where instead of solving flux values for a certain fixed source distribution, the principal target is to solve the criticality eigenvalue for the multiplicative system of fission neutrons. This eigenvalue problem can be formulated with the Boltzmann transport equation by just adding a fission production term on the right-hand side:

$$\nabla \cdot \vec{\Omega}\Psi(\vec{r},E,\vec{\Omega}) + \sigma^{T}(\vec{r},E,\vec{\Omega})\Psi(\vec{r},E,\vec{\Omega}) =$$

$$Q(\vec{r},E,\vec{\Omega}) + \iint \sigma^{S}(\vec{r},E,E',\vec{\Omega},\vec{\Omega}')\Psi(\vec{r},E',\vec{\Omega}')d\vec{\Omega}'dE'$$

$$+ \frac{\chi(\vec{r},E)}{k_{eff}} \iint \nu(\vec{r},E')\sigma^{f}(\vec{r},E')\Psi(\vec{r},E',\vec{\Omega}')d\vec{\Omega}'dE' \,. \qquad (3.3)$$

In equation (3.3), $\chi(\vec{r},E)$ is the fission spectrum, $\nu(\vec{r},E)$ is the number of neutrons emitted per fission, $\sigma^f(\vec{r},E)$ is the fission cross section, and k_{eff} is the multiplication eigenvalue. The k_{eff} parameter is introduced in order to bring the equation to a stable solution: physically the k_{eff} value can be interpreted as a ratio of the production rate of neutrons due to fission to the loss rate due to absorption and leakage.

The system (e.g. a nuclear reactor or a nuclear fuel transportation cask) is said to be sub-critical when $k_{\text{eff}} < 1$. In this case, the fission power, i.e. the total energy released by fission events, and amount of neutrons are decreasing to zero, unless the system has already reached the zero power level. If $k_{\text{eff}} = 1$, the system is critical and maintains a constant chain reaction at a constant power level. In order to make the fission power increasing, e.g. to raise the power of a nuclear reactor, the k_{eff} value has to be > 1, where the system is called overcritical.

Here one can make a general remark, not related to transport theory, but to reactor kinetics: a certain fraction β of fission neutrons is born delayed, in contrast to prompt neutrons which are released immediately in the fission event. For ^{235}U, $\beta = 0.65$ %. These delayed neutrons make it possible to control a nuclear reactor, as they slow down the exponential time behaviour of the number of neutrons, and give control systems sufficient time to react to the changing power level. If all the fission neutrons were born promptly, a controlled chain reaction and the production of electricity in nuclear power plants would be impossible.

Naturally, the radiation transport problems related to reactor physics are not only restricted to criticality problems, but there are many other types of problems as well. For example, calculated neutron flux is important for estimation of the embrittlement of reactor materials, such as the pressure vessel. The integrity of the pressure vessel is vital for nuclear safety. Or, as another example, calculated neutron flux distribution might be required for estimation of induced radioactivity of different reactor internals after an irradiation period. In these kinds of problems, a fixed source distribution (core power distribution) is usually used as a source term, without doing any criticality eigenvalue search.

Criticality and other issues of nuclear safety naturally require reliable and well benchmarked computational systems with known accuracy in order to be able to

use large enough safety margins. It has already been mentioned that 5 % accuracy in dose determination is also recommended for radiotherapy in order to ensure the safety and the success of the therapy [26]. Thus, in almost every application of radiation transport, the computational methods used have a high accuracy requirement.

3.1 Deterministic methods

The numerical solution of the Boltzmann transport equation (3.1) in realistic heterogeneous 3D problems always requires some approximations. There are a few approximations which are common for all deterministic methods, such as the Legendre expansion and the multigroup approximation of the cross sections.

With an assumption that scattering depends only on incident angle, an expansion of anisotropic scattering cross section can be made with the use of Legendre polynomials up to order L

$$\sigma^S(\vec{r},E,E',\vec{\Omega},\vec{\Omega}') \approx \sum_{l=0}^{L} \frac{2l+1}{4\pi} P_l(\mu_0)\sigma_l^S(\vec{r},E,E') \tag{3.4}$$

where the incident angle is

$$\mu_0 = \vec{\Omega}\cdot\vec{\Omega}' \ . \tag{3.5}$$

Another approximation that is always used in deterministic methods, also related to cross sections, is called the multigroup approximation. As the Boltzmann transport equation is energy-dependent, there has to be some way to reduce the problem involving scattering from one energy to another into a manageable form for numerical solution. In the multigroup approximation (Figure 4), the continuous (point-wise) cross sections are condensed into some energy group structure, in which each group has different energy width. The group flux denoted with index g becomes

$$\Psi^g(\vec{r},\vec{\Omega}) = \int_{E_g}^{E_{g-1}} \Psi(\vec{r},E,\vec{\Omega})dE \tag{3.6}$$

and the group total cross section, for instance, will be

$$\sigma_t^g(\vec{r}) = \frac{\int_{E_g}^{E_{g-1}} \sigma^T(\vec{r}, E, \vec{\Omega})\Phi(\vec{r}, E)dE}{\int_{E_g}^{E_{g-1}} \Phi(\vec{r}, E)dE} \tag{3.7}$$

where

$$\Phi(\vec{r}, E) = \int_{4\pi} \Psi(\vec{r}, E, \vec{\Omega})d\vec{\Omega} \tag{3.8}$$

is the scalar flux.

Similarly, the group scattering cross section becomes

$$\sigma_{s,l}^{g' \to g}(\vec{r}) = \frac{\int_{E_{g'}}^{E_{g'-1}} dE \int_{E_g}^{E_{g-1}} \sigma_l^S(\vec{r}, E, E')\Phi(\vec{r}, E')dE'}{\int_{E_g}^{E_{g-1}} \Phi(\vec{r}, E)dE} \tag{3.9}$$

It is worth noticing that, in equations (3.7) and (3.9), the scalar flux is used to weight the group cross section in order to define the exact and equivalent multigroup representation of the original transport equation. That is to say, to obtain the solution, $\Phi(\vec{r}, E)$, one needs the solution, $\Phi(\vec{r}, E)$. In practice, a certain approximative weighting spectrum has to be used in order to estimate the average group constants correctly. These weighting spectra are case-specific, i.e. they should represent a typical flux spectrum in the material and in the problem for which they are to be used. For instance, a very different weighting spectrum is used for the reactor core than for the concrete of the biological shield far from the core. The basic nuclear data also varies, some cross sections having strong resonance peaks within very small energy width. The multigroup approximation therefore always introduces some source of error, depending on how fine or broad the energy group widths are, and how accurately the used weighting spectrum represents the actual flux.

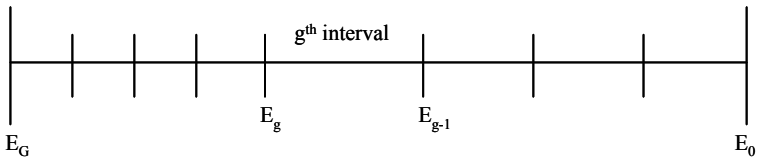

Figure 4. Division of the energy domain into G energy groups.

The Legendre expansion coefficients of the microscopic scattering cross sections are tabulated in multigroup format for different isotopes in the standard cross section libraries, such as BUGLE-96 (with 47 neutron groups and 20 photon groups) for instance [33]. The macroscopic cross sections can be calculated with corresponding coefficients (atomic densities) for different material constituents.

For a multigroup structure having G energy groups, the Boltzmann transport equation becomes

$$\nabla \cdot \vec{\Omega} \Psi^g(\vec{r},\vec{\Omega}) + \sigma_t^g(\vec{r}) \Psi^g(\vec{r},\vec{\Omega}) =$$

$$Q^g(\vec{r},\vec{\Omega}) + \sum_{g'=1}^{G} \sum_{l=0}^{L} \frac{2l+1}{4\pi} \sigma_{s,l}^{g'->g}(\vec{r}) \int P_l(\vec{\Omega} \cdot \vec{\Omega}') \Psi^{g'}(\vec{r},\vec{\Omega}') d\vec{\Omega}'$$

$$+ \sum_{g'=1}^{G} \frac{\chi^g(\vec{r})}{k_{eff}} \nu^{g'}(\vec{r}) \sigma_f^{g'}(\vec{r}) \int \Psi^{g'}(\vec{r},\vec{\Omega}') d\vec{\Omega}' . \qquad (3.10)$$

The terms $\Psi^g(\vec{r},\vec{\Omega})$ and $Q^g(\vec{r},\vec{\Omega})$ above are actually components of $1 \times G$ vector functions, where G is the total number of energy groups in the multigroup approximation. The group-to-group scattering cross sections $\sigma_{s,l}^{g'->g}(\vec{r})$ are components of $G \times G$ (possibly full) scattering matrix.

One can solve the multigroup equations successively as a sequence of effective one-group problems [34] by treating the contribution from other groups as an effective source term:

$$S^g(\vec{r},\vec{\Omega}) = Q^g(\vec{r},\vec{\Omega})$$

$$+ \sum_{g' \neq g} \sum_{l=0}^{L} \frac{2l+1}{4\pi} \sigma_{s,l}^{g'->g}(\vec{r}) \int P_l(\vec{\Omega} \cdot \vec{\Omega}') \Psi^{g'}(\vec{r},\vec{\Omega}') d\vec{\Omega}' . \qquad (3.11)$$

The fission source can be defined as

$$S_{fiss}(\vec{r}) = \sum_{g'=1}^{G} \nu^{g'}(\vec{r})\sigma_f^{g'}(\vec{r}) \int \Psi^{g'}(\vec{r},\vec{\Omega}')d\vec{\Omega}' \,. \tag{3.12}$$

It is important to note that the spatial dependence of the fission source is identical in each group equation [34]. The "in group" transport equation becomes

$$\nabla \cdot \vec{\Omega}\Psi^g(\vec{r},\vec{\Omega}) + \sigma_t^g(\vec{r})\Psi^g(\vec{r},\vec{\Omega}) = S^g(\vec{r},\vec{\Omega})$$
$$+ \sum_{l=0}^{L} \frac{2l+1}{4\pi} \sigma_{s,l}^g(\vec{r}) \int P_l(\vec{\Omega}\cdot\vec{\Omega}')\Psi^g(\vec{r},\vec{\Omega}')d\vec{\Omega}' + \frac{\chi^g(\vec{r})}{k_{eff}} S_{fiss}(\vec{r}) \cdot \tag{3.13}$$

3.1.1 Discrete ordinates method

In the discrete ordinates method (also known as S_N method), the angular variable is discretised into a small number of directions or rays [15, 16, 35, 36]. The particle transport equation is written for each ray, including various coupling terms describing ray-to-ray transfer. In the following sections, the S_N formalism presented in the book by Duderstadt and Martin [15] is more or less quoted.

A set of M discrete directions $\{\hat{\Omega}_m\}$ and corresponding quadrature weights $\{w_m\}$ need to be chosen. The quadrature weights can be thought to represent an area on the unit sphere of direction cosine triplets (μ_m, η_m, ξ_m). The numerical integration over angle in the Boltzmann transport equation can then be estimated as a weighted sum.

The choice of discrete directions is not obvious in many cases – particularly in multidimensional geometries. In the following, only 3D Cartesian co-ordinate system is considered.

Since $\hat{\Omega}_m$ is a unit vector, the directions cosine triplet (μ_m, η_m, ξ_m) must satisfy equation

$$\mu_m^2 + \eta_m^2 + \xi_m^2 = 1 \,. \tag{3.14}$$

Furthermore, if no *a priori* information on the angular flux solution exists, a symmetric distribution of direction cosines can be assumed. The angular direction set should then be invariant under arbitrary 90° rotations about the coordinate axes, and 180° reflections about the *xy*, *xz*, or *yz* planes. This means that only one octant of the unit sphere needs to be considered. The direction cosine sets have to be identical, i.e. $\{\mu_m\} = \{\eta_m\} = \{\xi_m\}$, and lie on latitudes on the unit sphere (Figure 5). Otherwise, the point arrangement would not be invariant under rotation of one axis into the other. The reflection property implies that each set $\{\alpha_m\}$ is symmetric about α=0. Therefore, one needs to choose only terms $\alpha_1, \alpha_2, \ldots, \alpha_{M/2}$.

The equation (3.14) means, for instance, that

$$\alpha_i^2 + \alpha_j^2 + \alpha_k^2 = 1, \qquad \alpha_{i-1}^2 + \alpha_{j+1}^2 + \alpha_k^2 = 1 .$$

Subtracting these two equations and noting that *i*, *j*, and *k* are arbitrary, one finds that

$$\alpha_i^2 - \alpha_{i-1}^2 = \alpha_{j+1}^2 - \alpha_j^2 = C ,$$

or

$$\alpha_i^2 = \alpha_1^2 + (i-1)C . \tag{3.15}$$

There is a direction $\hat{\Omega}_m$ corresponding to $(\alpha_1, \alpha_1, \alpha_{M/2})$, since there are $M/2$ points for α>0. This implies

$$\alpha_1^2 + \alpha_1^2 + \alpha_{M/2}^2 = 1 . \tag{3.16}$$

Combining equations (3.15) and (3.16) gives

$$\alpha_{M/2}^2 = \alpha_1^2 + (M/2 - 1)C = 1 - 2\alpha_1^2 .$$

Now one can calculate the constant *C* to derive a recursive relation

$$\alpha_i^2 = \alpha_{i-1}^2 + \frac{2(1 - 3\alpha_1^2)}{M - 2} . \tag{3.17}$$

This means that choosing α_1 will determine explicitly the direction cosine sets $\{\mu_m\} = \{\eta_m\} = \{\xi_m\}$. By choosing α_1 to be large or small, the points (Figure 5) can be clustered close to α=0 or near the poles α=±1.

From a practical point of view, a variety of quadrature sets is usually supplied with the discrete ordinates transport computer codes. Actually, the sets can also be "biased" or "asymmetric" in ξ, e.g., additional directions can be supplied along the -Z direction in order to give fine detail to polar streaming.

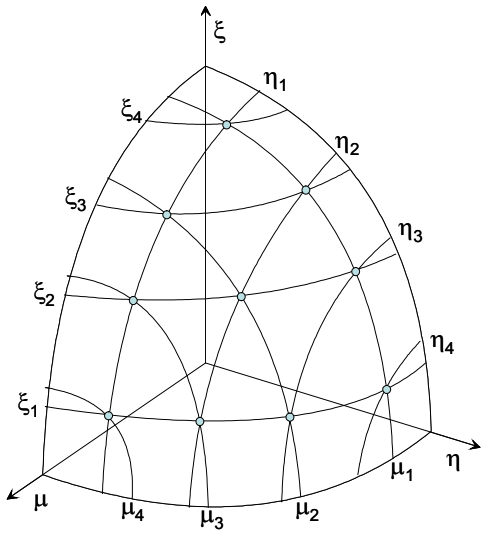

Figure 5. Symmetric point arrangement on one octant of unit sphere.

In addition to the selection of suitable quadrature sets, the resulting transport equations for each discrete direction have to be written as a set of algebraic equations adequate for numeric solution by computers. The S_N equation in the 3D Cartesian co-ordinate system has the form

$$\begin{aligned}
&\mu_m \left[A_{i+\frac{1}{2},j,k} N_{i+\frac{1}{2},j,k,m,g} - A_{i-\frac{1}{2},j,k} N_{i-\frac{1}{2},j,k,m,g} \right] \\
&+ \eta_m \left[B_{i,j+\frac{1}{2},k} N_{i,j+\frac{1}{2},k,m,g} - B_{i,j-\frac{1}{2},k} N_{i,j-\frac{1}{2},k,m,g} \right] \\
&+ \xi_m \left[C_{i,j,k+\frac{1}{2}} N_{i,j,k+\frac{1}{2},m,g} - C_{i,j,k-\frac{1}{2}} N_{i,j,k-\frac{1}{2},m,g} \right] \\
&+ \sigma^T_{i,j,k,g} V_{i,j,k} N_{i,j,k,m,g} = V_{i,j,k} S_{i,j,k,m,g} \,. \qquad (3.18)
\end{aligned}$$

Subscripts such as i+1/2 refer to the internal boundaries and N represents the angular flux. The coefficients A, B, and C are cell face areas perpendicular to the axes from which the direction cosines μ, η, and ξ are measured, and $\sigma^T_{i,j,k,g}$ is the total cross section. $V_{i,j,k}$ is the cell volume and $S_{i,j,k,m,g}$ is the source term.

Whereas the integro-differential form of the Boltzmann transport equation can be converted to a set of algebraic S_N equations by treating the angular integration with a weighted sum over discrete angular directions, this approach also causes certain problems. The rotational invariance of the original transport equation no longer holds for the S_N approach, due to angular discretisation. This sometimes leads to so-called "ray effect", i.e. non-physical artefacts in the flux solution by the discrete ordinates method [37, 38].

Another problem with the S_N method is that also false negative flux values can easily be generated. Non-physical negatives can cause wrong overall results and thwart convergence [36]. There are different fix-up methods for preventing this to happen. The easiest fix-up is to set all emerging negative flux values to zero, but this will underestimate the true result. Additionally, if false negatives are easily generated, it is apparent that inaccurate positive numbers can also be generated, and these errors are much harder to detect. The prevention of negative flux values is a characteristic problem for the S_N method. The undesired side effects of this problem can be avoided or at least minimised with a proper solution technique and by choosing suitable input parameters.

There are several numerical flux evaluation strategies for the S_N equations, such as the linear or diamond difference model, step model, linear zero and weighted difference model, as well as some semi-analytical methods like nodal and characteristic methods [36]. Details of these methods are beyond the scope of this review. However, the accuracy of the S_N approximation depends a lot on the solution method used and all the input parameters, including the discrete ordinates set. A user of the S_N codes should be aware of all the drawbacks and benefits of the different solution methods in order to be able to use these codes both efficiently and reliably in various transport problems.

3.1.2 Spherical harmonics method

The angular flux can be expanded by using spherical harmonics. The trigonometric form (instead of the imaginary exponential form) is used here to obtain more practical real equations for the flux. The flux expansion can be written as [18]

$$\Psi(\vec{r},E,\theta,\varphi) = \sum_{l=0}^{\infty}\sum_{m=0}^{l}(2l+1)P_l^m(\cos\theta)\left(\psi_{lm}(\vec{r},E)\cos m\varphi + \gamma_{lm}(\vec{r},E)\sin m\varphi\right) \tag{3.19}$$

where $P_l^m(\cos\theta)$ is an associated Legendre polynomial [28]

$$P_l^m(x) \equiv (1-x^2)^{m/2}\frac{d^m}{dx^m}P_l(x)\ . \tag{3.20}$$

Polar angle θ and azimuthal angle φ of the spherical co-ordinate system are illustrated in Figure 6.

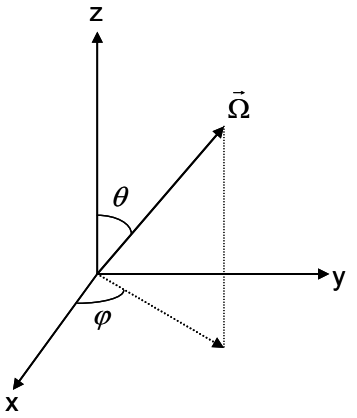

Figure 6. Direction vector $\vec{\Omega}$ in spherical co-ordinate system with polar angle θ and azimuthal angle φ.

Substituting the flux expansion (3.19) into the Boltzmann transport equation (3.1), multiplying it with an associated Legendre polynomial, and then integrating the resulting equation over direction space, a set of P_N transport equations can be derived for each associated Legendre polynomial by using the orthogonality of the base functions. For φ-terms the orthogonality integrals [28] are

$$\int_0^{2\pi} \sin(m\varphi)\sin(m'\varphi)d\varphi = \pi\delta_{m,m'},$$

$$\int_0^{2\pi} \cos(m\varphi)\cos(m'\varphi)d\varphi = \pi\delta_{m,m'}$$

and

$$\int_0^{2\pi} \sin(m\varphi)\cos(m'\varphi)d\varphi = 0$$

and the orthogonality integral for the associated Legendre polynomials is [28]

$$\int_0^{\pi} P_l^m(\cos\theta)P_{l'}^m(\cos\theta)\sin\theta\, d\theta = \frac{2}{2l+1}\cdot\frac{(l+m)!}{(l-m)!}\delta_{l,l'} .$$

The resulting streaming terms

$$\int d\vec{\Omega}P_{l'}^{m'}(\cos\theta)\cos m'\varphi\,\vec{\Omega}P_l^m(\cos\theta)\cos m\varphi$$

and

$$\int d\vec{\Omega}P_{l'}^{m'}(\cos\theta)\sin m'\varphi\,\vec{\Omega}P_l^m(\cos\theta)\sin m\varphi$$

are calculated by writing the direction vector in the form

$$\vec{\Omega} = \sin\theta\cos\varphi\,\vec{e}_x + \sin\theta\sin\varphi\,\vec{e}_y + \cos\theta\,\vec{e}_z$$

and using the trigonometric identities

$$\cos m\varphi\cos\varphi = \tfrac{1}{2}\left[\cos(m+1)\varphi + \cos(m-1)\varphi\right],$$

$$\cos m\varphi\sin\varphi = \tfrac{1}{2}\left[\sin(m+1)\varphi - \sin(m-1)\varphi\right],$$

$$\sin m\varphi\cos\varphi = \tfrac{1}{2}\left[\sin(m-1)\varphi - \sin(m+1)\varphi\right]$$

and

$$\sin m\varphi\sin\varphi = \tfrac{1}{2}\left[\cos(m-1)\varphi - \cos(m+1)\varphi\right]$$

and the recurrence relations [28] of the associated Legendre polynomials

$$\cos\theta\, P_l^m = \frac{l+m}{2l+1} P_{l-1}^m + \frac{l-m+1}{2l+1} P_{l+1}^m \ ,$$
$$\sin\theta\, P_l^m = \frac{1}{2l+1}\left(P_{l+1}^{m+1} - P_{l-1}^{m+1}\right)$$

and

$$\sin\theta\, P_l^m = \frac{1}{2l+1}\left[(l+m)(l+m-1)P_{l-1}^{m-1} - (l-m+1)(l-m+2)P_{l+1}^{m-1}\right] .$$

The scattering integral

$$\iint \sigma^S(\vec{r}, E, E', \vec{\Omega}, \vec{\Omega}')\Psi(\vec{r}, E', \vec{\Omega}')d\vec{\Omega}'dE'$$

is calculated with the use of the addition theorem [28]

$$P_{l'}(\mu_0) = P_{l'}(\cos\theta)P_{l'}(\cos\theta')$$
$$+ 2\sum_{m'=1}^{l'} \frac{(l'-m')!}{(l'+m')!} P_{l'}^{m'}(\cos\theta)P_{l'}^{m'}(\cos\theta')\cos m'(\varphi-\varphi')$$

and the trigonometric identity

$$\cos m(\varphi-\varphi') = \cos m\varphi \cos m\varphi' + \sin m\varphi \sin m\varphi' \ .$$

Separate equations are obtained for sine and cosine terms. The resulting P_N equations (derived by the author) are

$$2(l+m+1)\frac{\partial \psi_{l+1,m}}{\partial z} + 2(l-m)\frac{\partial \psi_{l-1,m}}{\partial z} + \left(\frac{\partial \psi_{l-1,m-1}}{\partial x} - \frac{\partial \gamma_{l-1,m-1}}{\partial y}\right)$$
$$-\left(\frac{\partial \psi_{l+1,m-1}}{\partial x} - \frac{\partial \gamma_{l+1,m-1}}{\partial y}\right) + (l+m+2)(l+m+1)\left(\frac{\partial \psi_{l+1,m+1}}{\partial x} + \frac{\partial \gamma_{l+1,m+1}}{\partial y}\right)$$
$$-(l-m-1)(l-m)\left(\frac{\partial \psi_{l-1,m+1}}{\partial x} + \frac{\partial \gamma_{l-1,m+1}}{\partial y}\right)$$
$$+ 2(2l+1)\sigma^T \psi_{l,m} = 2(2l+1)q_{l,m} + 2(2l+1)\int_0^\infty \sigma_l^s \psi_{l,m} dE' \qquad (3.21)$$

and

$$2(l+m+1)\frac{\partial \gamma_{l+1,m}}{\partial z}+2(l-m)\frac{\partial \gamma_{l-1,m}}{\partial z}+\left(\frac{\partial \psi_{l-1,m-1}}{\partial y}+\frac{\partial \gamma_{l-1,m-1}}{\partial x}\right)$$
$$-\left(\frac{\partial \psi_{l+1,m-1}}{\partial y}+\frac{\partial \gamma_{l+1,m-1}}{\partial x}\right)+(l+m+2)(l+m+1)\left(-\frac{\partial \psi_{l+1,m+1}}{\partial y}+\frac{\partial \gamma_{l+1,m+1}}{\partial x}\right)$$
$$-(l-m-1)(l-m)\left(-\frac{\partial \psi_{l-1,m+1}}{\partial y}+\frac{\partial \gamma_{l-1,m+1}}{\partial x}\right)$$
$$+2(2l+1)\sigma^{T}\gamma_{l,m}=2(2l+1)s_{l,m}+2(2l+1)\int_{0}^{\infty}\sigma_{l}^{s}\gamma_{l,m}dE' \qquad (3.22)$$

for each $l \in [0,N]$ and $m \in [-l,l]$, with the constraints that

$$\psi_{l,m}=\gamma_{l,m}\equiv 0 \text{ for } l<0 \text{ or } l>N .$$

The explicit spatial and energy dependency of the terms has been removed from the notation, for simplicity: e.g. the term σ^{T} stands for the total cross section $\sigma^{T}(\vec{r},E)$. It should be noted that also the source has been expanded in spherical harmonics

$$Q(\vec{r},E,\vec{\Omega})$$
$$=\sum_{l=0}^{\infty}\sum_{m=0}^{l}(2l+1)P_{l}^{m}(\cos\theta)\left(q_{l,m}(\vec{r},E)\cos m\varphi+s_{l,m}(\vec{r},E)\sin m\varphi\right) \qquad (3.23)$$

Fletcher [18] has derived equations which are very similar to equations (3.21) and (3.22), except that Fletcher's equations do not take anisotropic source terms into account. Similar (mathematically equivalent) P_N equations have also been derived for imaginary exponential form of the flux expansion [15], leading to a somewhat simpler approximation from the mathematical point of view, but less suitable for numerical solution (due to the resulting imaginary part).

It can be seen from equations (3.21) and (3.22) that a set of 15 coupled equations for 15 unknowns is obtained for Legendre order 3 approximation (i.e. P_3 approximation). For numerical solution, the first-order equations (3.21) and (3.22) are problematic, as the first-order derivatives will not be positive definite. However, by substituting odd moment terms (with l odd) into the even order

equations, it is possible to obtain equations in the second-order form, and also reduce the number of equations and unknowns. For instance, in the second-order multigroup P_3 approximation, "only" 6 coupled equations with 6 unknowns result:

$$2\sigma_{a0}^{g}\psi_{00}-\frac{2}{3\sigma_{a1}^{g}}\left[\partial_x^2+\partial_y^2+\partial_z^2\right]\psi_{00}+\frac{2}{3\sigma_{a1}^{g}}\left[\partial_x^2+\partial_y^2-2\partial_z^2\right]\psi_{20}$$
$$-\frac{4}{\sigma_{a1}^{g}}\partial_x\partial_z\psi_{21}-\frac{4}{\sigma_{a1}^{g}}\left[\partial_x^2-\partial_y^2\right]\psi_{22}-\frac{4}{\sigma_{a1}^{g}}\partial_y\partial_z\gamma_{21}-\frac{8}{\sigma_{a1}^{g}}\partial_x\partial_y\gamma_{22}=q_{00}^{g} \tag{3.24}$$

$$\frac{2}{3\sigma_{a1}^{g}}\left[\partial_x^2+\partial_y^2-2\partial_z^2\right]\psi_{00}-\frac{2}{3\sigma_{a1}^{g}}\left[\partial_x^2+\partial_y^2+4\partial_z^2\right]\psi_{20}-\frac{2}{\sigma_{a1}^{g}}\partial_x\partial_z\psi_{21}$$
$$+\frac{4}{\sigma_{a1}^{g}}\left[\partial_x^2-\partial_y^2\right]\psi_{22}-\frac{2}{\sigma_{a1}^{g}}\partial_y\partial_z\gamma_{21}+\frac{8}{\sigma_{a1}^{g}}\partial_x\partial_y\gamma_{22}+10\sigma_{a2}^{g}\psi_{20}$$
$$-\frac{12}{7\sigma_{a3}^{g}}\left[\partial_x^2+\partial_y^2\right]\psi_{20}-\frac{18}{7\sigma_{a3}^{g}}\partial_z^2\psi_{20}-\frac{6}{7\sigma_{a3}^{g}}\partial_x\partial_z\psi_{21}$$
$$+\frac{12}{7\sigma_{a3}^{g}}\left[\partial_x^2-\partial_y^2\right]\psi_{22}-\frac{6}{7\sigma_{a3}^{g}}\partial_y\partial_z\gamma_{21}+\frac{24}{7\sigma_{a3}^{g}}\partial_x\partial_y\gamma_{22}=0 \tag{3.25}$$

$$-\frac{4}{3\sigma_{a1}^{g}}\partial_x\partial_z\psi_{00}-\frac{2}{3\sigma_{a1}^{g}}\partial_x\partial_z\psi_{20}-\frac{2}{\sigma_{a1}^{g}}\left[\partial_x^2+\partial_z^2\right]\psi_{21}$$
$$-\frac{4}{\sigma_{a1}^{g}}\partial_x\partial_z\psi_{22}-\frac{2}{\sigma_{a1}^{g}}\partial_x\partial_y\gamma_{21}-\frac{4}{\sigma_{a1}^{g}}\partial_y\partial_z\gamma_{22}+10\sigma_{a2}^{g}\psi_{21}$$
$$-\frac{2}{7\sigma_{a3}^{g}}\partial_x\partial_z\psi_{20}-\frac{1}{7\sigma_{a3}^{g}}\left[16\partial_x^2+10\partial_y^2+16\partial_z^2\right]\psi_{21}$$
$$-\frac{12}{7\sigma_{a3}^{g}}\partial_x\partial_z\psi_{22}-\frac{6}{7\sigma_{a3}^{g}}\partial_x\partial_y\gamma_{21}-\frac{12}{7\sigma_{a3}^{g}}\partial_y\partial_z\gamma_{22}=0 \tag{3.26}$$

$$-\frac{1}{3\sigma_{a1}^{g}}\left[\partial_x^2-\partial_y^2\right]\psi_{00}+\frac{1}{3\sigma_{a1}^{g}}\left[\partial_x^2-\partial_y^2\right]\psi_{20}-\frac{1}{\sigma_{a1}^{g}}\partial_x\partial_z\psi_{21}$$
$$-\frac{2}{\sigma_{a1}^{g}}\left[\partial_x^2+\partial_y^2\right]\psi_{22}+\frac{1}{\sigma_{a1}^{g}}\partial_y\partial_z\gamma_{21}+10\sigma_{a2}^{g}\psi_{22}+\frac{1}{7\sigma_{a3}^{g}}\left[\partial_x^2-\partial_y^2\right]\psi_{20}$$
$$-\frac{3}{7\sigma_{a3}^{g}}\partial_x\partial_z\psi_{21}-\frac{16}{7\sigma_{a3}^{g}}\left[\partial_x^2+\partial_y^2\right]\psi_{22}-\frac{10}{7\sigma_{a3}^{g}}\partial_z^2\psi_{22}+\frac{3}{7\sigma_{a3}^{g}}\partial_y\partial_z\gamma_{21}=0 \tag{3.27}$$

$$-\frac{4}{3\sigma_{a1}^{g}}\partial_y\partial_z\psi_{00}-\frac{2}{3\sigma_{a1}^{g}}\partial_y\partial_z\psi_{20}-\frac{2}{\sigma_{a1}^{g}}\partial_x\partial_y\psi_{21}+\frac{4}{\sigma_{a1}^{g}}\partial_y\partial_z\psi_{22}$$
$$-\frac{2}{\sigma_{a1}^{g}}\left[\partial_y^2+\partial_z^2\right]\gamma_{21}-\frac{4}{\sigma_{a1}^{g}}\partial_x\partial_z\gamma_{22}+10\sigma_{a2}^{g}\gamma_{21}-\frac{2}{7\sigma_{a3}^{g}}\partial_y\partial_z\psi_{20}$$
$$-\frac{6}{7\sigma_{a3}^{g}}\partial_x\partial_y\psi_{21}+\frac{12}{7\sigma_{a3}^{g}}\partial_y\partial_z\psi_{22}-\frac{1}{7\sigma_{a3}^{g}}\left[10\partial_x^2+16\partial_y^2+16\partial_z^2\right]\gamma_{21}$$
$$-\frac{12}{7\sigma_{a3}^{g}}\partial_x\partial_z\gamma_{22}=0 \tag{3.28}$$

$$-\frac{2}{3\sigma_{a1}^{g}}\partial_x\partial_y\psi_{00}+\frac{2}{3\sigma_{a1}^{g}}\partial_x\partial_y\psi_{20}-\frac{1}{\sigma_{a1}^{g}}\partial_y\partial_z\psi_{21}-\frac{1}{\sigma_{a1}^{g}}\partial_x\partial_z\gamma_{21}$$
$$-\frac{2}{\sigma_{a1}^{g}}\left[\partial_x^2+\partial_y^2\right]\gamma_{22}+10\sigma_{a2}^{g}\gamma_{22}+\frac{2}{7\sigma_{a3}^{g}}\partial_x\partial_y\psi_{20}-\frac{3}{7\sigma_{a3}^{g}}\partial_y\partial_z\psi_{21}$$
$$-\frac{3}{7\sigma_{a3}^{g}}\partial_x\partial_z\gamma_{21}-\frac{1}{7\sigma_{a3}^{g}}\left[16\partial_x^2+16\partial_y^2+10\partial_z^2\right]\gamma_{22}=0 \tag{3.29}$$

The group transport cross sections are defined by subtraction of the corresponding Legendre component of the group scattering cross section from the group total cross section:

$$\sigma_{al}^{g}=\sigma_{t}^{g}-\sigma_{s,l}^{g->g}\ . \tag{3.30}$$

To the author's knowledge, these second-order P_3 equations (3.24)–(3.29) have not been explicitly published elsewhere. Fletcher has derived similar equations by setting extra constraints for the transport cross sections, that is, all σ_{al} are set equal except for σ_{a1} [18].

It is worth noticing that only the scalar source term q_{00} is taken into account in the source expansion (3.23) in the above second-order P_3 approximation, equations (3.24)–(3.29), for simplicity. The higher source moment terms can be included, but they increase the complexity of the equations even more.

The P_N approximation has been well established in transport theory [16]. However, for numerical solution it is rather ill suited. P_N equations have been used primarily for theoretical (i.e., analytical) investigations of solutions of the transport equation [15]. Especially in 3D, the complexity of the equations makes it very hard to construct a numerical algorithm. Despite these difficulties, Fletcher introduced as early as in the 1970s a small computer programme to derive second-order (odd) P_N equations of different Legendre orders for slab geometry, and also obtained numerical P_1 and P_3 multigroup solutions in XY and XYZ geometries [18, 19].

There are certain features that make the application of the P_N approximation for radiation transport problems very tempting. With the spherical harmonics approximation, the angular dependency of the flux actually becomes a property of the pre-Hilbert space with spherical harmonics as base polynomials of the vector function space. Thus, the resulting equations and unknowns depend only on energy and spatial co-ordinates. This is mathematically an elegant way to get rid of the problematic integro-differential form of the basic transport equation which contains implicit angular dependency! In addition, by using a higher Legendre order approximation, the solution will, in principle, approach the exact solution of the transport equation. Furthermore, the spherical harmonics base polynomials are rotationally invariant, so the rotational invariance of the original Boltzmann transport equation is also preserved. Thus, ray effects – encountered with the S_N method – will not emerge in the P_N approximation.

One drawback of the P_N approximation is that no exact vacuum boundary condition can be defined [16]. At the vacuum (or free surface) boundary,

particles escape from the geometry with no possibility to return. The problem is that this vacuum boundary condition [15, 16]

$$\Psi(\vec{\Omega}) \equiv 0 \text{ for } \vec{\Omega} \cdot \vec{n} < 0 , \tag{3.31}$$

where $\vec{n}$ is an outward normal to external surface, means that the flux is discontinuous at $\vec{\Omega} \cdot \vec{n} = 0$, which cannot be exactly represented by the continuous spherical harmonics base functions. Many approximative conditions are possible, though. Mark or Marshak boundary conditions are the most well-known [16, 39, 40, 41]. For instance, the Marshak vacuum boundary condition [41] is defined as

$$\int_{\vec{\Omega} \cdot \vec{n} < 0} d\vec{\Omega} P_l^m(\vec{\Omega}) \vec{\Omega} \cdot \vec{n} \Psi(\vec{\Omega}) = 0 . \tag{3.32}$$

Concerning the second-order form of the P_N equations, it is worth noticing, that by solving all the unknowns, only even moment terms are actually solved. Naturally, this includes the scalar flux (the ψ_{00} term), which is probably the most interesting quantity. However, if the angular flux has to be determined as well, then the odd moment terms should be solved in addition. As a final remark, it should be noted that spherical harmonics are sometimes used also with the discrete ordinates method discussed in the previous section in order to store the angular flux during the computation in a more compact manner. However, this has nothing to do with the actual P_N approximation of the transport equation.

3.1.3 Finite element method

The finite element method (FEM) is the name commonly applied to the expansion of the solution to a set of partial differential equations in a set of local basis functions [15, 17]. Finite element methods can be adapted to problems of great complexity and unusual geometry.

In radiation transport, the finite element method can be applied to both first and second-order forms of the transport equation. However, in the latter case, it is extremely difficult to implement anisotropic scattering in multidimensional geometries [15]. In the following, the theoretical background of the finite

element method found from radiation transport literature is briefly reviewed. The application of the method to second-order form of the transport equation will, however, not be covered in this context any further. In addition, the first-order form will only be covered superficially, just to give the reader a general idea of how the finite element method works.

The finite element method is always applied to an integral formulation of the original partial differential equation of interest. The Boltzmann radiation transport equation can also be written in so-called integral law (or weak) form. Multiplying the Boltzmann transport equation (3.1) with an arbitrary angular flux belonging to Sobolev space $\psi(\vec{r},\vec{\Omega}) \in H_E$ and integrating over the phase space, one can rewrite (considering for simplicity only one-speed form) the transport equation (3.1) as [15]

$$(\vec{\Omega}\cdot\nabla\Psi,\psi)+(K\Psi,\psi)=(Q,\psi)\,. \tag{3.33}$$

Here, the real inner product has been defined as

$$(f,g)\equiv\iint_V f(\vec{r},\vec{\Omega})g(\vec{r},\vec{\Omega})d\vec{r}d\vec{\Omega}$$

where *f* and *g* are two elements of the Sobolev space

$$H_E=\left\{\psi(\vec{r},\vec{\Omega}):\text{real}\,\psi(\vec{r},\vec{\Omega})\ \text{such that}\ \iint_V[|\psi|^2+|\nabla\psi|^2]d\vec{r}d\vec{\Omega}<\infty\right\},$$

which ensures that phase space integrals exist. In addition, a collision operator *K* has been introduced

$$K\circ\equiv\sigma^T(\vec{r})\circ-\int\sigma^S(\vec{r},\vec{\Omega},\vec{\Omega}')\circ\ .$$

If one assumes inhomogeneous boundary conditions

$$\Psi(\vec{r}_s,\vec{\Omega})=\Psi_0(\vec{r}_s,\vec{\Omega}),\quad \vec{\Omega}\cdot\vec{n}<0$$

and defines the inner product to characterise the boundary

$$\langle f,g\rangle\equiv\iint_{\partial V} f(\vec{r}_s,\vec{\Omega})g(\vec{r}_s,\vec{\Omega})(\vec{\Omega}\cdot\vec{n})dSd\vec{\Omega}$$

divided further for incoming and outgoing directions $\vec{\Omega}\cdot\vec{n}<0$ and $\vec{\Omega}\cdot\vec{n}>0$ as

$$\langle f,g\rangle = \langle f,g\rangle_+ - \langle f,g\rangle_-$$

then (after some manipulation including integration by parts of the streaming term) equation (3.33) can be rewritten in a form [15]

$$(\Psi,\vec{\Omega}\cdot\nabla\psi) + \langle\Psi,\psi\rangle_+ + (K\Psi,\psi) = (Q,\psi) + \langle\Psi_0,\psi\rangle_- \ . \qquad (3.34)$$

This is known as the *integral law* or *weak form* of the transport equation.

It is worth noticing that the boundary condition is included in the integral law (3.34). This is an example of a so-called *natural* boundary condition, and is a consequence of integration by parts.

In the finite element method one seeks the solution in a finite element subspace $S^h \subset H_E$, i.e., a solution $\Psi^h(\vec{r},\vec{\Omega}) \in S^h$ such that equation (3.34) is satisfied for all $\psi^h(\vec{r},\vec{\Omega}) \in S^h$. S^h is a specially constructed subspace with local basis functions $\psi_i^h(\vec{r},\vec{\Omega})$, i=1,2,…,N, where N is the dimension of S^h, typically the number of nodes in the mesh. In other words, the solution is expanded as a series

$$\Psi^h(\vec{r},\vec{\Omega}) = \sum_{j=1}^{N} \Psi_j \psi_j^h(\vec{r},\vec{\Omega}) \ ,$$

which is then inserted into equation (3.34), and a matrix system is obtained [15]

$$A\vec{\Psi} = \vec{S} \ , \qquad (3.35)$$

where

$$A_{ij} = -(\psi_j^h,\vec{\Omega}\cdot\nabla\psi_i^h) + \langle\psi_j^h,\psi_i^h\rangle_+ + (K\psi_j^h,\psi_i^h)$$

$$S_i \equiv (Q,\psi_i^h)$$

$$\vec{\Psi} = \mathrm{col}(\Psi_1,\Psi_2,\ldots,\Psi_N) \ .$$

There are different ways to construct the finite element subspace S^h. Just to illustrate how the basis functions could be chosen, a 1D triangular mesh is

considered next as an example. It should be noted that for multidimensional elements one can also formulate basis functions that are direct products of simple 1D basis functions [15].

Let x be the spatial co-ordinate and μ the angular direction cosine: a basis function for global node n is then defined [15] as a direct product of 1D basis functions for the spatial node i and angular node j

$$\psi_n(x,\mu) = \psi_i(x)\psi_j(\mu) \ .$$

Continuous standard "tent" functions can be used as local basis functions (see Figure 7):

$$\psi_i(x) = \begin{cases} \dfrac{x - x_{i-1}}{x_i - x_{i-1}}, & x_{i-1} \le x \le x_i \\ \dfrac{x_{i+1} - x}{x_{i+1} - x_i}, & x_i \le x \le x_{i+1} \\ 0, & \text{otherwise} \end{cases}$$

and

$$\psi_j(\mu) = \begin{cases} \dfrac{\mu - \mu_{j-1}}{\mu_j - \mu_{j-1}}, & \mu_{j-1} \le \mu \le \mu_j \\ \dfrac{\mu_{j+1} - \mu}{\mu_{j+1} - \mu_j}, & \mu_j \le \mu \le \mu_{j+1} \\ 0, & \text{otherwise} \end{cases} \ .$$

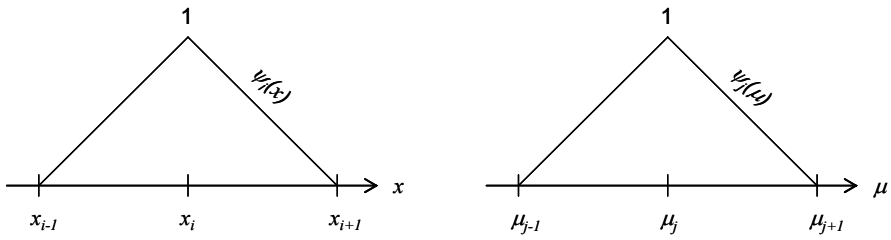

Figure 7. Standard "tent" basis functions of 1D triangular finite elements.

There are also other possibilities to construct the basis functions, such as using a higher order polynomial over a general element such as a triangle, or using a product of higher order 1D polynomials. For instance, in 1D one can introduce an additional node and define quadratic basis functions instead of triangular. However, higher order elements increase the coupling between the neighbour elements. For cubic elements the interaction would extend over the three nearest neighbours on either side. The increased coupling is undesirable, as it will also increase the bandwidth of coefficient matrix A of the matrix system (3.35).

The advantages of the first-order FEM approach to radiation transport are the ease of incorporating anisotropic scattering, mitigation of the ray effect, and convenient treatment of boundary conditions as natural. The major disadvantage is that the resulting asymmetric matrix system has to be solved by using direct matrix inversion methods, which are time consuming and in large problems severely limited by the memory requirements.

In the second-order FEM approach (not covered any further in this context) the resulting matrices are symmetric and positive definite, which makes it possible to use iterative solution techniques [15]. However, implementation of anisotropic scattering in multidimensional geometries is far from trivial. In addition, voids can present a problem because of the $(\sigma^T)^{-1}$ term [15]. Ray-tracing has been used to overcome this problem [42].

The major advantage of FEM is the possibility to model complicated geometries with a variably sized, unstructured mesh (Figure 8). For instance, an adaptive tetrahedral finite element mesh can be used in 3D, providing gains in efficiency that may not be realisable on uniformly defined grids. In many cases, also dynamic mesh refinement can be used, based on local error estimate of the

solution [43]. Thus, the mesh is locally refined, not only to adapt to the geometry, but to ensure accuracy of the solution everywhere based on feedback from the obtained error estimate.

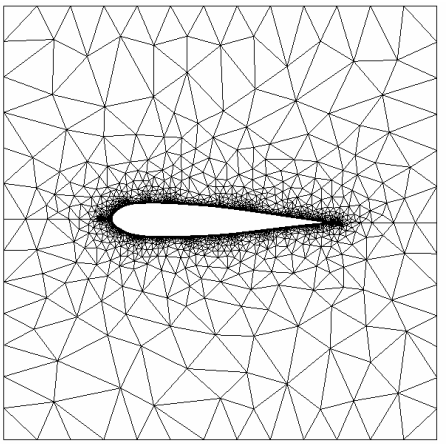

Figure 8. An illustration of an unstructured triangular finite element mesh (a Mesh2d example picture with permission from UCL Département de mécanique http://www.mema.ucl.ac.be/~wu/mesh2d/mesh2d.html).

There are also hybrid schemes where FEM has been combined with discrete ordinates or spherical harmonics solutions [42, 44–46]. FEM has been applied to reactor physics problems already for a long time [47–49]. FEM has been applied also to radiotherapy calculations, including solution of the Boltzmann-Fokker-Planck equation for charged particle transport [50, 51]. The applicability of the FEM for inverse problems encountered, for instance, in intensity modulated radiotherapy (IMRT) has also been studied lately [52, 53].

An interested reader can find in-depth studies, e.g. from the book by Ackroyd [49], concerning the use of FEM in reactor and radiation physics. In general, FEM is widely used in structural analysis, electromagnetics and computational fluid dynamics.

3.2 Statistical methods

3.2.1 Monte Carlo method

Monte Carlo methods [54, 55] and deterministic transport methods are fundamentally very different. Deterministic methods solve the transport equation for the average particle behaviour. By contrast, Monte Carlo does not solve an explicit equation, but rather obtains answers by simulating individual particles and recording some aspects of their average behaviour.

The Monte Carlo methods are based on statistical sampling techniques, and the term "Monte Carlo" naturally refers to the games of chance. It was Nicholas Metropolis who named this mathematical method during World War II at Los Alamos, where the first nuclear weapons were developed. However, the idea of random sampling to solve mathematical problems is much older: the method was used as early as in 1772 by Compte de Buffon, and in 1786 Laplace suggested that π could be evaluated by random sampling. Eventually, it was the development of computers that really made the Monte Carlo method a breakthrough.

The Monte Carlo method can be used to duplicate theoretically a statistical process, such as the interaction of nuclear particles with materials. The individual probabilistic events for each particle are simulated sequentially, in order to produce a particle track through the problem geometry. The particles are followed until escape or absorption, or some other terminal category. Probability distributions are randomly sampled for each particle interaction. The probability distribution for scattering angle, for instance, can be found from the primary sources of nuclear data, such as the Evaluated Nuclear Data File (ENDF) system [56].

The probability of a first collision for a particle between s and $s + ds$ along its line of flight is given by

$$p(s)ds = e^{-\sigma^T} \sigma^T ds \tag{3.36}$$

where σ^T is the macroscopic total cross section of the medium and is interpreted as the probability per unit length of a collision. The distance to the next collision can then be calculated from the expression

$$s = \frac{\ln(\zeta)}{\zeta} \tag{3.37}$$

where ζ is a random number uniformly distributed between 0 and 1.

After a collision occurs, the collision nuclide is identified, based on probability proportional to weight fractions of each material constituent. Then the collision type (absorption, elastic scattering, inelastic scattering, etc.) is sampled based on cross sections (i.e. probabilities for different events) taken from the material cross section library. In the case of the elastic scattering, for instance, the scattering angle is further sampled from the probability tables. The velocity of the scattered particle is then dictated by two-body kinematics, and the particle track can be continued.

Monte Carlo methods are very time consuming: in order to get results with sufficiently low statistical uncertainty for some tally volume, generally a huge number of source particles and particle tracks have to be simulated. Especially the tracking of electrons is tedious, as electron transport is dominated by the long-range Coulomb force, resulting in large numbers of scattering events. Additionally, Monte Carlo methods very seldom provide comprehensive data on flux details, but merely give answers in some user-specified points or geometry volumes. On the other hand, Monte Carlo methods can be considered very reliable when sufficiently low statistical uncertainty is achieved.

MCNP is the well-known successor of the early Monte Carlo codes developed at Los Alamos [57]. Among the radiation transport codes used in nuclear engineering, it has almost obtained the status of a standard, but there are also many other transport codes using the Monte Carlo method. In the medical physics community, Electron Gamma Shower (EGS) codes (e.g., EGS4 and EGSnrc) are widely used for photon and electron transport problems [58, 59, 60]. In electron transport problems, for example, in simulation of ionisation chamber responses in cases where c.p.e. condition is not met, EGSnrc seems to produce the most accurate results [60]. MCNP is capable for electron transport as well, but uses somewhat different algorithms from EGS codes, and can produce quite

inaccurate electron dose results with default options [60, 61]. This poses some extra difficulties for ionisation chamber modelling in BNCT beams, as EGS codes are not capable for neutron transport, and therefore MCNP is in practice the only viable option for coupled neutron-photon-electron simulations. However, it seems that with suitable input parameter options, also MCNP can produce good results for electron dose, and is also widely used in radiation dosimetry applications [62]. For high-energy physics, on the other hand, a special Monte Carlo code GEANT4 exists, having unique capabilities to simulate all kinds of particle interactions and heavy particle transport [63]. Quite recently the capacity of GEANT4 to simulate neutron transport in the thermal energy region has also been tested [64].

A new Monte Carlo code has been recently developed also at VTT. It is called PSG (named after Probabilistic Scattering Game), and it uses a modification of a fast Woodcock tracking method [65, 66]. The Woodcock tracking method is based on introducing virtual collisions in such a way that the effective total cross section (majorant cross section) can be set equal in all material regions. Therefore, when simulating particle tracks, it is not necessary to calculate the shortest optical distance to the material boundaries each time the path length is sampled, which makes the code performance more effective. PSG is used for calculation of multiplication eigenvalues, group constants, reactor kinetic parameters, pin-wise nuclear fuel power distributions, discontinuity factors and other parameters needed for nodal diffusion calculations and nuclear reactor analysis [34, 67, 68]. It is also planned to be used for burnup calculations. For many applications, the new PSG code is considerably faster than MCNP, for instance. The PSG code is, however, still at an early stage and needs further development.

In BNCT treatment planning, the Monte Carlo code SERA and its predecessor BNCT_rtpe have been used in Finland [7–10]. In SERA, uniform volume element (univel) reconstruction of the patient geometry is used, allowing integer arithmetics to be utilised in calculation of the distance to boundary, in order to speed up the particle tracking. In addition, SERA uses multigroup cross sections to improve efficiency even further.

The NCT_Plan system [69] has also been used by the BNCT community. NCT_Plan has been developed in connection with the clinical research

programme centred at Harvard and MIT. NCT_Plan has algorithms for creating voxelised patient geometry and uses customised radiation transport routines of MCNP, with a significant increase in the execution speed of the calculations [70] compared to the standard version of MCNP.

The Monte Carlo method has become more and more important over the years, due to increased computer capacity. Particle tracking by Monte Carlo method is also well suited for parallel computing.

4. Tree multigrids and simplified spherical harmonics approximation

4.1 Tree multigrid technique

4.1.1 Construction of the spatial tree structured domain

The simplest way to discretise a spatial domain is naturally to divide it into uniform, equidistant mesh. However, a very fine mesh might be required in problems which are large but contain small geometrical details. This will both affect the memory allocation required for the data storage of the unknowns, as well as the total amount of required arithmetical operations in order to solve the original numerical problem. Especially when using uniform mesh in complicated 3D problems, the required computational work and the overall dimension of the problem might become too demanding even for modern computers.

In the majority of practical problems there are sub-domains which require fine discretisation, but there may be other sub-domains that allow a considerably coarser grid. For instance, a fine grid is required near the borders and material interfaces, but a coarse grid can be used elsewhere. In such a case, the traditional finite difference methods, which introduce the simplest discretisation process and equations, can lead to an unnecessarily large discrete system.

There are methods in which the computational domain is divided into finite elements [15, 42–53], as already discussed in Section 3.1.3. These finite elements are often made triangular or polygonal. As the finite element method offers an elegant way to represent the geometry, the numerical algorithm for radiation transport is far from trivial, especially with anisotropic scattering in multidimensional geometry [15]. Also the generation of a suitable finite element mesh is more or less a difficult and time-consuming task, even though several algorithms and freeware codes exist.

The method discussed here is somewhat different from the FEM approach. In this method, the resulting tree structured grid is called quadtree or octree, depending on whether one is focused on a 2D or 3D method, respectively [71]. The basic mesh elements are quadratic or cubic. The idea is to use a conditional

subdivision procedure to generate a nested non-equidistant, non-uniform cell system through adaptive meshing [13]. Here we concentrate on the 3D octree method. One starts from a cube (called a root cell) which embodies the original geometry. This is then conditionally divided into eight sub-cubes. The sub-cubes are called children of the parent cell. Each child-cube can become a parent and have their own children. The subdivision procedure is continued until a pre-defined subdivision level is reached. The subdivision criteria can be based on some static geometrical features, such as number of points in a cell, or some dynamic features such as error estimate or flux gradient of some partial differential equation. The adaptive meshing is illustrated in Figure 9.

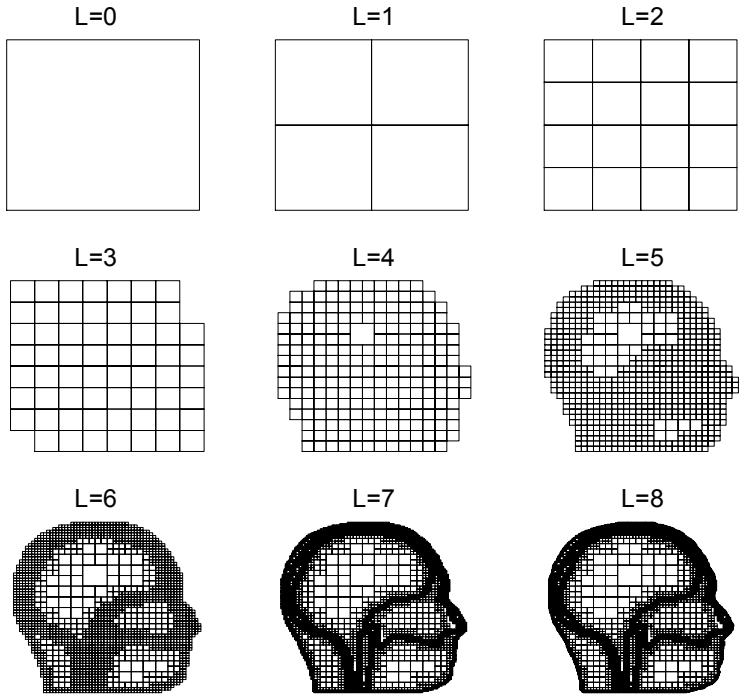

Figure 9. Adaptive meshing. L = subdivision level.

In 3D the octree cell structure can be indexed by spatial indexes i, j, and k and subdivision level L. Thus, if u is a cell in octree, it is indexed as $u^{L}_{i,j,k}$. Eight children cells of this octree cell would be indexed as

$$u^{L+1}_{2i,2j,2k}$$

$$u^{L+1}_{2i+1,2j,2k}$$

$$u^{L+1}_{2i,2j+1,2k}$$

$$u^{L+1}_{2i+1,2j+1,2k}$$

$$u^{L+1}_{2i,2j,2k+1}$$

$$u^{L+1}_{2i+1,2j,2k+1}$$

$$u^{L+1}_{2i,2j+1,2k+1}$$

$$u^{L+1}_{2i+1,2j+1,2k+1}$$

The parent of each cell can be found simply by subtracting 1 from the subdivision level L and by dividing each i, j, and k integer index by 2 (and forgetting the modulus). A 1D example of the discretisation of the spatial domain is shown in Figures 10 and 11, as an additional illustration of the subdivision and cell indexing.

When the minimum co-ordinates X_{min}, Y_{min}, and Z_{min} of the root cell are known, the minimum and maximum co-ordinates of any octree cell $u^{L}_{i,j,k}$ are

$$x_{min} = X_{min} + i\Delta \cdot 2^{-L}$$

$$y_{min} = Y_{min} + j\Delta \cdot 2^{-L}$$

$$z_{min} = Z_{min} + k\Delta \cdot 2^{-L}$$

$$x_{max} = X_{min} + (i+1)\Delta \cdot 2^{-L}$$

$$y_{max} = Y_{min} + (j+1)\Delta \cdot 2^{-L}$$

$$z_{max} = Z_{min} + (k+1)\Delta \cdot 2^{-L}$$

where Δ is the side length of the root cube.

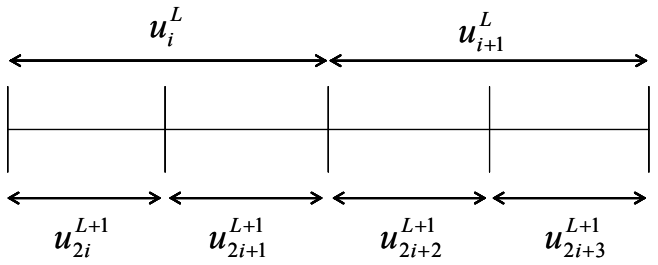

Figure 10. Division of the spatial domain in 1D.

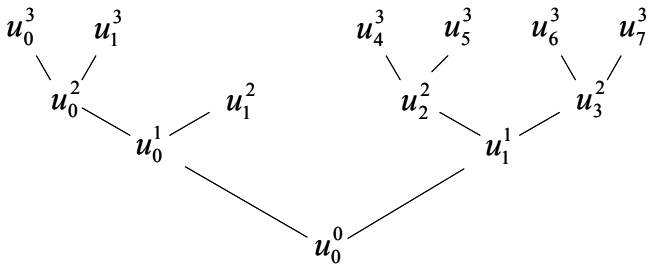

Figure 11. Tree structure of the spatial domain as a 1D example. Each cell division forms a branch, and the leaf cells are the cells which are not divided any further (e.g. u_0^3 and u_1^2 are both leaf cells).

In principle, the recursive subdivision of octree cells can be continued unlimitedly. In practice, the computer memory and the numerical efficiency of the iterative solution set constraints on the maximal subdivision level L. Usually a subdivision level L=7 or L=8 already gives a very fine mesh. The minimum cell side length $\Delta_{\min}$ is relative to the overall dimension of the geometry

$$\Delta_{\min} = \Delta \cdot 2^{-L}$$

where Δ is the side length of the root cube (which embodies the original geometry). For instance, for a human head geometry (Figure 9), the minimum cell side length is 1.55 mm for subdivision level L=7 and 0.77 mm for L=8.

The octree structure makes it possible to easily find parent or children cells and to build recursive functions for data handling on nested grids with different grid size (coarseness).

Self-adaptive quadtree or octree meshing is often used also as an intermediate stage in generation of the finite element mesh. However, this theme will not be covered in more detail here.

The advantage of the octree grid compared to more sophisticated finite element mesh is that, as the resulting cell system can be made regular, it is much easier to construct straightforward difference schemes, which will also have lower computational cost [13]. It is also worth noticing, that the octree grid algorithm automatically produces all the coarser grids at the same time (as illustrated in Figure 9), which enables the utilisation of fast multigrid acceleration methods in the numerical iteration [13].

4.1.2 Multigrid acceleration methods

Practical multigrid methods [72, 73] were first introduced by Brandt [74] in the 1970s. These methods can solve partial differential equations discretised on N grid points in $O(N)$ operations. For example Gauss-elimination would require $O(N^2)$ operations, and even "rapid" direct elliptic solvers require $O(N\log N)$ operations for solving elliptic equations. Thus, the multigrid method is very efficient for large problems (number of grid points N being large).

The efficiency of the multigrid methods is based on discretisation of the original problem on coarser and finer grids, i.e. with different mesh sizes. A multigrid is formed by nested grids with refined mesh size. On a coarse grid, much less iterations are required to obtain a converged solution. These coarse solutions can be interpolated into finer grids, and thus be used to accelerate the iteration process of the fine-grid solutions. In the multigrid methods, data is transferred both from coarser grids to finer grids, and backwards, in so-called multigrid cycles.

If we consider a linear elliptic problem

$$A\vec{u} = \vec{S} \tag{4.1}$$

where A is the matrix of the corresponding linear elliptic operator, $\vec{u}$ is the column vector, and $\vec{S}$ is the column source vector. If this problem is discretised

on a uniform grid with mesh size h, it can be written in a set of linear algebraic equations as

$$A_h u_h = S_h \ . \tag{4.2}$$

Let $\widetilde{u}_h$ denote some approximate solution of the equation, and let u_h be the exact solution. Then the error of the approximate solution is

$$v_h = u_h - \widetilde{u}_h \tag{4.3}$$

A quantity called residual can be defined as

$$r_h = S_h - A_h \widetilde{u}_h \tag{4.4}$$

As A is assumed to be linear, also the error satisfies the equation

$$A_h v_h = r_h \tag{4.5}$$

This residual equation can be approximated on a coarser grid with mesh size H

$$A_H v_H = r_H \tag{4.6}$$

where H=2h, for instance. Since this equation has a smaller dimension, it will be much easier to solve. To define the residual on the coarser grid, some restriction operator $\Re$ is needed:

$$r_H = \Re r_h \tag{4.7}$$

Once the equation (4.6) is solved on a coarse grid, the error can be interpolated to the finer grid by a proper prolongation operator $\wp$:

$$\widetilde{v}_h = \wp \widetilde{v}_H \tag{4.8}$$

Both $\Re$ and $\wp$ are chosen to be linear operators. Finally, the approximation $\widetilde{u}_h$ can be updated:

$$\widetilde{u}_h^{new} = \widetilde{u}_h + \widetilde{v}_h \tag{4.9}$$

Thus, a solution on a next coarser grid can be used to accelerate the solution on a finer grid. By constructing a sequence of nested grids (fine and coarse grids), one can define the multigrid cycle, which recursively leads the discrete problem from finest grid to coarser grids and back to finest grid again. The exact structure of the cycle depends on the number of two-grid iterations γ at each intermediate stage. If γ=1 the structure is called V-cycle, and if γ=2, W-cycle (Figure 12).

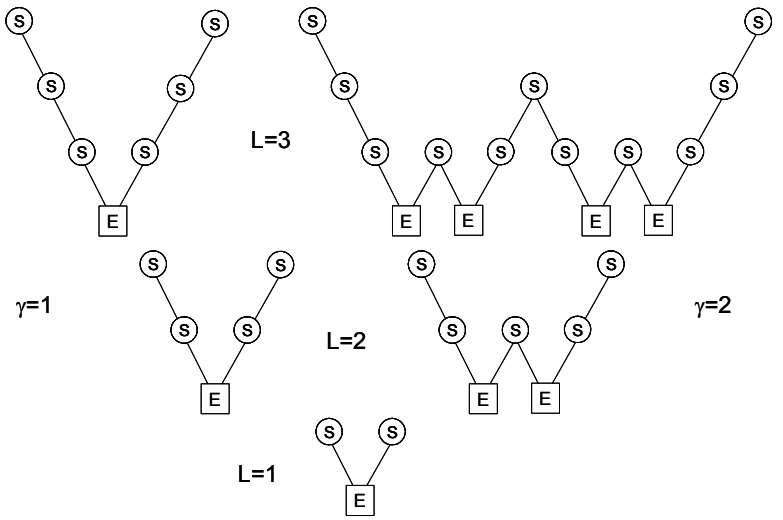

Figure 12. Structure of V and W multigrid cycles. S denotes smoothing while E denotes exact solution on the coarsest grid (the root cell). Leaf cells are at the top level of each diagram. Each descending line corresponds to restriction, and each ascending line to prolongation.

4.2 Simplified spherical harmonics approximation

4.2.1 Theory

Spherical harmonics P_N approximation has been already discussed in Section 3.1.2. Now, if only one-dimensional slab geometry is considered, the angular flux expansion can be made by Legendre polynomials

$$\Psi(x,\theta) = \sum_{l=0}^{\infty} \frac{2l+1}{2} \Phi_l(x) P_l(\cos\theta) \tag{4.10}$$

Inserting this into a 1D Boltzmann transport equation, whose directional derivative becomes now

$$\nabla \cdot \vec{\Omega}\Psi(\vec{r},\vec{\Omega}) = \cos\theta \frac{d}{dx}\Psi(x,\theta) \ ,$$

multiplying the resulting equation by Legendre polynomial and integrating over the angle, one can derive the corresponding P_N equations in 1D slab geometry. The recurrence relation

$$\cos\theta P_l(\cos\theta) = \frac{l+1}{2l+1} P_{l+1}(\cos\theta) + \frac{l}{2l+1} P_{l-1}(\cos\theta) \qquad (4.11)$$

and the orthogonality integral

$$\int_0^{\pi} P_l(\cos\theta) P_{l'}(\cos\theta) \sin\theta d\theta = \frac{2}{2l+1}\delta_{l,l'} \qquad (4.12)$$

are needed. The P_N equations in one-dimensional planar geometry simply become

$$\frac{l+1}{2l+1}\frac{d}{dx}\Phi_{l+1}^g(x) + \frac{l}{2l+1}\frac{d}{dx}\Phi_{l-1}^g(x) + \sigma_{al}^g \Phi_l(x) = q_l^g(x) \quad l = 0,...,N-1 \qquad (4.13)$$

where the group transport cross sections are defined by equation (3.30) as before. Also the source on the right-hand side of equation (4.13) has been expanded as a Legendre series.

Now, solving the odd moment terms and inserting them into even-order equations, the second-order equations can be derived in a similar manner as explained in Section 3.1.2 for the full P_N approximation. Furthermore, by replacing the 1D derivative in a formal manner with a 3D nabla operator ∇, as suggested by Gelbard [20–22], the simplified spherical harmonics 3D approximation is obtained (in a general form derived by the author):

$$
\begin{aligned}
&-\frac{l(l-1)}{(2l-1)(2l+1)\sigma^g_{a,l-1}}\nabla^2\Phi^g_{l-2}(\vec{r}) \\
&-\left[\frac{(l+1)^2}{(2l+1)(2l+3)\sigma^g_{a,l+1}}+\frac{l^2}{(2l-1)(2l+1)\sigma^g_{a,l-1}}\right]\nabla^2\Phi^g_{l}(\vec{r}) \\
&-\frac{(l+1)(l+2)}{(2l+1)(2l+3)\sigma^g_{a,l+1}}\nabla^2\Phi^g_{l+2}(\vec{r})+\sigma^g_{al}\Phi^g_{l}(\vec{r}) \\
&=q_l(\vec{r})-\frac{l}{(2l+1)\sigma^g_{a,l-1}}\nabla q_{l-1}(\vec{r})-\frac{(l+1)}{(2l+1)\sigma^g_{a,l+1}}\nabla q_{l+1}(\vec{r})
\end{aligned}
\qquad (4.14)
$$

for each $l = 0,2,...$ up to arbitrary (odd) Legendre order *N* with constraints that

$$\Phi_l(\vec{r}) = q_l(\vec{r}) \equiv 0 \text{ for } l < 0 \text{ or } l \geq N \ .$$

To the author's knowledge, such general second-order SP_N approximation for arbitrary (odd) Legendre order *N*, equation (4.14), has not been published elsewhere. From equation (4.14) one can derive also the SP_3 approximation, which has been used in the MultiTrans code as an approximation to Boltzmann's transport equation. SP_3 approximation is the lowest odd-order approximation after the diffusion theory. It is worth noticing that diffusion P_1 and SP_1 equations are congruent. In matrix form, the SP_3 equations are

$$
\begin{aligned}
&\begin{bmatrix} -D_0\nabla^2+\sigma_{a0} & -2\sigma_{a0} \\ -\frac{2}{5}\sigma_{a0} & -D_2\nabla^2+\sigma_{a2}+\frac{4}{5}\sigma_{a0} \end{bmatrix}^{i,g}\begin{bmatrix} \hat{\Phi}_0(\vec{r}) \\ \Phi_2(\vec{r}) \end{bmatrix}^{i,g} \\
&=\begin{bmatrix} 1 & -3D_0\nabla & 0 & 0 \\ -\frac{2}{5} & 0 & 1 & -\frac{7}{3}D_2\nabla \end{bmatrix}^{i,g}\begin{bmatrix} S_0(\vec{r}) \\ S_1(\vec{r}) \\ S_2(\vec{r}) \\ S_3(\vec{r}) \end{bmatrix}^{i,g} \ .
\end{aligned}
\qquad (4.15)
$$

The variable $\hat{\Phi}_0(\vec{r})$ is defined as

$$\hat{\Phi}_0(\vec{r}) \equiv \Phi_0(\vec{r}) + 2\Phi_2(\vec{r}) \ . \qquad (4.16)$$

The diffusion coefficients are defined by the transport cross sections as

$$D_0^{i,g} = \frac{1}{3\sigma_{a1}^{i,g}} \tag{4.17}$$

and

$$D_2^{i,g} = \frac{9}{35\sigma_{a3}^{i,g}} \quad . \tag{4.18}$$

The effective source moment terms are

$$\begin{bmatrix} S_0(\vec{r}) \\ S_1(\vec{r}) \\ S_2(\vec{r}) \\ S_3(\vec{r}) \end{bmatrix}^{i,g} = \begin{bmatrix} Q_0(\vec{r}) \\ Q_1(\vec{r}) \\ Q_2(\vec{r}) \\ Q_3(\vec{r}) \end{bmatrix}^{i,g} + \sum_{g'=1, g' \neq g}^{G} \begin{bmatrix} \sigma_{s0}^{g'->g} \Phi_0^{g'}(\vec{r}) \\ \sigma_{s1}^{g'->g} \Phi_1^{g'}(\vec{r}) \\ \sigma_{s2}^{g'->g} \Phi_2^{g'}(\vec{r}) \\ \sigma_{s3}^{g'->g} \Phi_3^{g'}(\vec{r}) \end{bmatrix}^{i,g} \tag{4.19}$$

where also anisotropic group-to-group scattering is taken into account through the sum terms. Actually, anisotropic source terms or anisotropic group-to-group scattering are usually not taken into account. Second-order SP_3 approximation including only scalar source terms and anisotropic in-group scattering would reduce to form

$$\begin{bmatrix} -D_0\nabla^2 + \sigma_{a0} & -2\sigma_{a0} \\ -\frac{2}{5}\sigma_{a0} & -D_2\nabla^2 + \sigma_{a2} + \frac{4}{5}\sigma_{a0} \end{bmatrix}^{i,g} \begin{bmatrix} \hat{\Phi}_0(\vec{r}) \\ \Phi_2(\vec{r}) \end{bmatrix}^{i,g} = S^{i,g}(\vec{r}) \begin{bmatrix} 1 \\ -\frac{2}{5} \end{bmatrix}. \tag{4.20}$$

The approximation (4.20) has been used in MultiTrans for most of the cases. However, in some cases it is useful to take the anisotropy of the source and the anisotropic group-to-group scattering into account. The first-order derivatives on the right-hand side of the equation (4.15) are in this form problematic for the numeric solution, as they distort the positive definite nature of the second-order SP_3 approximation. In Publication V, a solution to this problem has been suggested. By using the first-order equations (4.13) for the odd-moment terms (with ∇ operator),

$$\Phi_1^g(\vec{r}) = D_0^g(3S_1^g(\vec{r}) - \nabla\hat{\Phi}_0^g(\vec{r})) \tag{4.21}$$

and

$$\Phi_3^g(\vec{r}) = \frac{35D_2^g}{9}(S_3^g(\vec{r}) - \frac{3}{7}\nabla\Phi_2^g(\vec{r})) \ , \tag{4.22}$$

it is possible to transform the equation (4.15) into the form

$$\begin{bmatrix} -D_0\nabla^2 + \sigma_{a0} & -2\sigma_{a0} \\ -\frac{2}{5}\sigma_{a0} & -D_2\nabla^2 + \sigma_{a2} + \frac{4}{5}\sigma_{a0} \end{bmatrix}^{i,g} \begin{bmatrix} \hat{\Phi}_0(\vec{r}) \\ \Phi_2(\vec{r}) \end{bmatrix}^{i,g}$$
$$= \begin{bmatrix} 1 & 3D_0 & 0 & 0 \\ -\frac{2}{5} & 0 & 1 & D_2 \end{bmatrix}^{i,g} \begin{bmatrix} S_0(\vec{r}) \\ \hat{S}_1(\vec{r}) \\ S_2(\vec{r}) \\ \hat{S}_3(\vec{r}) \end{bmatrix}^{i,g} . \tag{4.23}$$

This matrix equation we have called in Publication V "the extended SP_3 approximation". The group source terms $\hat{S}_1^{i,g}(\vec{r})$ and $\hat{S}_3^{i,g}(\vec{r})$ containing group-to-group scattering are now

$$\hat{S}_1^{i,g}(\vec{r}) = -\nabla Q_1^{i,g}(\vec{r}) + \sum_{g'=1,g'\neq g}^{G} \sigma_{s1}^{i,g'->g} D_0^{i,g'} \left[\nabla^2\hat{\Phi}_0^{i,g}(\vec{r}) + 3\hat{S}_1^{i,g'}(\vec{r})\right] \tag{4.24}$$

and

$$\hat{S}_3^{i,g}(\vec{r}) = -\frac{7}{3}\nabla Q_3^{i,g}(\vec{r}) + \frac{35}{9}\sum_{g'=1,g'\neq g}^{G} \sigma_{s3}^{i,g'->g} D_2^{i,g'} \left[\nabla^2\Phi_2^{i,g}(\vec{r}) + \hat{S}_3^{i,g'}(\vec{r})\right] \tag{4.25}$$

where these odd-order source moment terms depend on the second-order derivatives of the even flux moment terms, and are much easier to solve numerically.

To further clarify equations (4.24) and (4.25), one can remark that these equations are not recursive: the $\hat{S}_1^{i,g}(\vec{r})$ and $\hat{S}_3^{i,g}(\vec{r})$ terms on the right-hand side of the equations are to take into account group-to-group scattering, i.e. with different energy group index *g* (inside sum terms) as on the left-hand side of the equations.

In addition to the ability to treat anisotropic group-to-group scattering, also anisotropies of any internal source terms can be treated by the variables $Q_1^{i,g}(\vec{r})$, $Q_2^{i,g}(\vec{r})$, and $Q_3^{i,g}(\vec{r})$: in this case, however, a first-order derivative is still encountered in source terms equations (4.24) and (4.25). Such anisotropic internal source terms emerge from first collision source algorithms, for instance. However, if an analytical solution exists for the uncollided flux in calculation of the first collision source, the derivatives can be calculated directly without problems. Also, if the uncollided flux is monotonically decreasing (which is true for an external beam source for instance), these source terms will always be positive.

Brantley and Larsen have derived material interface conditions and Marshak-like boundary conditions for second-order SP_3 approximation from the variational principle [25]. The material interface conditions for SP_3 approximation are:

$$\hat{\Phi}_0^{i,g}(\vec{r}) = \hat{\Phi}_0^{j,g}(\vec{r}) \ , \ \vec{r} \in \partial V_{ij} \ , \tag{4.26}$$

$$D_0^{i,g}(\vec{n}_i \cdot \nabla)\hat{\Phi}_0^{i,g}(\vec{r}) = D_0^{j,g}(\vec{n}_j \cdot \nabla)\hat{\Phi}_0^{j,g}(\vec{r}) \ , \ \vec{r} \in \partial V_{ij} \ , \tag{4.27}$$

$$\Phi_2^{i,g}(\vec{r}) = \Phi_2^{j,g}(\vec{r}) \ , \ \vec{r} \in \partial V_{ij} \tag{4.28}$$

and

$$D_2^{i,g}(\vec{n}_i \cdot \nabla)\Phi_2^{i,g}(\vec{r}) = D_2^{j,g}(\vec{n}_j \cdot \nabla)\Phi_2^{j,g}(\vec{r}) \ , \ \vec{r} \in \partial V_{ij} \ . \tag{4.29}$$

The Marshak-like boundary conditions suggested by Brantley and Larsen [25] are:

$$\frac{1}{2}\hat{\Phi}_0^{i,g}(\vec{r}) + D_0^{i,g}(\vec{n}_i \cdot \nabla)\hat{\Phi}_0^{i,g}(\vec{r})$$

and

$$= \frac{3}{8}\Phi_2^{i,g}(\vec{r}) + \int_0^{2\pi}\int_{-1}^{0} 2|\mu|\psi^b(\vec{r},\mu,\varphi)d\mu d\varphi \tag{4.30}$$

$$\frac{21}{40}\Phi_2^{i,g}(\vec{r}) + D_2^{i,g}(\vec{n}_i \cdot \nabla)\Phi_2^{i,g}(\vec{r})$$

$$= \frac{3}{40}\hat{\Phi}_0^{i,g}(\vec{r}) + \frac{3}{5}\int_0^{2\pi}\int_{-1}^{0} 2P_3(|\mu|)\psi^b(\vec{r},\mu,\varphi)d\mu d\varphi \tag{4.31}$$

where $\psi^b(\vec{r},\mu,\varphi)$ is the incident flux at boundary.

In the above, odd-SP_N approximations (SP_3, SP_5, etc.) have been examined. It is also possible to solve even moment terms and insert them into odd-order equations, obtaining even-SP_N approximations (SP_2, SP_4, etc.). The SP_2 approximation, for instance, consists of one diffusion-like equation instead of two, and would therefore have even lower computational cost compared to SP_3. The problem is that, in even-SP_N approximations, the flux will be discontinuous at material interfaces, which poses some extra problems for numerical solution. Brantley has suggested quite recently an approach where diffusion and SP_2 approximations are combined to solve these discontinuity problems [75, 76]. This mixed P_1–SP_2 synthetic method has given quite comparable results with SP_3 approximation for some cases. A similar approach using mixed P_1–DP_0 diffusion theory has also been suggested [77].

The original "derivation" of the SP_N equations by Gelbard by simply replacing the 1D derivative operator in slab equations with a 3D operator has been viewed with suspicion [23, 25]. That is, the theoretical basis of the SP_N approximation has historically been weak, though the numerical results obtained by the approximation have appeared promising. However, the theoretical basis of the SP_N approximation has evolved. An asymptotic derivation of the SP_N equations in the case of an inhomogeneous medium with multiple energy groups and anisotropic scattering was first provided by Larsen, Morel, and McGhee [23]. Pomraning has shown that SP_N equations with odd N are a variational approximation to the transport equation in an infinite homogeneous medium with one-group isotropic scattering [24]. Neither Pomraning's variational approximation nor the asymptotic derivation mentioned above produce outer boundary conditions. Only recently has it been shown by Brantley and Larsen that SP_3 equations with Marshak-like boundary conditions can be derived from variational principle for an inhomogeneous medium with multigroup anisotropic scattering [25]. These boundary and material interface conditions, equations (4.26)–(4.31), have been utilised for SP_3 equations in MultiTrans code, as explained earlier.

It should be noted that in a very similar manner compared to derivation of the second-order SP_N approximation, one can also derive simplified discrete ordinates SS_N approximation. Once again, one starts from the 1D slab equations, now written as a second-order S_N approximation, which are then generalised to 3D. Such Even-Parity SS_N approximation, for instance, has been studied by Longoni *et al.* [78–81].

There are certain limitations for the applicability of the SP_3 approximation. Both the particle absorption probability and the particle escape probability from the system should be <0.5, and the mean scattering cosine should not be too close to unity [23]. Also, when the system is heterogeneous, the transport solution should have only weak tangential derivatives at material interfaces [23]. For problems that have strong multidimensional transport effects, the SP_3 approximation is less accurate [23]. It is also well-known that with the spherical harmonics method in general, no exact vacuum boundary condition can be determined [15], and therefore the utilised Marshak-like boundary conditions are also approximative. For the above reasons, it has been necessary to test MultiTrans on various computational problems, in order to be able to see the applicability range of the SP_3 approximation in practice.

4.2.2 First collision source method

The first collision source method has been used in MultiTrans to process an external beam source into a distributed fixed source. The reason is that the collided flux emerging from a highly anisotropic (even monodirectional) beam source will become at least to some extent more isotropic when treated in this manner, and can be better approximated with a low-order spherical harmonics approximation. Similar first collision source methods have been applied earlier as a source processing option also in other codes [82, 83].

In the first collision source method, the uncollided flux (the flux of photons that have undergone zero collisions) is solved analytically. This uncollided flux is then used to generate the distributed fixed source terms for the collided flux. The collided flux can be solved by the SP_3 approximation with vacuum boundary conditions [25]. Total flux is then calculated as a sum of the collided and uncollided flux for each energy group.

The spherical harmonics P_N expansion of the uncollided flux in trigonometric form would be

$$\Psi^{(u)}(\vec{r},E,\vec{\Omega}) = \Psi^{(u)}(\vec{r},E,\theta,\varphi)$$
$$\approx \sum_{l=0}^{N}\sum_{m=0}^{l}(2l+1)P_l^m(\cos\theta)\left(\psi_{lm}^{(u)}(\vec{r},E)\cos m\varphi + \gamma_{lm}^{(u)}(\vec{r},E)\sin m\varphi\right) \tag{4.32}$$

where the expansion coefficients of the uncollided flux can be calculated (using orthogonality of the base functions) from integrals

$$\psi_{lm}^{(u),g} = \frac{1}{2\pi} \int_0^{2\pi} \int_0^{\pi} \frac{(l-m)!}{(l+m)!} P_l^m(\cos\theta) \cos m\varphi \, \Psi^{(u),g}(\vec{r},\theta,\varphi) \sin\theta \, d\theta \, d\varphi \tag{4.33}$$

and

$$\gamma_{lm}^{(u),g} = \frac{1}{2\pi} \int_0^{2\pi} \int_0^{\pi} \frac{(l-m)!}{(l+m)!} P_l^m(\cos\theta) \sin m\varphi \, \Psi^{(u),g}(\vec{r},\theta,\varphi) \sin\theta \, d\theta \, d\varphi \tag{4.34}$$

where $P_l^m(\cos\theta)$ are associated Legendre polynomials.

In the case of the simplified spherical harmonics SP_N approximation, the azimuthal dependency of the angular flux is suppressed:

$$\Psi^{(u)}(\vec{r},E,\vec{\Omega}) = \Psi^{(u)}(\vec{r},E,\theta) \approx \sum_{l=0}^{N} (2l+1) P_l(\cos\theta) \Phi_l^{(u)}(\vec{r},E) \ . \tag{4.35}$$

In this sense, the SP_N approximation is more restricted than full P_N approximation. Therefore, in the SP_N approximation, the moment terms of the uncollided flux can only be calculated when the uncollided flux has no azimuthal dependency:

$$\Phi_l^{(u),g}(\vec{r}) = \int_0^{\pi} P_l(\cos\theta) \Psi^{(u),g}(\vec{r},\theta) \sin\theta \, d\theta \ . \tag{4.36}$$

Here $P_l(\cos\theta)$ are the Legendre polynomials. It can be easily seen, that this equation also results in setting m=0 in equations (4.33) and (4.34).

The first collision source moment terms are

$$Q_l^{i,g}(\vec{r}) = \sigma_{sl}^{i,g} \Phi_l^{(u),i,g}(\vec{r}) \tag{4.37}$$

where $\sigma_{sl}^{i,g}$ is the Legendre expansion coefficient of the order l of the within-group scattering cross section and $\Phi_l^{(u),i,g}(\vec{r})$ is the corresponding moment term of the distributed uncollided flux.

For an isotropic point source the uncollided flux is

$$\Psi^{(u),g}(\vec{r},\vec{\Omega}) = \delta(\vec{\Omega}-\vec{\Omega}_r)q^g(\vec{r}_s)\frac{e^{-\beta(\vec{r},\vec{r}_s)}}{4\pi\left|\vec{r}-\vec{r}_s\right|^2} \tag{4.38}$$

where $q^g(\vec{r}_s)$ is the point source strength in energy group *g*, $\delta(\vec{\Omega}-\vec{\Omega}_r)$ is a delta function in angle, and $\beta(\vec{r},\vec{r}_s)$ is the number of mean-free-paths between the source point $\vec{r}_s$ and point $\vec{r}$.

As an azimuthal dependency exists, only the scalar term can be calculated from the integral equation (4.36). Thus, for an isotropic point source the first collision source is

$$Q_o^{i,g}(\vec{r}) = \sigma_{s0}^{i,g}q^g(\vec{r}_s)\frac{e^{-\beta(\vec{r},\vec{r}_s)}}{4\pi\left|\vec{r}-\vec{r}_s\right|^2} \tag{4.39}$$

and the higher moment terms cannot be taken into account. In other words, the SP_3 approximation cannot treat the anisotropy of the uncollided flux emerging from a point source, as the angular representation of the flux in the SP_3 approximation is in a sense one-dimensional. In a homogeneous case, a problem with an isotropic point source would naturally reduce to a one-dimensional problem in spherical geometry: the intention is, however, to develop deterministic transport methods for true three-dimensional heterogeneous problems, without limiting the applicability to some special cases.

Here we can remark that the underlying SP_3 equations are rotationally symmetric. For a point source one could rotate the base functions locally to eliminate the azimuthal terms, but this cannot be accomplished in the entire domain in a uniform manner.

For a monodirectional incident boundary surface flux, the uncollided flux is

$$\Psi^{(u),g}(\vec{r}) = \delta(\vec{\Omega}-\vec{\Omega}_s)q^g(\vec{r}_s)e^{-\beta(\vec{r},\vec{r}_s)} \tag{4.40}$$

where $q^g(\vec{r}_s)$ is the surface source strength in energy group *g*, and $\vec{\Omega}_s$ is the direction vector of the source surface.

Now the rotational symmetry of the SP_3 equations can be used to make the incident monodirectional beam oriented to the z-direction. Then the equation (4.40) becomes

$$\Psi^{(u),g}(\vec{r}) = \delta(\theta) q^g(\vec{r}_s) e^{-\beta(\vec{r},\vec{r}_s)} \tag{4.41}$$

and the first collision source moment terms can be calculated to be

$$Q_l^{i,g}(\vec{r}) = \sigma_{sl}^g q^g(\vec{r}_s) e^{-\beta(\vec{r},\vec{r}_s)} \quad (\vec{r} - \vec{r}_s) \parallel \vec{e}_z \ . \tag{4.42}$$

In a case of the extended SP_3 approximation, the first-order derivatives needed for equations (4.24) and (4.25) are simply

$$-\nabla Q_l^{i,g}(\vec{r}) = \overline{\sigma}_t^g \sigma_{sl}^{i,g} q^g(\vec{r}_s) e^{-\beta(\vec{r},\vec{r}_s)} \quad (\vec{r} - \vec{r}_s) \parallel \vec{e}_z \tag{4.43}$$

where $\overline{\sigma}_t^g$ is the average total cross section along the path between the source point $\vec{r}_s$ and point $\vec{r}$, parallel to z-axis.

Additionally, second-order derivatives of the uncollided flux are needed for the even moments of the source terms (in order to consider the total flux in group-to-group scattering, not only collided flux):

$$\nabla^2 \Phi_l^{(u),i,g}(\vec{r}) = \left(\overline{\sigma}_t^g\right)^2 q^g(\vec{r}_s) e^{-\beta(\vec{r},\vec{r}_s)} \quad (\vec{r} - \vec{r}_s) \parallel \vec{e}_z \ . \tag{4.44}$$

The first collision source produced by several point sources is easily calculated by superposition. In practice, the source is never exactly point-like, but will instead occupy a certain source volume. The first collision source method for point sources might therefore be more useful in computational exercises than in practice. As noted above, the SP_3 approximation cannot treat the anisotropy of the uncollided flux emerging from a point source, and the first collision source method for (more mathematical than real) point sources in conjunction with the SP_3 approximation is generally not so useful. Instead, small volumetric isotropic sources could be directly inserted as scalar source terms.

With the beam geometry (an accelerator source for instance) the first collision source method should be applicable also in practice. The methodology described above has been restricted to monodirectional beams, albeit arbitrary shaped. For

divergent beams, the azimuthal dependency cannot be defined by the first collision source method: however, the source moment terms can, in principle, be calculated in the direction of beam orientation. The calculation of the uncollided flux would require some additional ray tracing technique in this case.

4.3 Numerical transport algorithm

For a numerical solution, it is necessary to discretise SP_3 equations into the octree grid structure. The octree grid has been made regular, that is, the ratio of the sizes of any adjacent cells is restricted to be at most 2, which facilitates the discretisation of the equations. The tree structure still makes the grid non-uniform, and some proper difference scheme must be used. In the MultiTrans code, the so-called integrated difference scheme has been chosen.

Integrating the Laplacian of the function u over a cell C and applying Green's formula, one obtains

$$\int_C \nabla^2 u \, \mathrm{d}\Omega = \int_{\partial C} (\vec{n} \cdot \nabla) u \, \mathrm{d}\Gamma \tag{4.45}$$

where $\vec{n}$ is the normal vector of the cell surface. This is the basis of the integrated scheme. When the face neighbour cells are the same size, flux over the side of the cell is approximated by using central difference

$$(\vec{n} \cdot \nabla) u \approx \frac{1}{h}(u_N - u_C) \tag{4.46}$$

where h is the mesh size; u_C and u_N are the flux values in the cell and its neighbour, respectively. Otherwise, the parent of the smaller cell is used:

$$(\vec{n} \cdot \nabla) u \approx \begin{cases} \frac{1}{2h}(u_N - u_{P(C)}), \text{ neigbour } N \text{ is bigger than } C \\ \frac{1}{2h}(u_{P(N)} - u_C), \text{ neigbour } N \text{ is smaller than } C \end{cases} \tag{4.47}$$

where the value of the parent cells $u_{P(C)}$ and $u_{P(N)}$ is the average of their children's values. This averaging can also be seen as a special choice of the fine-to-coarse restriction operation of the multigrid technique.

The discretised standard SP_3 approximation solved by MultiTrans code in iterative diagonal form is

$$\begin{bmatrix} -D_0 h^2\left(\vec{n}\cdot\nabla\right)+h^3\sigma_{a0} & 0 \\ 0 & -D_2 h^2\left(\vec{n}\cdot\nabla\right)+h^3\sigma_{a2} \end{bmatrix}_h^{i,g} \begin{bmatrix} \hat{\Phi}_0 \\ \Phi_2 \end{bmatrix}_h^{i,g,l+1} = h^3\sigma_{a0}\begin{bmatrix} 2\Phi_2 \\ \frac{2}{5}\hat{\Phi}_0 - \frac{4}{5}\Phi_2 \end{bmatrix}_h^{i,g,l} + h^3 S_h^{i,g}\begin{bmatrix} 1 \\ -\frac{2}{5} \end{bmatrix} \tag{4.48}$$

where $\left(\vec{n}\cdot\nabla\right)$ denotes the central difference determined by equations (4.46) or (4.47), depending on the local octree grid structure. Similarly, the discretised extended SP_3 approximation is:

$$\begin{bmatrix} -D_0 h^2\left(\vec{n}\cdot\nabla\right)+h^3\sigma_{a0} & 0 \\ 0 & -D_2 h^2\left(\vec{n}\cdot\nabla\right)+h^3\sigma_{a2} \end{bmatrix}_h^{i,g} \begin{bmatrix} \hat{\Phi}_0 \\ \Phi_2 \end{bmatrix}_h^{i,g,l+1}$$

$$= h^3\sigma_{a0}\begin{bmatrix} 2\Phi_2 \\ \frac{2}{5}\hat{\Phi}_0 - \frac{4}{5}\Phi_2 \end{bmatrix}_h^{i,g,l} + h^3\begin{bmatrix} 1 & 3D_0 & 0 & 0 \\ -\frac{2}{5} & 0 & 1 & D_2 \end{bmatrix}^{i,g} \begin{bmatrix} S_0 \\ \hat{S}_1 \\ S_2 \\ \hat{S}_3 \end{bmatrix}_h^{i,g} \tag{4.49}$$

Now the multigrid acceleration technique from Section 4.1.2 can be utilised for these discretised matrix equations.

Starting from an initial flux guess (usually set to zero) one first calculates the residual at the leaf cell level from the right-hand side of equation (4.48) or (4.49). Then the residual is restricted into coarser grids by simple averaging. The error terms are smoothed by using the diagonal part of the matrix on the left-hand side of the equations. The error terms are then prolongated to finer grids. This is done in multigrid cycles: eight V-cycles have been used as a default in MultiTrans, but this value can be modified by the user. At the leaf cells, the flux terms are updated. The whole procedure is repeated until the total error at the leaf cells is small enough, that is, below pre-specified convergence criteria.

The multigroup transport problem is solved by solving a nested sequence of one-group problems, starting from the highest energy group. The down-scattering

from higher energy to lower energy groups is taken into account through an effective source term on each one-group problem, calculated with the use of corresponding group-to-group scattering cross sections. However, if up-scattering exists (at low thermal neutron energies this is the case), outer source iterations are required. In other words, the sweep through the multigroups has to be restarted from an energy level where up-scattering still has a contribution and repeated until the source converges. A similar need for outer source iterations is encountered also in the case of photon-electron calculation with full coupling, that is, when photons create electrons, but electrons also create photons (e.g. bremsstrahlung), and therefore "up-scattering" from electron groups to photon groups also exists.

The outer source iteration strategy is required also in the multiplication eigenvalue search. The multiplication eigenvalue for criticality problems is solved by the MultiTrans code with an algorithm similar to the standard source iteration method for multigroup diffusion equations [34]. First, some initial guess for the fission source and the multiplication eigenvalue are set. Next, the multigroup SP_3 equations are solved iteratively with the tree multigrid technique, by starting from the highest energy group and proceeding towards the lowest. Having done so, a new fission source

$$S_f^{(1)}(\vec{r}) = \sum_{g'=1}^{G} \nu^{g'} \sigma_f^{i,g'} \Phi_0^{g'(1)}(\vec{r})$$

and a new multiplication eigenvalue

$$k^{(1)} = \frac{\int S_f^{(1)}(\vec{r}) d^3 r}{\frac{1}{k^{(0)}} \int S_f^{(0)}(\vec{r}) d^3 r}$$

are calculated, and a new sweep for solving the multigroup SP_3 equations is started. The whole procedure is repeated until the multiplication eigenvalue and the fission source converge. The convergence criterion is defined as

$$\left| \frac{k^{(n)} - k^{(n-1)}}{k^{(n)}} \right| < \varepsilon_1 \quad \text{and / or} \quad \max \left| \frac{S_f^{(n)} - S_f^{(n-1)}}{S_f^{(n)}} \right| < \varepsilon_2 .$$

The solution strategy for multigroup problems including outer source iterations is shown on a general level in Figure 13.

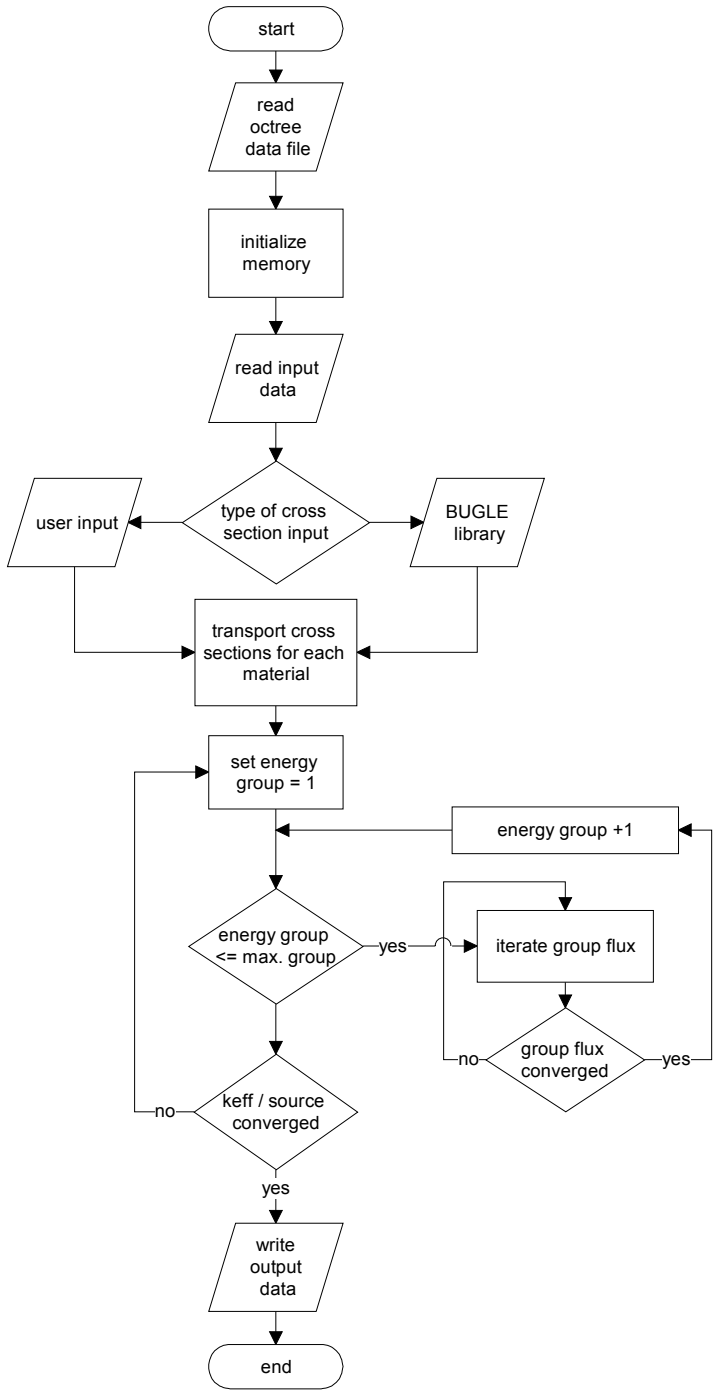

Figure 13. Flow chart of the iteration strategy in the MultiTrans code for solving multigroup and outer source iteration problems (on a general level).

5. Applicational scope of the new radiation transport code

The new MultiTrans radiation transport code – having no especial geometrical restrictions – could in principle be applied to any 3D radiation transport problem. However, the applicability range of the used SP_3 approximation limits the accuracy of MultiTrans, and therefore careful validation between different computational methods and verification against measurements are required for different applications. The validation and verification process has been the major objective of the research work reported in Publications II–V. The main results and some application specific issues are reviewed and discussed in the following sections.

5.1 Dose planning in BNCT

BNCT patients can be different in their size and shape and have tumours in different locations. Individual treatment planning is therefore required for accurate absorbed dose delivery. The primary aim of the treatment planning is to ensure a high enough tumour dose for meaningful and ethically acceptable treatment, with sufficiently low radiation risk to sensitive organs and tissues outside the planning target volume (PTV). The accuracy requirements of radiation therapy have already been briefly discussed in the Introduction, Section 1. It is worth repeating, that 5 % accuracy is recommended for absorbed dose delivery in radiotherapy [26]. An important limiting factor is the narrowness of the therapeutic window for the patient dose: often the adverse effects start to appear in the healthy tissue at lower absorbed doses before the complete tumour control (see Figure 2 in Section 1).

A treatment planning system (TPS) suitable for BNCT requires a verified beam model, methods for handling the patient geometry – e.g. software to create a voxelised geometry from computed tomography (CT) or magnetic resonance imaging (MRI) –, and some radiation transport algorithm to calculate the dose to various parts of the geometry [84]. The construction of an FiR 1 epithermal neutron beam model and dose calculations for verification of TPS used at the Finnish BNCT facility have been described in the academic dissertation of Tiina Seppälä [10].

In addition to treatment planning, computational methods are required for dosimetrical purposes, e.g. for planning different measurement setups and suitable irradiation times for detectors. Comparison of the dosimetrical results to the dose planning calculations can supply important knowledge on the accuracy of the computational method. This is vital for verification of the computational system used for treatment planning.

The whole MultiTrans code development started from the intention to replace the time-consuming Monte Carlo method in BNCT dose planning with a fast, deterministic and accurate radiation transport method. The tree multigrid technique was recognised as a promising tool for this purpose, as the self-adaptive meshing could be used to model the complicated structure of organs and tissues with great accuracy. As one of the first progresses, the self-adaptive meshing was tested for segmented CT images of a human head. The cross section of the resulting tree multigrid is shown in Figure 14.

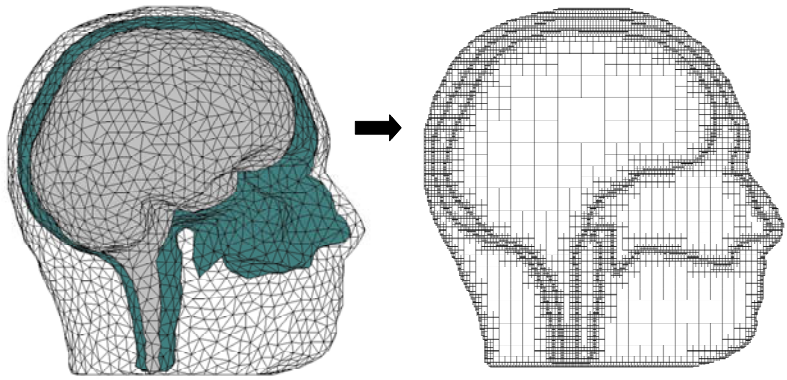

Figure 14. Segmented CT image (left) and a cross section of the corresponding tree multigrid (right).

As a radiation transport approximation, second-order P_3 equations, Eqs. (3.21)–(3.26), were first considered. However, the implementation of these equations into an iterative tree multigrid algorithm was found too complicated. Especially the discretisation of the mixed derivatives ($\partial_x \partial_y$ for example) in an effective way on a regular but non-uniform 3D tree multigrid was far from trivial. For this reason, it was decided to implement a simpler but less accurate SP_3 transport

approximation. However, the implementation of full P_3 approximation with an iterative tree multigrid solver should not be entirely excluded.

For BNCT dose planning purposes, it was necessary to be able to read the boundary source, i.e. the FiR 1 treatment planning source plane, into MultiTrans for dose-planning calculation. The treatment-planning source has been first derived by 2D calculations with the discrete ordinates code DORT [85], including the FiR 1 core model and subsequent transport calculation through the moderator and collimator structures of the FiR 1 epithermal beam [10]. The design of the Finnish BNCT facility is described elsewhere [4, 5, 10], but generally speaking, the fast fission neutron spectrum of the reactor core has been moderated into a more suitable energy range and collimated into a purpose-built treatment room. Special moderator material, Fluental™, has been developed at VTT in order to obtain a good epithermal neutron flux with high enough intensity and low, fast neutron and gamma contamination, even with a small research reactor such as FiR 1 TRIGA Mark II with 250 kW nominal power [4, 86].

Separate aperture plates of the FiR 1 BNCT collimator structure, made from lithiated polyethylene, can be easily added or removed, giving beam diameter options of 8, 11, 14, 17 and 20 cm. The 14 cm aperture has most often been used in patient treatments. The treatment-planning source for a 14 cm diameter beam aperture is situated 5 cm inwards of the beam direction into the collimator structures. It has been first calculated by DORT and then further processed for use in TPS by averaging the forward current over a 22 cm diameter circular area for each BUGLE energy group (47 neutron groups and 20 gamma groups) of DORT calculation [10]. Separate angular distributions by 10 cosine cut points in the forward direction have been defined for each energy group.

The treatment planning source for a 14 cm aperture has been used in MultiTrans. However, for some reason, using the source plane directly in the boundary condition seemed to thwart the convergence with the tree multigrid technique. This was perhaps just due to some mistake in the implementation of source values on different grid levels. Yet, instead of defining the source as a boundary condition, it was decided to use the first collision source method. The first collision source method has already been discussed in Section 4.2.2. The advantage of the first collision source in conjunction with the SP_3 approximation

is that the collided flux is more isotropic than the uncollided one, and therefore can be better approximated with a low-order spherical harmonics approximation.

As a suitable benchmark for validation and verification of the MultiTrans code, a cylindrical polymethyl-methacrylate (PMMA) phantom situated in the FiR 1 epithermal neutron beam with a 14 cm aperture was chosen. The solid PMMA phantom has a 20 cm diameter and 24 cm length, and PMMA is one of the tissue substitutes used in radiation dosimetry [87]. The phantom has removable centre pieces with 2 cm diameter and various shapes, e.g. to attach ionisation chambers, thermoluminescent detectors (TLD's) or small diluted manganese-aluminium (Mn-Al) or gold-aluminium (Au-Al) foils at different depths at the central axis of the phantom.

To be more specific, the above-mentioned Mn-Al and Au-Al foils are used for neutron activation measurements: ^{55}Mn and ^{197}Au have a large probability to capture neutrons and as a consequence to become activated. The activation products emit gamma radiation with distinctive energies. These photo-peaks can be measured after the irradiation with a gamma spectrometer, and taking the decay and the geometry of the measurement setup into account, the specific saturation activity of the foils can be defined [88]. The reason why Mn and Au ingredients have been diluted in Al is to avoid self-shielding in the neutron field due to strong neutron absorption, i.e. capture reaction.

The neutron activation measurements are a very accurate method to measure the neutron field, and insensitive to other radiation qualities, which is usually not the case with other measurement techniques. If the energy cross sections for neutron capture reactions are known, it is possible to calculate the corresponding responses from neutron energy spectra. Thus, it is possible to directly compare the measured and calculated activation reaction rates. It is also possible to adjust a calculated spectra based on measurements over a large set of different reactions with different response energies: such a procedure has been applied for the TPS source of the FiR 1 epithermal neutron beam, to further improve the source model [10, 89–92].

An extensive number of measurements have been performed in the FiR 1 beam with different phantom geometries and phantom materials, and multiplicity of measurement techniques [89–102]. The cylindrical PMMA phantom has been

perhaps most widely used. For instance, in each week having patient irradiation, diluted Mn-Al (1 wt-% Mn) and Au-Al (1 wt-% Au) foils are irradiated in the PMMA phantom at 2 cm depth, in order to check the neutron activation for quality assurance of the beam monitors used to control irradiation [103].

In Publication II, MultiTrans calculations have been compared to measured and calculated $^{197}Au(n,\gamma)$ and $^{55}Mn(n,\gamma)$ reaction rates at the central axis of the PMMA cylinder. The computational comparison included the discrete ordinates (S_N) code DORT and the Monte Carlo codes MCNP and SERA, the SERA calculations being made by Tiina Seppälä. Also different physical dose components, such as fast neutron hydrogen proton recoil dose, proton dose from nitrogen neutron capture reaction $^{14}N(n,p)$, and the gamma dose (mainly from hydrogen neutron capture), were compared to the values calculated by DORT. The same BUGLE-80 cross section library with 47 neutron and 20 gamma energy groups was used with both MultiTrans and DORT.

It was noted for instance, that $^{197}Au(n,\gamma)$ and $^{55}Mn(n,\gamma)$ reaction rates at 2 cm depth in the phantom (at thermal maximum) calculated by MultiTrans differed -3 % and +1 % from the measured values, respectively, and were within the measurement uncertainty, approximated to be 5 %. The total neutron dose at 2 cm depth in the phantom calculated by MultiTrans differed -4 % compared to the DORT result. The major disadvantage in the MultiTrans calculations was the inability to calculate the neutron-induced gamma dose accurately enough. A notable discrepancy was found in the gamma dose calculated by MultiTrans, being -16 % at 2.5 cm depth (at gamma dose maximum) compared to the DORT result. The shape of the depth curve of the gamma dose calculated by MultiTrans was also different from that calculated by DORT. The reason for this discrepancy was probably the long mean free paths of energetic 2.2 MeV photons induced from the hydrogen neutron capture reaction: the transport problem for energetic photons might not be optically thick enough for SP_3 approximation to be valid.

The MultiTrans calculations took 14 minutes on a desktop PC with a 200 MHz Pentium processor. The minimum octree cell side length was 0.38 cm. The MCNP and SERA simulations were run on a Sun Ultra60 SPARC station. The MCNP simulation was run for five days resulting in over 150 million particle histories. The SERA calculations took one hour with 10 million particle histories

and 1 cm^3 voxel size. It should be noted, however, that in order to produce the same statistical uncertainty with SERA having a 0.38 cm voxel side length (0.055 cm^3 volume) instead of 1 cm (1 cm^3 volume), approximately 18 times longer running time and amount of particle histories would have been required. With the same resolution, MultiTrans would therefore be about 2 magnitudes faster. However, this value is only speculative.

5.2 Radiation transport of photons and electrons in conventional radiotherapy

Despite the difficulties encountered in calculation of the gamma dose in BNCT by MultiTrans, it was decided to study further the applicability range of SP_3 approximation in photon transport problems of conventional radiotherapy. In addition, also transport of electrons as secondary charged particles was considered. This work was done in collaboration with Varian Medical Systems Finland Oy, and the main results have been reported in Publication V.

The idea was that, even though the photon transport seemed not to work so well for high-energy photons such as 2.2 MeV gammas from hydrogen neutron capture in BNCT, the SP_3 approximation might still work for low-energy photon sources, used for instance in brachytherapy. The specific goal was to find out the applicability range of the SP_3 approximation in coupled photon-electron transport problems.

Brachytherapy, also known as sealed source radiotherapy or endocurietherapy, is a form of radiotherapy where a radioactive source is placed inside or next to the area requiring treatment [104]. Encapsulated ^{125}I, ^{137}Cs, and ^{192}Ir are currently the most widely used sources in brachytherapy and are used to treat localised malignancies in nearly every body site. However, the influence of tissue and applicator heterogeneities on brachytherapy dose distributions is not well understood, despite widespread use of shielded applicators in intracavitary therapy [30, 31, 105–107].

Electrons induced in photon interactions are the secondary particles which finally deposit the energy into tissue and after all cause the physical dose. It is possible to estimate the dose from photon fluence by using mass-energy

absorption coefficients [29]. However, for this estimation to be valid, a sufficient local secondary charged particle equilibrium (c.p.e.) condition is required. By calculating the electron transport in detail, and then converting the electron fluence into deposited energy, the absorbed dose can be calculated more accurately, without the requirement of the c.p.e. condition. This is an important issue with strong material heterogeneities.

Electron transport is in general described by the Boltzmann-Fokker-Planck equation, but using the continuous-slowing-down approximation (CSDA) and defining electron "pseudo" cross sections, the Boltzmann equation for neutral particles can be applied for electrons as well [32]. Thus, it was realised, that by suitable modification of the cross sections, it was possible to solve also electron transport by MultiTrans without any code changes, except for the library routines for handling the coupled photon-electron cross sections. The modification of the electron cross sections into "pseudo" cross sections was done with the CEPXS code [108].

Calculations were performed for different coupled photon-electron transport problems, which are described in detail in Publication V. These test problems included monoenergetic photon point sources from 10 keV to 2 MeV in water [109] representing a simplified brachytherapy source in homogeneous media, and different dose-planning problems for monoenergetic monodirectional beam sources, including also some heterogeneous test problems. Comparison calculations were performed by Varian using the EGS4 Monte Carlo code system [58, 110]. Both standard and what we have called "extended SP_3 approximation" (Section 4.2.1 and Publication V) were used in the MultiTrans calculations, the latter one taking also anisotropic group-to-group scattering into account. For example, in the case with monoenergetic photon point source, the dose calculated by MultiTrans agreed within 6 % compared to the EGS4 results with 25, 35, 70 and 125 keV energies. However, with higher energies the results were in larger disagreement, with maximal +18 % difference between MultiTrans and EGS4 for 1.75 MeV source photons, at about 10 cm distance from the point source. As another example, with a monodirectional 125 mm × 125 mm beam source of 7 MeV photons exposed to a large water cylinder, the dose at 2, 5 and 10 cm depths along the beam centreline calculated by MultiTrans differed -6 %, -6 % and -9 % with extended SP_3 approximation, and +7 %, 0 % and -4 % with standard SP_3 approximation, respectively, compared to

EGS4 results. Even though the extended SP_3 approximation disagreed more than the standard approximation from the absolute value of the EGS4 solution, the conclusion of the study was that the extended SP_3 approximation seemed to be advantageous when compared to the standard formulation, as it better duplicated the shape of the depth-dose curve, the position of the dose build-up maximum and the profile shape of the off-axis ratios (Publication V). However, with high photon energies both approximations failed to produce accurate results. Therefore we further concluded that the method was not directly applicable for treatment planning in conventional radiotherapy, where the uncertainty of the dose to the patient should not exceed 5 % [26].

In the future, the accurate Monte Carlo method will probably be more and more applied in clinical radiotherapy treatment planning. At the moment, computer capacity limits the wider use of the Monte Carlo method, and semi-empirical methods (utilising measured dose distributions in water) are still often used for clinical dose planning. It is worth noting, that clinical treatment-planning software using the Monte Carlo method do exist [111, 112]. Fast deterministic transport methods such as MultiTrans would be advantageous compared to the semi-empirical approach, especially in the case of strong tissue heterogeneities that cannot be correctly taken into account with the traditional methods. However, the accuracy of the SP_3 approximation used in MultiTrans seems not to be good enough for treatment-planning purposes. This is especially the case with the accuracy of the photon transport. For electron transport, the SP_3 approximation might work much better, as for electrons one can expect the system to be optically thicker. In Publication V we have suggested a hybrid scheme where photon transport would be solved by Monte Carlo and subsequent secondary particle (electron) transport by MultiTrans. This would use the best sides of both methods, as the Monte Carlo method is capable for accurate photon transport but handles electron transport very slowly due to Coulomb interactions; this electron transport might be solved by MultiTrans in an accurate and efficient way. Accuracy of the transport of secondary electrons with SP_3 approximation in 3D, however, remains to be seen.

5.3 Reactor physics

Radiation transport codes have been traditionally developed and applied in the field of reactor physics. Typical radiation transport problems are, for instance, criticality safety analysis, radiation protection calculations, determination of various detector responses, and out-of-core neutron dose calculations.

Fission source and neutron transport calculations of the reactor core are often handled by simplistic 1D or 3D nodal methods: the core is divided into homogenised segments and only few-group (for instance 2-group) nodal calculations are performed. Such simplistic but efficient methods for neutron transport and fission source modelling are especially needed in transient and accident analysis, where fission source and related power density and heat generation is coupled with thermal hydraulics in order to model the overall dynamic behaviour of the reactor core under different operating conditions.

In more detailed calculations, such as 3D modelling of (unhomogenised) fuel bundles or modelling of the axial and radial leakage terms of the core, more sophisticated radiation transport methods are required. Especially 3D out-of-core calculations with streaming and deep penetration of the radiation are very demanding. Such calculations are needed, for instance, to estimate the pressure vessel steel embrittlement or in activity inventory calculations of a nuclear power plant for decommissioning planning. It should also be noted that reactor physics problems are not restricted to the reactor core, but often the problem is to determine the criticality safety, radiation protection or heat generation in transportation casks or fuel storage pools, etc. Such problems often require detailed modelling of the criticality eigenvalue or source terms, sometimes coupled with burn-up and depletion calculations in order to estimate the isotopic concentration.

In the reactor physics field, the MultiTrans code was first applied to a simplistic two-group pressurised water reactor (PWR) benchmark with a fixed source, reported in Publication I. Since the demonstration of the applicability of the MultiTrans code to various dose-planning problems in BNCT and conventional radiotherapy, MultiTrans has increasingly been tested also in traditional reactor physics problems. Implementation of an outer source iteration method for

multiplication eigenvalue problems, for instance, has been described in Publication III, and discussed in Section 4.3.

For testing the multiplication eigenvalue search algorithm, two problems were chosen from the proposal of 3D neutron transport benchmarks by the Osaka University to OECD Nuclear Energy Agency (NEA) Committee on Reactor Physics [113, 114]. The first one is a small light-water reactor (LWR) with a core model of Kyoto University Critical Assembly (KUCA), and the second one is a small fast breeder reactor (FBR). The LWR and FBR geometries and the cross sections of the corresponding octree grids are shown in Figures 15 and 16, respectively.

The LWR benchmark was a 2-group problem, and the FBR benchmark a 4-group problem. In both benchmarks, the objective was to calculate the control-rod-worth. In the LWR benchmark the control rod was either inserted or withdrawn, the control rod position being empty void in the latter case. In the FBR benchmark the control rod was inserted or half inserted, the empty position being replaced by sodium coolant. The control-rod-worth was defined to be the value

$$\left.\frac{1}{k_{eff}}\right|_{\text{rod in}} - \left.\frac{1}{k_{eff}}\right|_{\text{rod out}}.$$

For the FBR benchmark, the calculated multiplication eigenvalues and the corresponding control-rod-worth agreed well with Monte Carlo results reported by Takeda and Ikeda [114]. For the case with the control rod half inserted, the difference in MultiTrans results for k_{eff} was +0.37 %, and for the case with control rod inserted +0.32 %, compared to the Monte Carlo results, respectively. For calculated control-rod-worth, the difference between the MultiTrans and Monte Carlo results was +3.4 %. Also for the LWR benchmark, the k_{eff} agreed in the case when the control rod was inserted, with +0.24 % difference between the MultiTrans and Monte Carlo results. However, in the LWR rod-out case with void region, the MultiTrans value for k_{eff} was inaccurate with -2.6 % difference compared to the Monte Carlo result, which also led to negative control-rod-worth. This inaccurate result for the rod-out case was concluded to happen due to long neutron streaming paths in the void region, which is problematic for the SP_3 approximation.

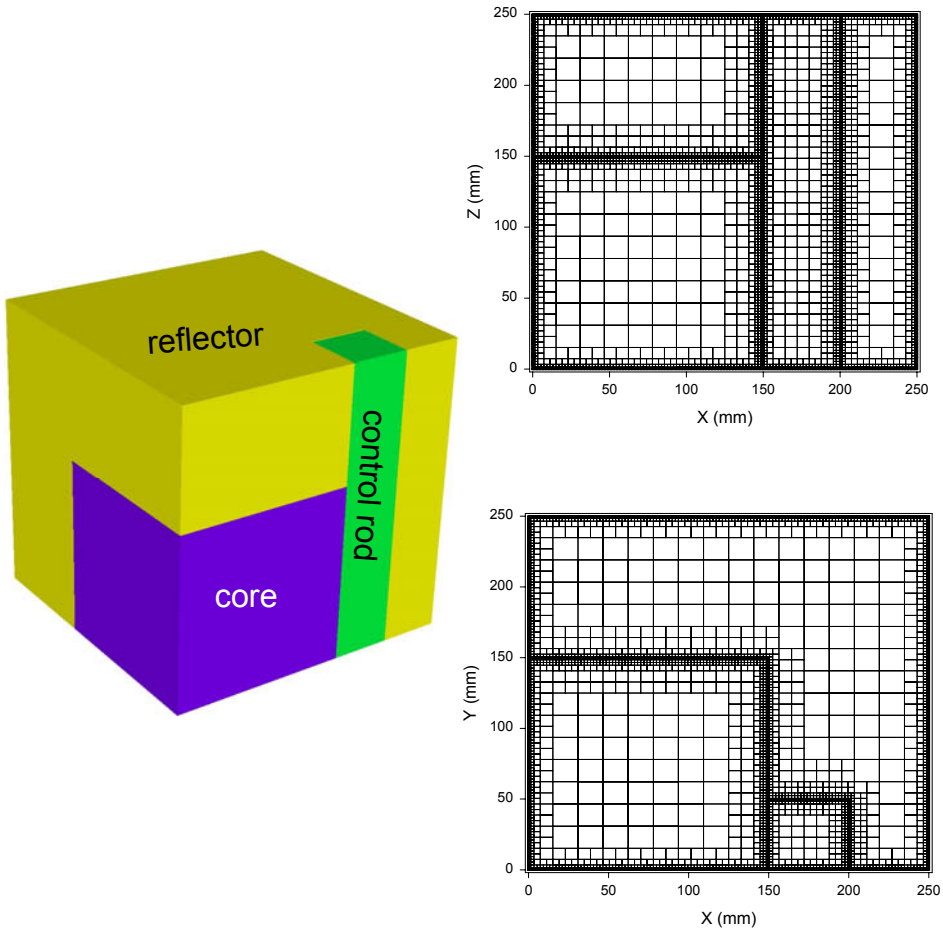

Figure 15. CAD model of the KUCA LWR core benchmark (left) and cross sections of the corresponding octree grid (right).

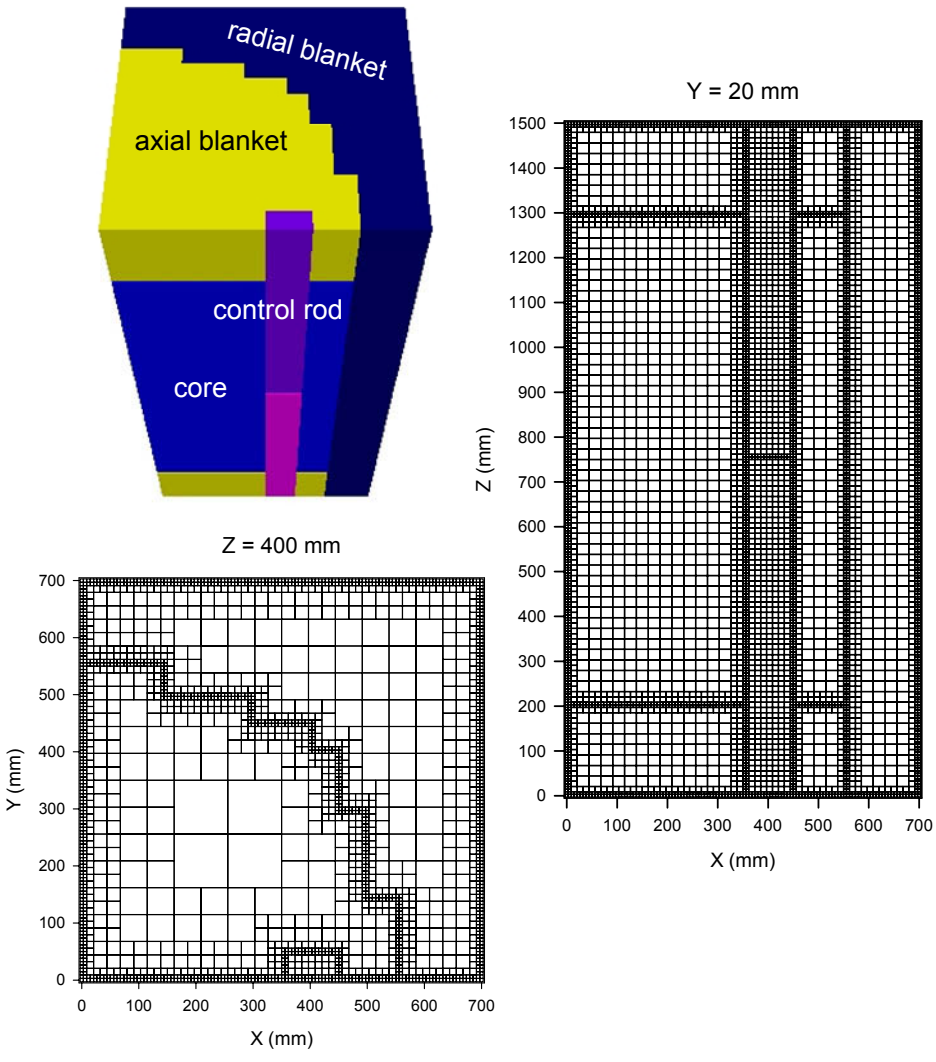

Figure 16. CAD model of the FBR core benchmark (top left) and cross sections of the corresponding octree grid.

The calculated LWR and FBR benchmarks demonstrated the applicability of the new MultiTrans code to criticality problems for the first time. However, in order to test more thoroughly the applicability of the MultiTrans code in reactor dosimetry problems, two VENUS benchmarks were calculated.

The VENUS Critical Facility is a zero power reactor located in Mol, Belgium, used to study LWR core designs. Measured data exists for verification of the

computational results, and benchmarks have been calculated with several different codes, offering a good resource for experimental and computational data to test a new transport code.

Many commercial power plants in Europe and Japan use reprocessed mixed oxide (MOX) uranium and plutonium fuel (UO_2-PuO_2) in addition to the uranium oxide (UO_2) fuel. The use of MOX fuel in LWRs presents different neutron characteristics, and therefore the VENUS-2 MOX-fuelled reactor dosimetry benchmark [115] was launched by OECD NEA in 2004 to test the current state-of-the-art computation methods of calculating neutron flux to reactor components against the measured data of the VENUS-2 MOX-fuelled critical experiments.

Twelve groups worldwide participated in the VENUS-2 blind benchmark providing 15 different solutions [116]. VTT attended with 3 different codes: MultiTrans, TORT and MCNP [116, 117]. The task was to calculate ^{58}Ni(n,p), ^{115}In(n,n'), ^{103}Rh(n,n'), ^{64}Zn(n,p), ^{237}Np(n,f), and ^{27}Al(n,α) reaction rates and the corresponding equivalent fission fluxes measured on the core mid-plane at specific positions outside the core of the VENUS-2 MOX-fuelled reactor. The benchmark geometry is shown in Figure 17. In the MultiTrans calculations, all material regions were modelled in detail, except that the fuel pin, fuel cladding, and water regions were homogenised over each fuel zone. The external regions outside the jacket inner wall (air, jacket outer wall, reactor vessel, water, and reactor room) were omitted from the model, as they can be assumed to have no significant effect on the responses at the measurement points.

The BUGLE-96 cross section library with 47 neutron groups was used in the transport calculations by MultiTrans. ^{235}U and ^{239}Pu fission spectra were taken also from the BUGLE-96 library, weighted by the relative portions of the main fissile isotopes in the VENUS-2 core. The International Reactor Dosimetry File (IRDF) was used in calculation of the dosimetry responses. IRDF-90 version 2 dosimetry cross sections for reactions ^{58}Ni(n,p), ^{115}In(n,n'), ^{103}Rh(n,n'), ^{64}Zn(n,p), ^{237}Np(n,f), and ^{27}Al(n,α) were condensed into the BUGLE energy group structure from the SAND-II energy group structure (640 groups) by using X333 utility program from the neutron metrology file NMF-90 [118]. The combined Maxwell, 1/E, and fission weighting spectrum was used. The MultiTrans criticality calculation with 2,530,817 mesh cells took 16.0 hours on a

desktop PC with a 3.0 GHz Pentium4 processor [117]. TORT criticality calculation with 648,270 mesh cells took 18.7 hours on an AlphaServer ES45 workstation with four EV6.8CB 1.0 GHz processors [117].

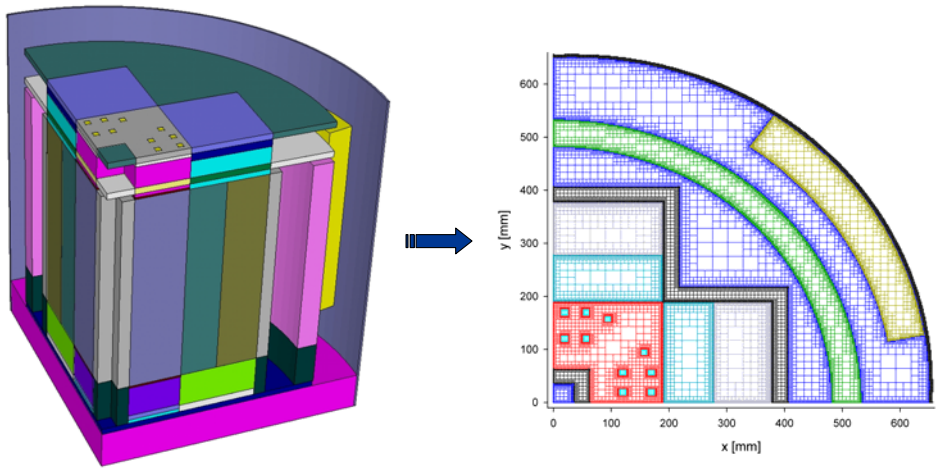

Figure 17. CAD model of the VENUS-2 MOX-fuelled reactor dosimetry benchmark (left) and a cross section of the corresponding octree grid at core mid-plane (right).

The results obtained by MultiTrans were fairly comparable to other reported results of the VENUS-2 benchmark [116]. For instance, equivalent fission fluxes calculated in 32 ^{58}Ni(n,p) detector positions by MultiTrans were all within ±20 %, and most of them within ±10 %, compared to measured values. The equivalent fission flux values calculated by MultiTrans for the ^{115}In(n,n') detector positions, on the other hand, showed about ±20 % of scatter band in stainless steel zones and about ±30 % in water zones [116]. Especially, discrepancies were noted in the MultiTrans results in the detector positions where the solution starts to behave more transport-like and the applicability of the SP_3 approximation becomes more limited.

In Publication IV, application of the MultiTrans code to VENUS-3 benchmark has been reported. The core loading in VENUS-3 is completely different from the VENUS-2 benchmark described above. VENUS-3 is a LWR pressure vessel steel benchmark with partial length shielded assemblies [119], and the results of the computational benchmark have been published by NEA [120]. The well-

documented experimental and computational data has been a good resource to test the performance of the MultiTrans code.

The VENUS-3 benchmark geometry is shown in Figure 18. Again, the material regions were modelled in detail, except that the fuel pin, fuel cladding, and water regions were homogenised over each fuel zone and external regions outside the jacket inner wall were left out of the model, as their effect is negligible.

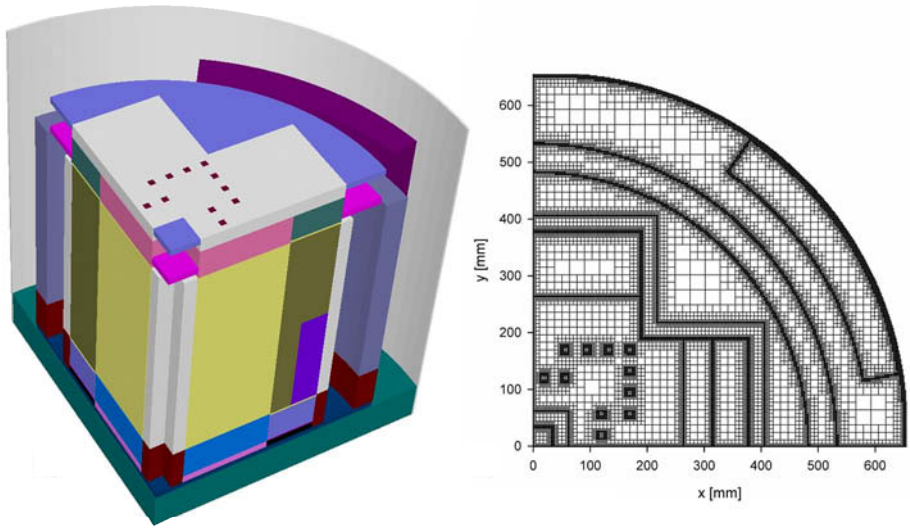

Figure 18. CAD model of the VENUS-3 LWR pressure vessel steel benchmark with partial length shielded assemblies (left) and a cross section of the corresponding octree grid at 10 cm below the core mid-plane (right).

The partial length shielded assemblies make the VENUS-3 benchmark especially a 3D radiation transport exercise. The task was to calculate ^{58}Ni(n,p), ^{115}In(n,n'), and ^{27}Al(n,α) reaction rates in specific in-core and out-of-core detector positions distributed also axially: a total of 244 detector positions were defined for nickel, 104 detector positions for indium, and 38 positions for aluminium. The reaction rates calculated by MultiTrans agreed well with the experimental values: the majority of the values were within 5 % for Ni and Al, and within 7 % for In. The deviation was larger than 20 % only in 2 detector positions of Ni in the uppermost region of the partial length shielded assemblies, and in one detector position of In and Al in the core barrel near the corner of the partial length shielded assemblies. In these positions, the solution behaves

probably more transport-like and the SP_3 approximation is, once again, less valid. In this VENUS-3 benchmark, the results obtained by MultiTrans are very comparable to the reported results obtained by other computational methods [120]. The MultiTrans calculations for 47 BUGLE neutron groups took 70 minutes on a desktop PC with a 3.0 GHz Pentium4 processor.

For the VENUS-3 benchmark, a fixed source from venus3.src file from NEA-1517/69 SINBAD-VENUS-3 distribution CD was used. This required implementation of a new source routine that could read the source file and distribute the source into the octree cell structure with correct weighting. That is, the average source in each octree cell is calculated from an arbitrary source distribution given in an external file, with no need that this source distribution data should match the boundaries of the octree cells. The use of this source routine is not restricted to the VENUS core, but can be used to describe the power distribution of any reactor in a very general format.

In addition to the distributed source routine, a special interpolation algorithm was developed and implemented into MultiTrans for both VENUS benchmarks. In order to be able to define the reaction rate in the precise detector position, the cell averaged values had to be interpolated correctly. Interpolation would be rather straightforward in an equidistant mesh, but in a non-uniform octree mesh the interpolation becomes more complicated. A kind of 2-step linear interpolation method was implemented, where one first interpolates the vertex values of the cubic voxel containing the specific point, and then uses these vertex values for the final linear interpolation inside the cell.

An attempt to use MultiTrans code in the calculation of the C5G7 MOX benchmark extension has also been made [121, 122]. However, in this particular benchmark, no results could be obtained due to memory limitations. In the C5G7 benchmark geometry the fuel assemblies are non-homogenised, that is, each fuel rod is included in the model, see Figure 19. With cubic elements the required number of octree cells becomes extremely high if one tries to distinguish the heterogeneous fuel and moderator material regions, resulting in an inevitable computer memory overflow.

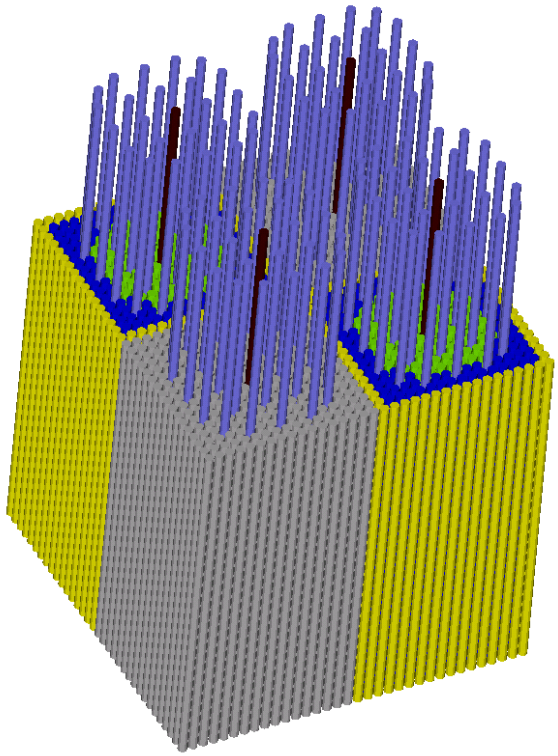

Figure 19. CAD model of the NEA C5G7 MOX benchmark extension, excluding the moderator region. In the picture the different fuel pins of the core are shown, as well as the control rods and the fission chambers extending above the core into the upper axial reflector.

The cubic cells are problematic in the C5G7 benchmark, as the axial meshing becomes oversized for heterogeneous fuel bundles. It might be possible, with some modifications to use a different axial length for the octree cells. The octree cells could perhaps be made rectangular in the axial dimension. In this way, the required number of octree cells for modelling a non-homogenised fuel bundle could be greatly reduced and the application of the MultiTrans code to such problems might become feasible. This would require further studying, however.

In general, the applicability of the MultiTrans code to reactor physics problems has been demonstrated. The VENUS-2 and VENUS-3 benchmarks show that the calculated results by MultiTrans are fairly comparable to the results obtained by

other methods. Void regions are problematic for the SP_3 approximation, though, as shown by the KUCA LWR rod-out case. At the moment, the ability of MultiTrans to model heterogeneous fuel assemblies is also restricted due to large memory requirement encountered in such cases: application of a deterministic code to such heterogeneous 3D problems would represent the real state-of-the-art.

6. Summary and conclusions

Neutral and charged particle transport theory in conjunction with the tree multigrid technique has been studied. A new deterministic radiation transport method, based on the tree multigrid technique and simplified spherical harmonics SP_3 approximation, has been developed and applied to 3D neutron transport modelling (Publication I) and to BNCT neutron and photon dose planning (Publication II). The applicability of the novel MultiTrans radiation transport code has been further extended to multiplicative systems (Publication III) and to coupled photon-electron transport problems (Publication V). In order to validate and verify the code performance, MultiTrans has been tested for a wide variety of different types of neutral and charged particle transport problems encountered both in radiotherapy and in reactor physics (Publications I–V).

The results obtained with the new MultiTrans code are somewhat twofold: in some cases the results are pretty good and promising, but in some other cases obviously inaccurate. For instance, in BNCT dose-planning problems, the neutron dose and related dosimetric responses seem to be modelled rather accurately, but the calculated photon dose is in disagreement with other computational methods and measurements. The problems have been related to the used SP_3 approximation of the transport equation. Especially geometrical areas with low density – or low optical thickness for the radiation quality, to be more specific – have been problematic for the simplified spherical harmonics approximation. For air inhomogeneities, some ray-tracing technique might overcome this problem [42].

Sometimes combining different methods can lead to the best results [123]. For example, deterministic radiation transport methods (even quite approximative) can be used to solve the adjoint flux and thereby determine the optimal importance distribution for Monte Carlo variance reduction [124, 125]. Then the accurate Monte Carlo method can be used in an effective manner to solve the actual forward problem. Another combination of different methods is to use an approximative solution (such as diffusion solution) as a preconditioner for some more accurate deterministic method. In other words, the problem is first solved with one method, and the solution is then used as an initial guess to accelerate the iterative solution by the more accurate method. Recently, Even-Parity SS_N

approximation (very similar to SP_N) has been used as such a preconditioner for S_N method with great success [78–81]. The multigrid acceleration can also be seen as sort of preconditioner.

In Publication V we have suggested a combination of Monte Carlo method and deterministic solution of SP_3 approximation with the tree multigrid technique. The idea would be to solve the photon flux by the accurate Monte Carlo method, and then do the subsequent electron transport calculation by MultiTrans. The electron transport calculations are handled very slowly by the Monte Carlo technique, while MultiTrans might produce the solution both fast and accurately. The combined performance of the methods might prove to be both fast and accurate, and could be useful in radiotherapy dose planning, especially in the cases with strong material heterogeneities.

As a conclusion, it seems that SP_3 approximation is best suited for radiation transport problems which are diffusion-like and have low void fraction, such as homogenised PWR core calculations. In that kind of transport or criticality problems the SP_3 approximation should produce much better results than simple diffusion theory. For out-of-core calculations SP_3 approximation is less suited, especially if there is streaming or deep penetration of radiation, that is, if the solution behaves very transport-like. For such cases, more accurate methods exist and should be applied. In radiotherapy applications some hybrid methods would be required to meet the required accuracy. Such methods might be worth further study.

The tree multigrid technique has proved to be efficient. The CAD interface makes MultiTrans a flexible design tool. The CT interface enables radiotherapy applications. The usefulness of the new MultiTrans code has been indicated by verifying and validating the code performance for different types of neutral and charged particle transport problems, reported in separate publications (Publications I–V).

Bibliography

[1] Kankaanranta, L., *et al.*, "First clinical results on the Finnish study on BPA-mediated BNCT in glioblastoma", in *9th International Symposium on Neutron Capture Therapy for Cancer, Program & Abstracts*, (Osaka, Japan, 2000), pp. 31–32.

[2] Joensuu, H., *et al.*, "Boron neutron capture therapy of brain tumors: clinical trials at the Finnish facility using boronophenylalanine", *J. Neuro-Oncol.* **62** (2003), pp. 123–134.

[3] Kouri, M., *et al.*, "Undifferentiated sinonasal carcinoma may respond to single-fraction boron neutron capture therapy", *Radiother. Oncol*. **72(1)** (2004), pp. 83–85.

[4] Auterinen, I. and Hiismäki, P., "Epithermal BNCT neutron beam design for a Triga II reactor", in A. H. Soloway and R. F. Barth (Eds.), *Proceedings of the 5th International Symposium on Neutron Capture Therapy,* (Columbus, Ohio, 1992), *Advances in Neutron Capture Therapy*, (Plenum Press, New York, 1993), pp. 81–84.

[5] Auterinen, I., *et al.*, "Metamorphoses of a 35 year-old Triga reactor into a modern BNCT facility", in M. F. Hawthorne, K. Shelly and R. J. Wiersema (Eds.), *Frontiers in Neutron Capture Therapy*, (Kluwer Academic, New York, 2001), pp. 267–275.

[6] Barth, R. F., *et al.*, "Boron Neutron Capture Therapy of Cancer: Current Status and Future Prospects", *Clin. Cancer Res.* **11(11)** (2005), pp. 3987–4002.

[7] Nigg, D. W., "Methods for radiation dose distribution analysis and treatment planning in boron neutron capture therapy", *Int. J. Radiat. Oncol. Biol. Phys.* **28** (1994), pp. 1121–1134.

[8] Nigg, D. W., *et al*., "Computational dosimetry and treatment planning for boron neutron capture therapy", *J. Neuro-Oncol.* **33** (1997), pp. 93–104.

[9] Nigg, D. W., "Computational dosimetry and treatment planning considerations for neutron capture therapy", *J. Neuro-Oncol.* **62** (2003), pp. 75–86.

[10] Seppälä, T., *FiR 1 Epithermal Neutron Beam Model and Dose Calculation for Treatment Planning in Neutron Capture Therapy*, Ph.D. thesis, University of Helsinki (2002), Report Series in Physics, HU-P-D103, 46 p. + appendices.

[11] Seppälä, T., *et al.*, "Aspects of dose planning and patient positioning for BNC-treatment at FiR 1", *Med. Biol. Eng. Comput.* **37** (1999), pp. 402–403.

[12] Simbierowicz, P. and Olin, M., "Investigation of the influence of heterogeneous porosity on matrix diffusion: A novel approach using adaptive tree-multigrid technique and real porosity data", in W. Gray and I. Triay (Eds.), *Scientific Basis for Nuclear Waste Management XX*, *Symposium Proceedings*, vol. 465, (Materials Research Society, Pittsburgh, 1997), pp. 847–854.

[13] Gaspar, C. and Simbierowicz, P., "Difference schemes in tree-structured multigrid context", *Computational Methods in Water Resources IX*, vol. 1, (Elsevier Applied Science, 1992), pp. 555–562.

[14] Gaspar, C., Jozsa, J. and Simbierowicz, P., "Lagrangian modelling of the convective diffusion problem using unstructured grids and multigrid technique", in L. C. Wrobel and C. A. Brebbia (Eds.), *Proceedings of the 1st International Conference on Water Pollution*, (Southampton, 1991), *Water Pollution: Modelling, measuring and prediction*, (Elsevier Applied Science, Computational Mechanics Publications, 1991), pp. 299–312.

[15] Duderstadt, J. and Martin, W., *Transport Theory*, (Wiley, New York, 1979).

[16] Davison, B., *Neutron Transport Theory*, (Oxford University Press, London, 1957).

[17] Lewis, E. E. and Miller, W. F. Jr., *Computational methods of neutron transport*, (Wiley-Interscience, New York, 1984).

[18] Fletcher, J. K., *The Solution of the Multigroup Transport Equation Using Spherical Harmonics*, UKAEA TRG-Report-2547 (R), (United Kingdom Atomic Energy Agency, Risley, 1974).

[19] Fletcher, J. K., *Further Work on the Solution of the Static Multigroup Neutron Transport Equation Using Spherical Harmonics*, UKAEA TRG-Report-2849 (R), (United Kingdom Atomic Energy Agency, Risley, 1976).

[20] Gelbard, E. M., *Application of Spherical Harmonics Methods to Reactor Problems*, WAPD-T-1182, (Bettis Atomic Power Laboratory, 1961).

[21] Gelbard, E. M., *Simplified Spherical Harmonics Equations and Their Use in Shielding Problems*, WAPD-T-1182, (Bettis Atomic Power Laboratory, 1961).

[22] Gelbard, E. M., *Applications of the Simplified Spherical Harmonics Equations in Spherical Geometry*, WAPD-TM-294, (Bettis Atomic Power Laboratory, 1962).

[23] Larsen, E. W., Morel, J. E. and McGhee, J. M., "Asymptotic Derivation of the Multigroup P_1 and Simplified P_N Equations with Anisotropic Scattering", *Nucl. Sci. Eng.* **123** (1996), pp. 328–342.

[24] Pomraning, G. C., "Asymptotic and Variational Derivations of the Simplified P_N Equations", *Ann. Nucl. Energy* **20** (1993), pp. 623–637.

[25] Brantley, P. S. and Larsen, E. W., "The Simplified P_3 Approximation", *Nucl. Sci. Eng.* **134** (2000), pp. 1–21.

[26] International Commission on Radiation Units and Measurements, *Determination of absorbed dose in a patient irradiated by beams of X or gamma rays in radiotherapy procedures*, ICRU Report 24, (ICRU Publications, Bethesda, 1976).

[27] Perez, C. A. and Brady, L. W., *Principles and Practice of Radiation Oncology*, (Lippincott–Raven Publishers, Philadelphia, 1997), third ed., 13 p.

[28] Arfken, G., *Mathematical Methods for Physicists*, (Academic Press, San Diego, 1985), third ed., 867 p.

[29] International Commission on Radiation Units and Measurements, *Photon, Electron, Proton and Neutron Interaction Data for Body Tissues*, ICRU Report 46, (ICRU Publications, Bethesda, 1992).

[30] Hunt, M. A., Desobry, G. E., Fowble, B. and Coia, L. R., "Effect of low-density lateral interfaces on soft-tissue doses", *Int. J. Radiat. Oncol. Biol. Phys.* **37** (1997), pp. 475–482.

[31] Wong, J. W. and Purdy, J. A., "On methods of inhomogeneity corrections for photon transport", *Med. Phys.* **17** (1990), pp. 807–814.

[32] Josef, J. A. and Morel, J. E., "Simplified spherical harmonic method for coupled electron-photon transport calculations", *Phys. Rev. E* **57** (1998), pp. 6161–6171.

[33] White, J. E., *et al.*, *BUGLE-96: Coupled 47 Neutron, 20 Gamma-Ray Group Cross Section Library Derived from ENDF/B-VI for LWR Shielding and Pressure Vessel Dosimetry Applications*, RSICC Data Library Collection, DLC-185, (Oak Ridge National Laboratory, 1996).

[34] Duderstadt, J. J. and Hamilton, L. J., *Nuclear Reactor Analysis*, (Wiley, New York, 1976).

[35] Carlson, B. G., *Solution of the Transport Equation by S_N Approximations*, LA-1599, (Los Alamos Scientific Laboratory, 1953).

[36] Rhoades, W. A. and Simpson, D. B., *The TORT Three-Dimensional Discrete Ordinates Neutron/Photon Transport Code (TORT Version 3)*, ORNL/TM-13221, (Oak Ridge National Laboratory, 1997).

[37] Lathrop, K. D., "Ray Effects in Discrete Ordinates Equations", *Nucl. Sci. Eng.* **32** (1968), pp. 357–369.

[38] Lathrop, K. D., "Remedies for Ray Effects", *Nucl. Sci. Eng.* **45** (1971), pp. 255–268.

[39] Davis, J. A., "Transport Error Bounds Via P_N Approximations", *Nucl. Sci. Eng.* **31** (1968), pp. 127–146.

[40] Mark, J. C., *The Spherical Harmonic Method*, Technical Report, CRT-340, (Atomic Energy of Canada, Ontario, 1947).

[41] Marshak, R. E., "Note on the Spherical Harmonic Method As Applied to the Milne Problem for a Sphere", *Phys. Rev.* **71** (1947), pp. 443–446.

[42] De Oliveira, C. R. E., Eaton, M. D., Umpleby, A. P. and Pain, C. C., "Finite element-spherical harmonics solutions of the 3D Kobayashi benchmarks with ray-tracing void treatment", *Prog. Nucl. Energ.* **39** (2001), pp. 243–261.

[43] Babuška, I., Zienkiewicz, O. C., Gago, J. and Oliveira, E. R. de A., *Accuracy Estimates and Adaptive Refinements in Finite Element Computations*, (John Wiley & Sons, Chichester, 1986).

[44] Wareing, T. A., McGhee, J. M., Morel, J. E. and Pautz, S. D., "Discontinuous Finite Element S_N Methods on Three-Dimensional Unstructured Grids", *Nucl. Sci. Eng.* **138** (2001), pp. 256–268.

[45] De Oliveira, C. R. E., "An Arbitrary Geometry Finite Element Method for Multigroup Neutron Transport with Anisotropic Scattering", *Prog. Nucl. Energ.* **18** (1986), pp. 227–236.

[46] Keller, S. E. and de Oliveira, C. R. E., "Two-Dimensional C5G7 MOX Fuel Assembly Benchmark Calculations Using the FEM-PN Code EVENT", *Prog. Nucl. Energ.* **39** (2001), pp. 243–261.

[47] Martin, W. R. and Duderstadt, J. J., "Finite Element Solutions of the Neutron Transport Equation with Applications to Strong Heterogeneities", *Nucl. Sci. Eng.* **62** (1977), pp. 371–390.

[48] Ackroyd, R. T., "A finite element method for neutron transport. Part I. Some theoretical considerations", *Ann. Nucl. Energy* **5** (1978), pp. 75–94.

[49] Ackroyd, R. T., *Finite Element Methods for Particle Transport: Applications to Reactor and Radiation Physics*, (John Wiley & Sons, Chichester, 1997).

[50] Boman, E., Tervo, J. and Vauhkonen, M., "Modelling the transport of ionizing radiation using the finite element method", *Phys. Med. Biol.* **50** (2005), pp. 265–280.

[51] Gifford, K. A., Horton Jr., J. L., Wareing, T. A., Failla, G. and Mourtada, F., "Comparison of a finite-element multigroup discrete-ordinates code with Monte Carlo for radiotherapy calculations", *Phys. Med. Biol.* **51** (2006), pp. 2253–2265.

[52] Tervo, J., Kolmonen, P., Vauhkonen, M., Heikkinen, L. M. and Kaipio, J. P., "A finite-element model of electron transport in radiation therapy and a related inverse problem", *Inverse Probl.* **15** (1999), pp. 1345–1361.

[53] Tervo, J. and Kolmonen, P., "Inverse radiotherapy treatment planning model applying Boltzmann-transport equation", *Math. Mod. Meth. Appl. S.* **12** (2002), pp. 109–141.

[54] Hammersley, J. M. and Handscomb, D. C., *Monte Carlo Methods*, (John Wiley & Sons, New York, 1964).

[55] Dupree, S. A. and Fraley, S. K., *A Monte Carlo Primer: A Practical Approach to Radiation Transport*, (Kluwer Academic, New York, 2002).

[56] Kinsey, R., *Data Formats and Procedures for the Evaluated Nuclear Data File, ENDF*, BNL-NCS-50496, (Brookhaven National Laboratory, 1979).

[57] Briesmeister, J. F., *MCNP – A General Monte Carlo N-Particle Transport Code, Version 4C*, LA-13709 M, (Los Alamos National Laboratory, 2000).

[58] Bielajew, A. F., Hirayama, H., Nelson, W. R. and Rogers, D. W. O., *History, overview and recent improvements of EGS4*, Technical Report PIRS-0436, (National Research Council of Canada, 1994).

[59] Kawrakow, I. and Rogers, D. W. O., *The EGSnrc code system: Monte Carlo simulation of electron and photon transport*, Technical Report PIRS-701, (National Research Council of Canada, 2000).

[60] Rogers, D. W. O., "Fifty years of Monte Carlo simulations for medical physics", *Phys. Med. Biol.* **51** (2006), pp. 287–301.

[61] Jeraj, R., Keall, P. J. and Ostwald, P. M., "Comparisons between MCNP, EGS4 and experiment for clinical electron beams", *Phys. Med. Biol.* **44** (1999), pp. 705–717.

[62] Solberg, T. D., *et al.*, "A review of radiation dosimetry applications using the MCNP Monte Carlo code", *Radiochim. Acta* **89** (2001), pp. 337–355.

[63] Agostinelli, S., *et al.*, "GEANT4 – a simulation toolkit", *Nucl. Instrum. Meth.* **A 506** (2003), pp. 250–303.

[64] Enger, S. A., Munck af Rosenschöld, P., Rezaei, A. and Lundqvist, H., "Monte Carlo calculations of thermal neutron capture in gadolinium: A comparison of GEANT4 and MCNP with measurements", *Med. Phys.* **33** (2) (2006), pp. 337–341.

[65] Woodcock, E. R., Murphy, T., Hemmings, P. J. and Longworth, S. C., "Techniques used in the GEM code for Monte Carlo neutronics calculations in reactors and other systems of complex geometries", in *Proceedings of the Conference on Applications of Computing Methods to Reactor Problems*, ANL-7050, (Argonne National Laboratory, 1965), 557 p.

[66] Leppänen, J., “A new assembly-level Monte Carlo neutron transport code for reactor physics calculations”, in *Proceedings of the International Topical Meeting on Mathematics and Computation, Supercomputing, Reactor Physics and Nuclear and Biological Applications*, American Nuclear Society (2005), on CD-ROM, 12 p.

[67] Zweifel, P. F., *Reactor Physics*, (McGraw-Hill, New York, 1973).

[68] Lamarsh, J. R., *Introduction to Nuclear Reactor Theory*, (Addison-Wesley, Reading, 1972).

[69] Zamenhof, R. G., *et al.*, “Monte Carlo based treatment planning for boron neutron capture therapy using custom designed models automatically generated from CT data”, *Int. J. Radiat. Oncol. Biol. Phys.* **35** (1996), pp. 383–397.

[70] Goorley, T., McKinney, G., Adams, K. and Estes, G., “MCNP enhancements, parallel computing, and error analysis for BNCT”, in M. F. Hawthorne, K. Shelly and R. J. Wiersema (Eds.), *Frontiers in Neutron Capture Therapy*, (Kluwer Academic, New York, 2001), pp. 599–604.

[71] Cheng, J. H., Finnigan, P. M., Hathaway, A. F., Kela, A. and Schroeder, W. J., “Quadtree/Octree Meshing with Adaptive Analysis”, in *Numerical Grid Generation in Computational Fluid Mechanics*, (Pineridge Press, Swansea, 1988), pp. 633–642.

[72] Hackbusch, W., *Multi-grid Methods and Applications*, (Springer, Berlin, 1985).

[73] Wesseling, P., *An Introduction to Multigrid Methods*, (Wiley, New York, 1992).

[74] Brandt, A., “Multi-level adaptive solutions to boundary-value problems”, *Math. Comput.* **31** (1977), pp. 333–390.

[75] Brantley, P. S. and Tomašević, D. I., "Spatially continuous mixed simplified P_2–P_1 solutions for multidimensional geometries", in *Proceedings of the International Topical Meeting on Mathematics and Computation, Supercomputing, Reactor Physics and Nuclear and Biological Applications*, American Nuclear Society (2005), on CD-ROM, 10 p.

[76] Prinsloo, R., Tomašević, D. I., Albornoz, F. and Brantley, P. S., "Application of SP_2 and the spatially continuous SP_2-P_1 equations to the PBMR reactor", in *Proceedings of the International Topical Meeting on Mathematics and Computation, Supercomputing, Reactor Physics and Nuclear and Biological Applications*, American Nuclear Society (2005), on CD-ROM, 8 p.

[77] Brantley, P. S., "A mixed P_1–DP_0 diffusion theory for planar geometry", *Ann. Nucl. Energy* **32** (2005), pp. 1525–1545.

[78] Longoni, G. and Haghighat, A., "The Even-Parity Simplified S_N Equations Applied to a MOX Fuel Assembly Benchmark Problem on Distributed Memory Environments", in *PHYSOR 2004 – The Physics of Fuel Cycles and Advanced Nuclear Systems: Global Developments*, American Nuclear Society (2004), on CD-ROM.

[79] Longoni, G., *Advanced Quadrature Sets, Acceleration and Preconditioning Techniques for the Discrete Ordinates Method in Parallel Computing Environments*, Ph.D. thesis, University of Florida (2004), UF Online Dissertations, 202 p.

[80] Longoni, G., Haghighat, A. and Sjoden, G., "A New Synthetic Acceleration Technique Based on the Simplified Even-Parity S_N Equations", *Transport Theor. Stat.* **33** (2004), pp. 347–360.

[81] Longoni, G., Haghighat, A., Yi, C. and Sjoden, G., "Benchmarking of PENTRAN-SS_N Parallel Transport Code and FAST Preconditioning Algorithm Using the VENUS-2 MOX-Fueled Benchmark Problem", *J. ASTM Int.* **3** Issue 7 (2006), 10 p.

[82] Lillie, R. A., "GRTUNCL3D: A Discontinuous Mesh Three-Dimensional First Collision Source Code", in *Proceedings of the ANS Radiation* Protection and Shielding Division Topical Conference, American Nuclear Society (1998), pp. 368–375.

[83] Wareing, T. A., Morel, J. E. and Parsons, D. K., "A First Collision Source Method For ATTILA, An Unstructured Tetrahedral Mesh Discrete Ordinates Code", in Proceedings of the ANS Radiation Protection and Shielding Division Topical Conference, American Nuclear Society (1998), pp. 376–382.

[84] Bjugg, H., *BNCT-annossuunnittelun teoreettiset perusteet*, M.Sc. thesis (in Finnish), University of Helsinki (2000), 64 p.

[85] Rhoades, W. A. and Childs, R. L., "The DORT Two-Dimensional Discrete Ordinates Transport Code", Nucl. Sci. Eng. 99 (1988), pp. 88–89.

[86] Hiismäki, P. and Auterinen, I., Patent FI-92890 (1995).

[87] International Commission on Radiation Units and Measurements, *Tissue Substitutes in Radiation Dosimetry and Measurement*, ICRU Report 44 (ICRU Publications, Bethesda, 1989).

[88] Knoll, G. F., *Radiation Detection and Measurement*, (John Wiley & Sons, New York, 1988).

[89] Kaita, K., *Characterisation of the epithermal neutron beam at the Triga BNCT-station using activation detectors*, M.Sc. in Engineering thesis, Helsinki University of Technology (1996), 65 p. + appendices.

[90] Serén, T., *et al.*, "A Tale of Two Beams – Comparison of the Radiation Fields at the BMRR and FiR 1 Epithermal BNCT Facilities", *Med. Biol. Eng. Comput.* **37** (1999), pp. 396–397.

[91] Serén, T., Auterinen, I., Seppälä, T. and Kotiluoto, P., "Spectrum measurements and calculations in the epithermal neutron beam at the

FiR 1 BNCT facility", in *Proceedings of the 15th European TRIGA Conference*, VTT Symposium 197, (VTT, Espoo, 1999), pp. 167–179.

[92] Serén, T., Kotiluoto, P. and Auterinen, I., "Correct Treatment of Covers in Adjustment of Epithermal Neutron Spectra", in *Advances in Neutron Capture Therapy 2006*, International Society for Neutron Capture Therapy (2006), pp. 474–477.

[93] Auterinen, I., Serén, T., Uusi-Simola, J., Kosunen, A. and Savolainen, S., "A toolkit for epithermal neutron beam characterisation in BNCT", *Radiat. Prot. Dosim.* **110** (2004), pp. 587–593.

[94] Kosunen, A., *Metrology and quality of radiation therapy dosimetry of electron, photon and epithermal neutron beams*, Ph.D. thesis, STUK-A164, STUK – Radiation and Nuclear Safety Authority (1999), 50 p. + appendices.

[95] Aschan, C., *Applicability of thermoluminescent dosimeters in x-ray organ dose determination and in the dosimetry of systemic and boron neutron capture radiotherapy*, Ph.D. thesis, University of Helsinki (1999), Report Series in Physics, HU-P-D77, 31 p. + appendices.

[96] Uusi-Simola, J., *Microdosimetry and Its Application in Epithermal Neutron Beam*, M.Sc. thesis, University of Helsinki (2002), 70 p.

[97] Kosunen, A., *et al.*, "Twin ionisation chambers for dose determinations in phantom in an epithermal neutron beam", *Radiat. Prot. Dosim.* **81** (1999), pp. 187–194.

[98] Binns, P. J., *et al.*, "An international dosimetry exchange for boron neutron capture therapy, Part I: Absorbed dose measurements", *Med. Phys.* **32** (2005), pp. 3729–3736.

[99] Uusi-Simola, J., *et al.*, "Dosimetric comparison at FiR 1 using microdosimetry, ionisation chambers and computer simulation", *Appl. Radiat. Isotopes* **61** (2004), pp. 845–848.

[100] Auterinen, I., Serén, T., Anttila, K., Kosunen, A. and Savolainen, S., "Measurement of free beam neutron spectra at eight BNCT facilities worldwide", *Appl. Radiat. Isotopes* **61** (2004), pp. 1021–1026.

[101] Uusi-Simola, J., *et al.*, "Study of the relative dose-response of BANG-3® polymer gel dosimeters in epithermal neutron irradiation", *Phys. Med. Biol.* **48** (2003), pp. 2895–2906.

[102] Aschan, C., Toivonen, M., Savolainen, S., Seppälä, T. and Auterinen, I., "Epithermal neutron beam dosimetry with thermoluminescence dosemeters for boron neutron capture therapy", *Radiat. Prot. Dosim.* **81** (1999), pp. 47–56.

[103] Auterinen, I., Serén, T., Kotiluoto, P., Uusi-Simola, J. and Savolainen, S., "Quality assurance procedures for the neutron beam monitors at the FiR 1 BNCT facility", *Appl. Radiat. Isotopes* **61** (2004), pp. 1015–1019.

[104] Williams, J. R. and Thwaites, D. I., *Radiotherapy Physics in Practice*, (Oxford University Press, 1993).

[105] Williamson, J. F., Perera, H., Li, Z. and Lutz, W. R., "Comparison of calculated and measured heterogeneity correction factors for ^{125}I, ^{137}Cs, and ^{192}Ir brachytherapy sources near localized heterogeneities", *Med. Phys.* **20** (1993), pp. 209–222.

[106] Das, R. K., *et al.*, "Validation of Monte Carlo dose calculations near ^{125}I sources in the presence of bounded heterogeneities", *Int. J. Radiat. Oncol. Biol. Phys.* **38** (1997), pp. 843–853.

[107] Kirov, A. S., Williamson, J. F., Meigooni, A. S. and Zhu, Y., "Measurement and calculation of heterogeneity correction factors for an Ir-192 high dose-rate brachytherapy source behind tungsten alloy and steel shields", *Med. Phys.* **23** (1996), pp. 911–919.

[108] Lorence, L. J. Jr., Morel, J. E. and Valdez, G. D., *Physics guide to CEPXS: a multigroup coupled electron-photon cross-section generating code*, SAND89-1685, (Sandia National Laboratory, 1989).

[109] Luxton, G. and Jozsef, G., "Radial dose distribution, dose to water and dose rate constant for monoenergetic photon point sources from 10 keV to 2 MeV: EGS4 Monte Carlo model calculation", *Med. Phys.* **26** (1999), pp. 2531–2538.

[110] Nelson, W. R., Hirayama, H. and Rogers, D. W. O., *The EGS4 code system*, SLAC-265, (Stanford Linear Accelerator Center, 1985).

[111] Hartmann Siantar, C. L., *et al.*, "Description and dosimetric verification of the PEREGRINE Monte Carlo dose calculation system for photon beams incident on a water phantom", *Med. Phys*. **28** (2001), pp. 1322–1337.

[112] Boudreau, C., Heath, E., Seuntjens, J., Ballivy, O. and Parker, W., "IMRT head and neck treatment planning with a commercially available Monte Carlo based planning system", *Phys. Med. Biol*. **50** (2005), pp. 879–890.

[113] Takeda, T., Tamitani, M. and Unesaki, H., *Proposal of 3-D neutron transport benchmark problems*, NEACRP A-953 Rev. 1, (OECD/NEA Committee on Reactor Physics, 1988).

[114] Takeda, T. and Ikeda, H., *3-D neutron transport benchmarks*, NEACRP-L-330, (OECD/NEA Committee on Reactor Physics, 1991).

[115] Han, C. Y., Shin, C.-H., Kim, H.-C., Kim, J. K., Messaoudi, N. and Na, B.-C., *VENUS-2 MOX-fuelled Reactor Dosimetry Calculations, Benchmark Specification*, NEA/NSC/DOC(2004)6, (OECD/NEA Nuclear Science Committee, 2004).

[116] OECD NEA, *VENUS-2 MOX-fuelled Reactor Dosimetry Calculations, Final Report*, NEA/NSC/DOC(2005)22, (OECD/NEA Nuclear Science Committee, 2006).

[117] Kotiluoto, P. and Wasastjerna, F., "VENUS-2 MOX-fuelled reactor dosimetry benchmark calculations at VTT", in *Proceedings of the International Topical Meeting on Mathematics and Computation,*

Supercomputing, Reactor Physics and Nuclear and Biological Applications, American Nuclear Society (2005), on CD-ROM, 12 p.

[118] Zsolnay, É. M., Szondi, E. J. and Nolthenius, H. J., *The Neutron Metrology File NMF-90*, IAEA-NDS-171, Rev. 1, (International Atomic Energy Agency, 1999).

[119] Leenders, L., *LWR-PVS Benchmark Experiment VENUS-3 (with Partial Lenght Shielded Assemblies)*, FCP/VEN/01, (SCK, CEN, 1988).

[120] OECD NEA, *Prediction of Neutron Embrittlement in the Reactor Pressure Vessel*, NEA/NSC/DOC(2000)5, (OECD/NEA Nuclear Science Committee, 2000).

[121] Lewis, E. E., Palmiotti, G., Taiwo, T. A., Smith, M. A. and Tsoulfanidis, N., *Benchmark Specification for Deterministic MOX Fuel Assembly Transport Calculations without Spatial Homogenisation (3-D extension C5G7 MOX)*, NEA/NSC/DOC(2003)6, (OECD/NEA Nuclear Science Committee, 2003).

[122] Kotiluoto, P., "The new deterministic 3-D radiation transport code MultiTrans: C5G7 MOX fuel assembly benchmark", in *Proceedings of the International Conference on Supercomputing in Nuclear Applications*, Paris, France (2003), on CD-ROM, 7 p.

[123] Haghighat, A., "Recent Advances in Hybrid Methods Applied to Neutral Particle Transport Problems", in *Proceedings of the International Nuclear Atlantic Conference – INAC 2005*, Santos, Brazil (2005), 24 p.

[124] Haghighat, A. and Wagner, J., "Monte Carlo Variance Reduction with Deterministic Importance Functions", *Prog. Nucl. Energ.* **42** (2003), pp. 25–53.

[125] Wagner, J. and Haghighat, A., "Automated Variance Reduction of Monte Carlo Shielding Calculations Using the Discrete Ordinates Adjoint Function", *Nucl. Sci. Eng.* **128** (1998), pp. 186–2

PUBLICATION I

Fast tree multigrid transport application for the simplified P_3 approximation

In: Nuclear Science and Engineering 2001.
Vol. 138, pp. 269–278.

NUCLEAR SCIENCE AND ENGINEERING: **138**, 269–278 (2001)

Fast Tree Multigrid Transport Application for the Simplified P_3 Approximation

Petri Kotiluoto*

VTT Chemical Technology, Nuclear Applications, P.O. Box 1404, FIN-02044 VTT, Finland

Received June 29, 2000
Accepted October 10, 2000

Abstract—*Calculation of neutron flux in three-dimensions is a complex problem. A novel approach for solving complicated neutron transport problems is presented, based on the tree multigrid technique and the Simplified P_3 (SP_3) approximation. Discretization of the second-order elliptic SP_3 equations is performed for a regular three-dimensional octree grid by using an integrated scheme. The octree grid is generated directly from STL files, which can be exported from practically all computer-aided design-systems. Marshak-like boundary conditions are utilized. Iterative algorithms are constructed for SP_3 approximation with simple coarse-to-fine prolongation and fine-to-coarse restriction operations of the tree multigrid technique. Numerical results are presented for a simple cylindrical homogeneous one-group test case and for a simplistic two-group pressurized water reactor pressure vessel fluence calculation benchmark. In the former homogeneous test case, a very good agreement with 1.6% maximal deviation compared with DORT results was obtained. In the latter test case, however, notable discrepancies were observed. These comparisons show that the tree multigrid technique is capable of solving three-dimensional neutron transport problems with a very low computational cost, but that the SP_3 approximation itself is not satisfactory for all problems. However, the tree multigrid technique is a very promising new method for neutron transport.*

I. INTRODUCTION

Computer programs for radiation transport are based either on deterministic solution of the Boltzmann transport equation or on stochastic simulation (i.e., Monte Carlo method). The Monte Carlo method is extremely time consuming and often cannot present all radiation distribution details. Conventional deterministic programs, on the other hand, are mainly based on the discrete ordinates (S_N) method. S_N methods have their own problems, e.g., ray effects, which arise from the discrete representation of directional fluxes that does not preserve rotational invariance, and the problem of prevention of negative flux values.

An alternative solution is the well-established P_N approximation,[1] which is obtained by expanding the flux in spherical harmonics up to order $N + 1$ and using the orthogonality of these base functions. Thus, the angular dependency of the flux can be separated into spherical harmonics (or into the vector function space, i.e., Hilbert's space), and second-order elliptic differential equations for the spatial part of the moment flux can be obtained. The first two terms in the expansion are the scalar flux and current, and further terms are of smaller magnitude. The P_N equations in multidimensional geometries, however, form a very complicated set of equations that involve both coupling of the angular moments and their mixed derivatives. Gelbard[2–4] proposed in the early 1960s a simplification to this scheme, the Simplified P_N (SP_N) approximation. The SP_N equations were "derived" by simply replacing the second derivatives in the one-dimensional planar geometry P_N equations with general three-dimensional Laplacian operators.

The theoretical basis of the SP_N approximation has historically been weak, although the numerical results obtained by the approximation have always appeared promising. However, since 1991 a theoretical basis of the SP_N approximation has developed. Asymptotic derivation of the SP_N equations in the case of an inhomogeneous medium with multiple energy groups and

*E-mail: Petri.Kotiluoto@vtt.fi

anisotropic scattering was first provided by Larsen, Morel, and McGhee.[5] Pomraning[6] showed that SP_N equations with odd N are a variational approximation to the transport equation in an infinite homogeneous medium with one-group isotropic scattering. Neither Pomraning's variational approximation nor the asymptotic derivation mentioned earlier produce outer boundary conditions. Only recently has it been shown by Brantley and Larsen[7] that SP_3 equations with Marshak-like boundary conditions can be derived from the variational principle for inhomogeneous medium with multigroup anisotropic scattering.

In this paper, the theoretical basis of SP_3 equations lies on the developments of Brantley and Larsen[7] and on the improved iteration strategy[7,8] based on "explicit" formulation of SP_3 equations. Attention is paid to direct application of advanced multigrid[9] methods.

SP_3 equations form a coupled set of two second-order elliptic differential equations. In the explicit form, a best convergence rate[7,8] is expected for these equations. The most efficient numerical method to solve elliptic differential equations is the tree multigrid technique. To apply the efficient tree multigrid technique to SP_3 approximation, it is first necessary to discretize the equations into tree-structured, nonuniform, nonequidistant grids.[10]

In the multigrid solution technique, the iteration procedure is accelerated by first solving the problem on a coarser grid and then transferring data to finer grids, and vice versa. In the tree multigrid technique, an adaptive subdivision procedure enables refinement of the calculation grid on material surfaces or by computational demand. The tree structure enables the modeling of complicated geometries and surfaces accurately with only a limited number of mesh cells. The tree multigrid iteration technique offers a way to solve elliptic second-order differential equations with a minimum number of iterations required. Thus, the tree multigrid technique applied to SP_3 approximation makes the deterministic solution of the radiation transport possible in complicated three-dimensional geometries with decent running times, and it forms the basis of the radiation transport method outlined in this paper.

II. SP_3 APPROXIMATION

The derivation of the SP_3 approximation from the variational principle can be found from Brantley and Larsen.[7] Let us here just restate the "explicit" iterative multigroup formulation of SP_3 approximation in the case of a finite, piecewise-homogeneous medium with anisotropic scattering.

If one defines the unknown,

$$\hat{\Phi}_0(\vec{r}) \equiv \Phi_0(\vec{r}) + 2\Phi_2(\vec{r}) \ , \tag{1}$$

where $\Phi_0(\vec{r})$ is the scalar flux and $\Phi_2(\vec{r})$ is the P_2 moment term, the explicit SP_3 equations are given by[7] (where superscript g is the energy group, i is the material zone, and l is the iteration index)

$$-D_0^{i,g}\nabla^2\hat{\Phi}_0^{i,g,(l+1)}(\vec{r}) + \sigma_{a0}^{i,g}\hat{\Phi}_0^{i,g,(l+1)}(\vec{r}) = 2\sigma_{a0}^{i,g}\Phi_2^{i,g,(l)}(\vec{r}) + S^{i,g}(\vec{r}) \tag{2}$$

and

$$-D_2^{i,g}\nabla^2\Phi_2^{i,g,(l+1)}(\vec{r}) + \sigma_{a2}^{i,g}\Phi_2^{i,g,(l+1)}(\vec{r}) = \tfrac{2}{5}\{\sigma_{a0}^{i,g}[\hat{\Phi}_0^{i,g,(l+1)}(\vec{r}) - 2\Phi_2^{i,g,(l)}(\vec{r})] - S^{i,g}(\vec{r})\} \ , \tag{3}$$

where the group removal or transport cross sections are defined by subtraction of the corresponding Legendre component of the scattering cross section from the total cross section:

$$\sigma_{an}^{i,g} = \sigma_t^{i,g} - \sigma_{sn}^{i,g\to g}, \ n \geq 0 \ . \tag{4}$$

The diffusion coefficients are defined by transport cross sections $\sigma_{a1}^{i,g}$ and $\sigma_{a3}^{i,g}$ as

$$D_0^{i,g} = \frac{1}{3\sigma_{a1}^{i,g}} \tag{5}$$

and

$$D_2^{i,g} = \frac{9}{35\sigma_{a3}^{i,g}} \ . \tag{6}$$

The group source is

$$S^{i,g}(\vec{r}) = \sum_{g'=1, g'\neq g}^{G} \sigma_{s0}^{i,g'\to g}\Phi_0^{g'}(\vec{r}) + \frac{\chi^g}{k}\sum_{g'=1}^{G}\nu^{g'}\sigma_f^{i,g'}\Phi_0^{g'}(\vec{r}) + Q^g(\vec{r}) \ , \tag{7}$$

using standard multigroup neutronics notation.

The Marshak-like boundary conditions for SP_3 [Eqs. (2) and (3)] are[7]

$$\frac{1}{2}\hat{\Phi}_0^{i,g,(l+1)}(\vec{r}) + D_0^{i,g}(\vec{n}_i\cdot\nabla)\hat{\Phi}_0^{i,g,(l+1)}(\vec{r}) = \frac{3}{8}\Phi_2^{i,g,(l)}(\vec{r}) + \int_0^{2\pi}\int_{-1}^{0} 2|\mu|\psi^b(\vec{r},\mu,\varphi)\,d\mu d\varphi \tag{8}$$

and

$$\frac{21}{40}\Phi_2^{i,g,(l+1)}(\vec{r}) + D_2^{i,g}(\vec{n}_i\cdot\nabla)\Phi_2^{i,g,(l+1)}(\vec{r}) = \frac{3}{40}\hat{\Phi}_0^{i,g,(l+1)}(\vec{r}) + \frac{3}{5}\int_0^{2\pi}\int_{-1}^{0} 2P_3(|\mu|)\psi^b(\vec{r},\mu,\varphi)\,d\mu d\varphi \ , \tag{9}$$

where $\psi^b(\vec{r},\mu,\varphi)$ is the incident flux at boundary.

It should be noted, that depending on the detailed structure of the underlying functional, different variational boundary conditions may occur. The boundary conditions in Eqs. (8) and (9) are termed Marshak-like[7] because they reduce to the traditional Marshak boundary conditions[1] in one-dimensional geometries.

III. INTEGRATED DIFFERENCE SCHEME FOR SP_3 EQUATIONS

To apply the multigrid technique to the SP_3 approximation, one has to define a sequence of nested grids (fine and coarse grids), discretize the SP_3 equations on each grid, and define intergrid transfer operators (restriction and prolongation).

In the tree multigrid technique, the calculation grid is formed by a recursive subdivision procedure, which in three dimensions is often referred to as an octree algorithm.[11] After a subdivision, the eight obtained subcubes are called the children of the parent cell. The resulting cell system has a tree structure, in which the subdivisions form the branches and the leaves are the children, which are not divided further. Each cell can thus have in three dimensions eight children cells, which can have their own children, and so on, depending on computational or geometric requirements. One important rule is, however, applied to the subdivision procedure: All the face neighbor cells of each cell must be either same size, half the size, or twice the size of the cell. In other words, the ratio of the sizes of any adjacent cells is at most 2, and the resulting cell system (octree grid) is said to be regular. In this manner, the amount of possible neighbor cell configurations for each cell will be reduced, and the solution will also be more stable.

Because the tree structure makes the grid nonuniform, some proper difference scheme must be used. To be efficient and useful, this difference scheme should be as simple as possible. There are several approaches for a Laplace operator.[10]

Integrating the Laplacian of the function u over a cell C and applying Green's formula, one obtains

$$\int_C \nabla^2 u \, d\Omega = \int_{\partial C} (\vec{n}\cdot\nabla) u \, d\Gamma \ , \tag{10}$$

where $\vec{n}$ is the normal vector of the cell surface. This is the basis of the integrated scheme.[10] When the face neighbor cells are the same size, flux over the side of the cell is approximated by using the central difference

$$(\vec{n}\cdot\nabla) u \approx \frac{1}{h} (u_N - u_C) \ , \tag{11}$$

where h is the mesh size, and u_C and u_N are the flux values in the cell and its neighbor, respectively. Otherwise, the parent of the smaller cell is used:

$$(\vec{n}\cdot\nabla) u \approx \begin{cases} \dfrac{1}{2h} (u_N - u_{P(C)}) \ , \\ \qquad \text{neighbor } N \text{ is bigger than C} \\ \dfrac{1}{2h} (u_{P(N)} - u_C) \ , \\ \qquad \text{neighbor } N \text{ is smaller than C} \ , \end{cases} \tag{12}$$

where the value of the parent cells $u_{P(C)}$ and $u_{P(N)}$ is the average of their children's values. This averaging can also be seen as a special choice of the fine-to-coarse restriction operation of the multigrid technique.

The integrated difference scheme introduced is symmetric, which makes it relatively easy to apply in a regular octree-grid structure. Only face neighbors are used, which also makes application of the scheme easier. The integrated scheme is inconsistent with the Laplacian in the Taylor series sense.[10] However, it can be proved to be convergent and stable for a Laplace-Poisson equation supplied with Dirichlet boundary conditions by the Bramble-Hilbert lemma.[10] The proof is based on a specific linear functional that is bounded in $H^2(\Omega)$ and vanishes for every polynomial of at most first order. Details are omitted. This proof might be applicable also for SP_3 approximation, but it should be strongly pointed out that no theoretical studies have yet been made, and thus no such proof exists.

The SP_3 Eqs. (2) and (3) form a linear elliptic problem

$$Lu = f \ , \tag{13}$$

where L is the matrix of the corresponding linear elliptic operator, u is the column vector, and f is the column source vector. Explicitly, Eq. (13) becomes

$$\begin{bmatrix} -D_0\nabla^2 + \sigma_{a0} & -2\sigma_{a0} \\ -\frac{2}{5}\sigma_{a0} & -D_2\nabla^2 + \sigma_{a2} + \frac{4}{5}\sigma_{a0} \end{bmatrix}^{i,g} \begin{bmatrix} \hat{\Phi}_0 \\ \Phi_2 \end{bmatrix}^{i,g} = S^{i,g} \begin{bmatrix} 1 \\ -\frac{2}{5} \end{bmatrix} . \tag{14}$$

Equation (14) now has to be discretized into the regular octree grid. Integrating over a volume of an octree cell with cell size h, and using Eq. (10), one obtains

$$\begin{bmatrix} -D_0 h^2(\vec{n}\cdot\nabla) + h^3\sigma_{a0} & -2h^3\sigma_{a0} \\ -\frac{2}{5}h^3\sigma_{a0} & -D_2 h^2(\vec{n}\cdot\nabla) + h^3\sigma_{a2} + \frac{4}{5}h^3\sigma_{a0} \end{bmatrix}_h^{i,g} \begin{bmatrix} \hat{\Phi}_0 \\ \Phi_2 \end{bmatrix}_h^{i,g} = h^3 S_h^{i,g} \begin{bmatrix} 1 \\ -\frac{2}{5} \end{bmatrix} , \tag{15}$$

where $(\vec{n}\cdot\nabla)$ denotes the central difference determined by Eq. (11) or (12), depending on the octree structure, i.e., the size of the face neighbor cells. Thus, Eq. (15) represents the resulting set of discretized linear algebraic equations

$$L_h u_h = f_h \ , \tag{16}$$

which can be transformed to iterative diagonal form:

$$\begin{bmatrix} -D_0 h^2(\vec{n}\cdot\nabla) + h^3\sigma_{a0} & 0 \\ 0 & -D_2 h^2(\vec{n}\cdot\nabla) + h^3\sigma_{a2} \end{bmatrix}_h^{i,g} \begin{bmatrix} \hat{\Phi}_0 \\ \Phi_2 \end{bmatrix}_h^{i,g,l+1} = h^3 S_h^{i,g} \begin{bmatrix} 1 \\ -\frac{2}{5} \end{bmatrix} + h^3\sigma_{a0} \begin{bmatrix} 2\Phi_2 \\ \frac{2}{5}\hat{\Phi}_0 - \frac{4}{5}\Phi_2 \end{bmatrix}_h^{i,g,l} \ . \tag{17}$$

Now, let $\tilde{u}_h$ denote some approximate solution to Eq. (16), and let u_h be the exact solution of Eq. (16). Then the error is

$$v_h = u_h - \tilde{u}_h \ , \tag{18}$$

and the residual can be defined as

$$d_h = -L_h\tilde{u}_h + f_h \ . \tag{19}$$

Because L_h is linear, the error satisfies

$$L_h v_h = d_h \ . \tag{20}$$

The next step toward a tree multigrid algorithm is to "coarsify" the L_h operator to a coarser grid with mesh size $H = 2h$:

$$L_H v_H = d_H \ . \tag{21}$$

Because L_H has a smaller dimension, Eq. (21) is easier to solve than Eq. (20). As a restriction operator,

$$d_H = R d_h \ , \tag{22}$$

simple averaging is used. Cross sections are also averaged into coarser grids. The error, on the other hand, is prolongated (interpolated) to finer grids by a prolongation operator,

$$\tilde{v}_h = P\tilde{v}_H \ , \tag{23}$$

where $\tilde{v}_H$ is an iterative solution to Eq. (20), and at the leaf cell, approximation $\tilde{u}_h$ can be updated:

$$\tilde{u}_h^{new} = \tilde{u}_h + \tilde{v}_h \ . \tag{24}$$

At the coarse-to-fine prolongation, a simple piecewise constant prolongation can be performed; i.e., all the children's values can be taken directly from the parent cell. Another way to construct the prolongation is a weighting technique (a straightforward generalization of the two-dimensional scheme presented by Gáspár and Simbierowicz[10]):

$$(Pv)_C = \tfrac{1}{6}\cdot(3\cdot v_{P(C)} + v_N^1 + v_N^2 + v_N^3) \ , \tag{25}$$

where v_N^1, v_N^2, and v_N^3 are the error terms in the three nearest face neighbors of the parent cell. Because of the regularity of the octree grid, these neighbors always exist (except at boundary).

Now, by starting with an initial guess (set to zero) at the finest multigrid level, i.e., the leaf cells of an octree grid, a tree multigrid algorithm can be constructed. First, the residual of the leaf cells is calculated using Eqs. (17) and (19). Then the residual is restricted into coarser grids by Eq. (22). The error terms are smoothed by using the diagonal part of the elliptic operator Eq. (17) in Eq. (20), and then prolongated toward the finer grids. This is all done by performing a prespecified number of multigrid cycles. At the leaf cells, the scalar flux and the second moment term of the solution are updated by Eq. (24). If the total error at the leaf cells is small enough, convergence is concluded. The problem converges to an asymptotic solution when the number of multigrid cycles is large enough (i.e., the iteration error is small) and the mesh at leaf level is small enough (i.e., the truncation error is small). The sufficient number of multigrid cycles and tree subdivision levels can be determined empirically. This asymptotic solution obtained by the tree multigrid technique is assumed to be the converged solution of the SP_3 approximation, although no theoretical proof exists.

The coding of the tree multigrid algorithm just described has been performed in the C++ language. This coding has been partly based on previous work of Pawel Simbierowicz at VTT Chemical Technology in Finland for some specific diffusion applications, although the source code kernel was totally rewritten for the multigroup solution and the SP_3 approximation. The octree generating procedure used so far in radiation transport is static; i.e., the octree grid is generated once from the geometry files and not changed during the calculation. In other applications—e.g., in collision detection algorithms used in robotics—dynamic grid generating procedures have been used. Plans are being made to connect the octree grid refining and coarsening to the transport solution dynamically so that the mesh would automatically adapt to the solution and thus ensure the desired level of accuracy.

It is known that multigrid methods can solve partial differential equations discretized on N grid points in $O(N)$ operations.[9] Thus, multigrid methods are even more efficient than the rapid direct elliptic solvers that can solve special kinds of elliptic equations in $O(N\log N)$ operations. With a tree structure, the number of cells and grid points is significantly reduced, and the tree multigrid method requires a much lesser computational cost even compared with the traditional multigrid methods working on uniform grids. When getting the most out of the

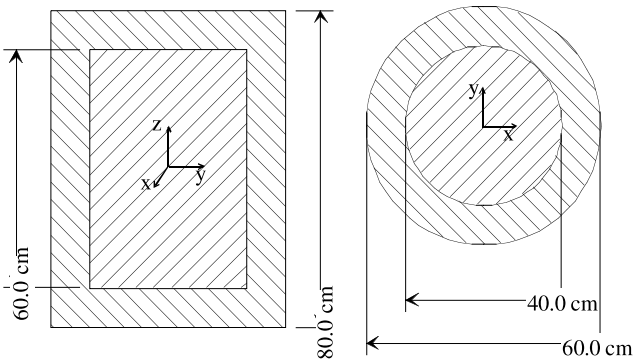

Fig. 1. Geometry of the three-dimensional calculational benchmarks.

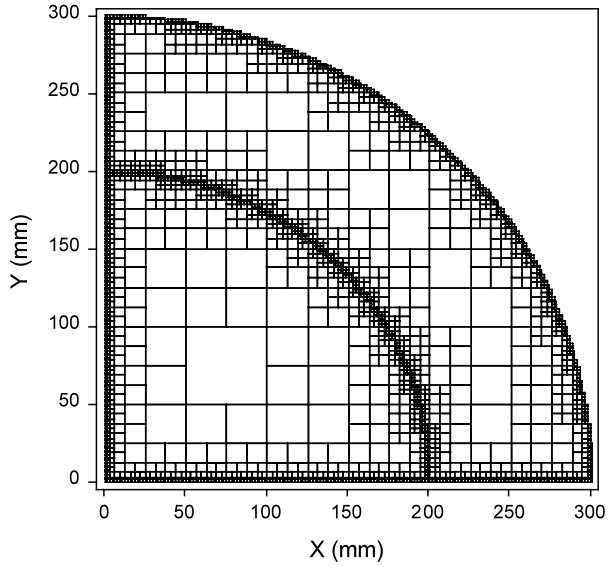

Fig. 2. Cross section of an octree grid for the three-dimensional calculational benchmarks.

tree multigrid technique, a simple difference scheme such as the integrated scheme introduced earlier, play an important role.

If the size of the resulting linear system is to be estimated, the number of cells in a regular octree grid roughly behaves like $\propto 4^L$, where L is the subdivision level. The eventual amount of the cells naturally depends on the underlying geometry of the problem. If a uniform grid were used, the number of cells would be comparable to $\propto 8^L$, resulting in a considerably larger linear system.

IV. NUMERICAL RESULTS

Two simple benchmarks have been performed for initial verification of the new transport code. Both benchmarks have the same geometry but different material specifications. The cylindrical benchmark geometry is shown in Fig. 1. Cylinder symmetry enables easy comparison calculations with DORT (Ref. 12).

The geometry consists of an inner cylinder that has a 20-cm radius and is 60 cm long (extending axially from -30 to $+30$ cm), and an outer cylinder that has a 30-cm radius and is 80 cm long (extending axially from -40 to $+40$ cm). For the SP_3 calculation, however, only one octant of the geometry needs to be modeled for symmetry reasons, and reflective boundary conditions have been utilized on the *X-Y*, *Y-Z*, and *X-Z* planes (Fig. 2). The octree grid has been generated directly from STL files offering a computer-aided design (CAD) interface.

The first benchmark is a simple one-group problem with homogeneous material all over and a fixed uniform volume source (1 n/cm^3) in the inner cylinder. Cross sections are presented in Table I. Cross sections are chosen to represent radiation transport in a medium with a relatively small absorption cross section and a short mean free path (1 cm) in order to ensure the validity of the SP_3 approximation.[5]

The second benchmark is a simplistic two-group pressurized water reactor (PWR) pressure vessel benchmark (suggested by Bojan Petrovic at http://gracie.nuce.psu.edu/~Petrovic/3Dbench/cyl1.html), with a fixed uniform volume source in the inner cylinder representing fuel; the outer cylinder water acts as a reflector. Source spectrum is given in Table II. Only the first two groups of the 47-group structure are used. Cross sections for these two groups are presented in Tables III and IV.

A different number of multigrid cycles and maximum octree subdivision levels were tested to ensure the convergence. This study is summarized in Table V. As a stopping criterion, an error $<10^{-4}$ was used. From Table V

TABLE I

Macroscopic Cross Sections (1/cm) for the First Benchmark Problem

Total Cross Section, σ_t	P_0 Scattering Cross Section, σ_{s0}	P_1 Scattering Cross Section, σ_{s1}	P_2 Scattering Cross Section, σ_{s2}	P_3 Scattering Cross Section, σ_{s3}
1.0	0.9	0.7	0.5	0.2

TABLE II

Fixed Source Spectrum for the Second Benchmark Problem

Energy Group	Group Upper Bound (eV)	Group Lower Bound (eV)	Fixed Source (n/cm^3)
1	1.73300E+07[a]	1.41910E+07	4.25838E−05
2	1.41910E+07	1.22140E+07	1.84253E−04

[a]Read as 1.73300×10^{7}.

TABLE III

Macroscopic Within-Group Cross Sections (1/cm) for the Second Benchmark Problem

Material	Energy Group	Total Cross Section, σ_t	P_0 Scattering Cross Section, σ_{s0}	P_1 Scattering Cross Section, σ_{s1}	P_2 Scattering Cross Section, σ_{s2}	P_3 Scattering Cross Section, σ_{s3}
Fuel	1	1.21840E−01[a]	5.09136E−02	4.50458E−02	3.82193E−02	3.19044E−02
Fuel	2	1.22186E−01	5.03877E−02	4.37986E−02	3.65188E−02	3.00574E−02
Water	1	7.34132E−02	1.91451E−02	1.68160E−02	1.36171E−02	1.07626E−02
Water	2	7.63243E−02	1.94962E−02	1.70019E−02	1.35168E−02	1.05149E−02

[a]Read as 1.21840×10^{-1}.

TABLE IV

Macroscopic Group-to-Group Cross Sections (1/cm) for the Second Benchmark Problem, with No Upscatter

Material	P_0 Scattering Cross Section, $\sigma_{s0}^{1\to2}$	P_1 Scattering Cross Section, $\sigma_{s1}^{1\to2}$	P_2 Scattering Cross Section, $\sigma_{s2}^{1\to2}$	P_3 Scattering Cross Section, $\sigma_{s3}^{1\to2}$
Fuel	1.04403E−02[a]	5.14301E−03	2.21054E−03	1.60152E−03
Water	1.05554E−02	6.32764E−03	3.54165E−03	2.70906E−03

[a]Read as 1.04403×10^{-2}.

TABLE V

Convergence Study

Multigrid Cycles, γ	Octree Subdivision Level, L	Memory Usage (K)	CPU Time	Maximal Difference Compared with ($\gamma = 6$, $L = 7$) Solution (%)
4	6	4936	19 s	1.69
5	6	4936	22 s	1.65
6	6	4936	23 s	1.43
7	6	4936	26 s	1.43
5	7	19240	1 min 41 s	0.04
6	7	19240	1 min 57 s	0.00

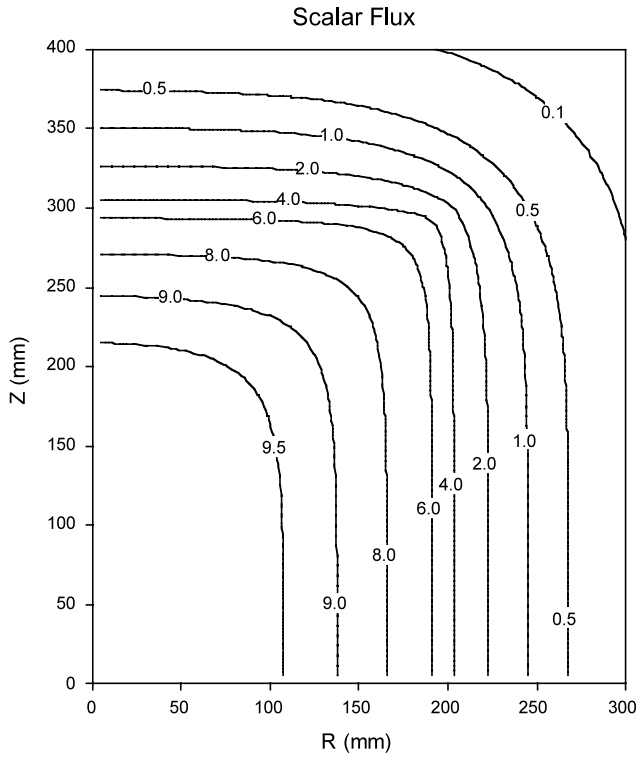

Fig. 3. *R-Z* plot of the SP_3 scalar flux results of the first benchmark.

one can see that the iteration error due to a different number of multigrid cycles is rather small and that five multigrid cycles are sufficient with a maximum octree subdivision level of seven. It should be noted that some truncation error might still exist. This could be tested by the dynamic refinement of the octree grid discussed in Sec. III or partly by higher octree subdivision levels. However, calculations with a higher subdivision level than seven were not performed because of run time memory requirements [a desktop personal computer (PC) with a 128-Mb memory was used]. It should be noted that when results of the calculations with different maximum numbers of the octree subdivision levels are compared, some interpolation error also has consequence. However, the truncation error was assumed to be small enough and the final SP_3 calculations reported in this paper for the described cylinder-in-cylinder benchmarks were performed with five multigrid cycles and a maximum octree subdivision level of seven, resulting in minimum cell size of 3.16 mm. Both the simple piecewise constant prolongation and the weighting technique (Sec. III) were tested, but in the final implementation, the piecewise constant prolongation was preferred; the more complicated weighting technique seemed to have no significance on results whatsoever. Scalar flux values for the selected set of data points were approximated by linear interpolation. In the second benchmark, isotropic downscattering was assumed (only the P_0 term was used from Table IV). Because no upscattering nor fission was present in these fixed source problems, no source iterations needed to be performed.

Comparison calculations in cylindrical two-dimensional geometry with DORT were performed with a 150 × 200 mesh, resulting in a cell size of 2 mm. Full symmetric S_8 quadrature (48 discrete directions) was used with directional theta weighting. S_8 calculations were carried out for both benchmark problems, but comparison of the SP_3 results of the second benchmark was performed against the DORT S_{16} directional theta weighted results given by Petrovic. S_8 and S_{16} results had a maximum difference (in the given set of data points) of 6.1% for group 1 and 5.8% for group 2 at $Z = 325$ mm and $R = 275$ mm.

Scalar flux results of the SP_3 octree calculation for the first benchmark are presented in Fig. 3. The DORT comparison of results is presented in Table VI. The maximum difference between SP_3 and DORT S_8 results is only 1.6% among the chosen data points, showing good accuracy of SP_3 octree approximation in this simple homogeneous case.

Scalar flux results of the SP_3 octree calculation for the second benchmark are presented in Figs. 4 and 5.

TABLE VI

Difference between SP_3 and DORT S_8 Results for the First Benchmark

R (cm)	Z (cm)							
	2.5	7.5	12.5	17.5	22.5	27.5	32.5	37.5
2.5	0.0%	0.0%	0.0%	0.0%	−0.1%	−0.4%	−1.2%	−0.1%
7.5	0.1	0.0	0.0	0.0	0.0	−0.3	−0.8	−0.3
12.5	0.1	0.1	0.1	0.1	0.1	−0.2	−0.6	−0.4
17.5	−0.1	−0.1	0.0	0.0	0.0	−0.2	−0.7	−0.8
22.5	−0.8	−0.5	−0.4	−0.3	−0.3	−0.6	−1.3	−1.5
27.5	−0.2	0.2	0.3	0.5	0.4	−0.1	−1.2	−1.6

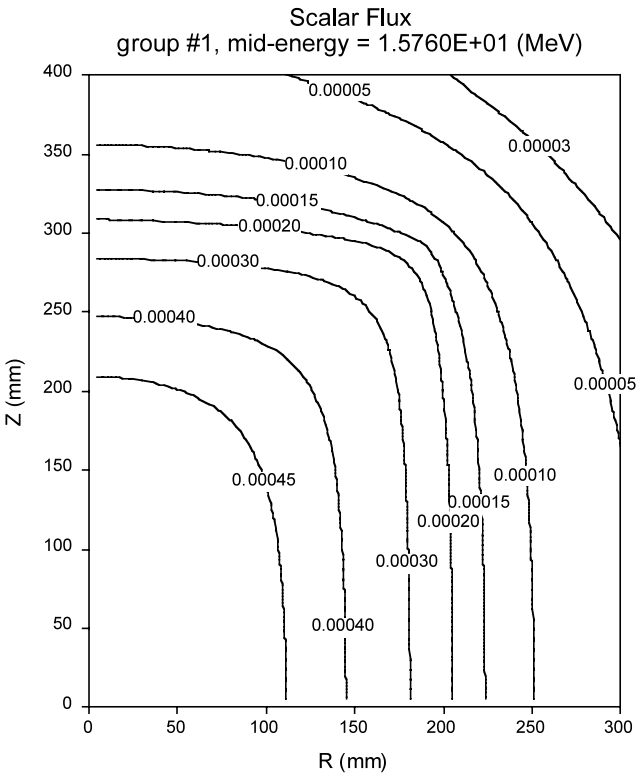

Fig. 4. *R-Z* plot of the SP_3 scalar flux results of the second benchmark, group 1.

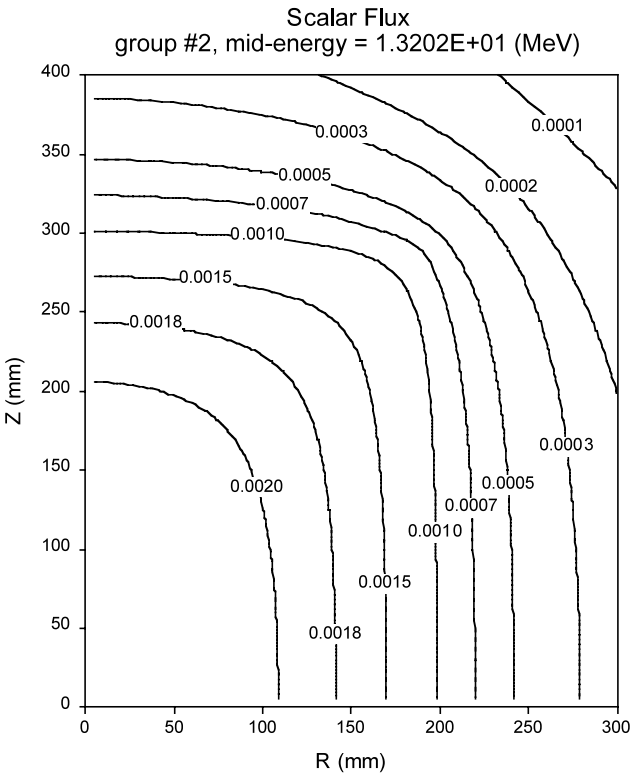

Fig. 5. *R-Z* plot of the SP_3 scalar flux results of the second benchmark, group 2.

The DORT S_{16} comparison is provided in Tables VII and VIII, showing a maximum difference of 18% between SP_3 and S_{16} in the chosen set of data points. In this benchmark case of fast neutrons (in the 12.2- to 17.3-MeV energy range) with mean free paths up to 13.6 cm in the outer cylinder, the validity of the SP_3 approximation itself is questionable. The SP_3 octree calculation seems to produce a much smoother solution than S_{16}. However, SP_3 approximation does not suffer from the ray effects illustrated in Figs. 6 and 7 by a radial profile plot of SP_3 and S_8 results near the vacuum boundary at $Z = 395$ mm.

SP_3 octree calculations were performed on a PC with a 200-MHz Pentium processor and 128 Mb of memory. A fully three-dimensional two-group problem with five multigrid cycles and an octree subdivision level of seven took 1 min 41 s CPU time. With four multigrid cycles and with an octree subdivision level of six, quite good results (within 2% compared with the former case) were obtained in 19 s CPU time (Table V). The program was executed in debug mode, however, and no optimization has yet been done for a code or compilation procedure. Thus, fully three-dimensional problems can effectively

TABLE VII

SP_3 Results for Group 1 Compared with DORT S_{16} Results

R (cm)	*Z* (cm)							
	2.5	7.5	12.5	17.5	22.5	27.5	32.5	37.5
2.5	0%	0%	0%	−1%	−2%	−10%	5%	8%
7.5	−1	0	−1	−1	−3	−10	5	8
12.5	−2	−2	−2	−3	−4	−12	4	8
17.5	−9	−10	−10	−10	−12	−18	3	8
22.5	6	7	7	7	6	6	6	6
27.5	9	9	10	11	10	10	5	4

TABLE VIII

SP_3 Results for Group 2 Compared with DORT S_{16} Results

R (cm)	Z (cm)							
	2.5	7.5	12.5	17.5	22.5	27.5	32.5	37.5
2.5	0%	0%	0%	0%	−2%	−9%	6%	7%
7.5	0	0	0	−1	−2	−9	5	7
12.5	−2	−2	−2	−2	−4	−11	5	7
17.5	−9	−9	−9	−9	−11	−17	4	7
22.5	7	7	7	7	7	6	6	5
27.5	8	8	9	9	9	9	4	1

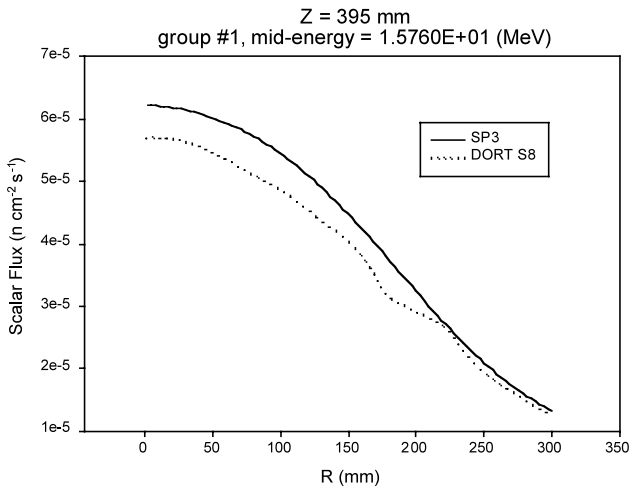

Fig. 6. SP_3 and S_8 scalar flux radial profiles at $Z = 395$ mm for the second benchmark, energy group 1. Mild ray effects can be seen in the S_8 solution.

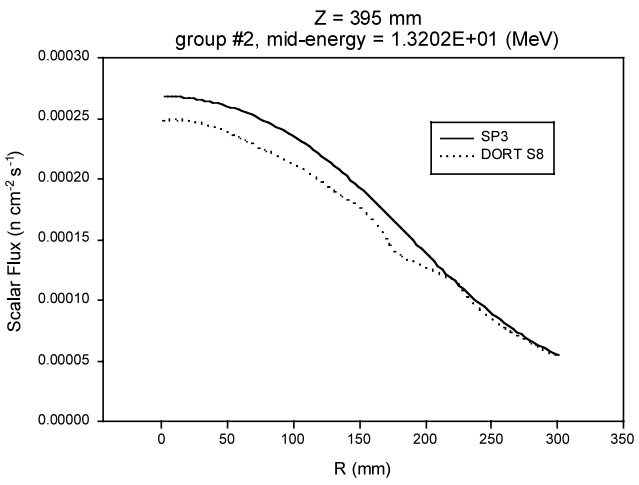

Fig. 7. SP_3 and S_8 scalar flux radial profiles at $Z = 395$ mm for the second benchmark, energy group 2. Mild ray effects can be seen in the S_8 solution.

be solved by the tree multigrid technique with running times comparable to two-dimensional DORT performance.

V. DISCUSSION

In this paper the tree multigrid application of the SP_3 approximation was described. The regular three-dimensional octree grid used in calculations has been generated from STL files that can be exported from practically all CAD systems. Calculations show that efficiency of this novel method is competitive, even though the full optimization of the code has not yet been carried out. Comparison of numerical results with DORT in the simple one-group benchmark shows good accuracy of the method in the validity range of the SP_3 approximation. The illustrated simple PWR benchmark shows notable discrepancies in some mesh points. Many of these discrepancies are deduced to originate from the SP_3 approximation itself, not from the tree multigrid technique applied. Larsen, Morel, and McGhee[5] list three conditions that a problem should meet in order to have a valid SP_3 approximation:

1. The physical system should be several mean free paths thick so that the probability for neutrons to leak out is sufficiently small (<0.5).
2. The probability of absorption should not be too high (<0.5).
3. The mean scattering cosine should not be too close to unity.

For the two fast neutron groups of the illustrated simple PWR benchmark, the physical system is not optically thick enough to meet these criteria. For thermal neutron energies, one might expect much better accuracy. Thus,

the overall suitability of the SP_3 tree multigrid technique for reactor core calculations (e.g., criticality calculations) might still be adequate. The test case nevertheless emphasizes that the SP_3 approximation is not satisfactory for all problems. However, the tree multigrid technique is considered to be a very promising new method for neutron transport.

ACKNOWLEDGMENTS

I wish to thank Pekka Hiismäki (VTT) and Sauli Savolainen (Helsinki University Central Hospital) for their supervision. I especially wish to acknowledge Edward Larsen (University of Michigan) for his kind help and useful advice. I am also grateful to Pawel Simbierowicz (VTT) for many enlightening discussions. Funding from TEKES (Technology Development Centre, Finland) is also acknowledged.

REFERENCES

1. B. DAVISON, *Neutron Transport Theory*, Oxford University Press, London (1957).

2. E. M. GELBARD, "Application of Spherical Harmonics Methods to Reactor Problems," WAPD-BT-20, Bettis Atomic Power Laboratory (1960).

3. E. M. GELBARD, "Simplified Spherical Harmonics Equations and Their Use in Shielding Problems," WAPD-T-1182, Bettis Atomic Power Laboratory (1961).

4. E. M. GELBARD, "Applications of the Simplified Spherical Harmonics Equations in Spherical Geometry," WAPD-TM-294, Bettis Atomic Power Laboratory (1962).

5. E. W. LARSEN, J. E. MOREL, and J. M. McGHEE, "Asymptotic Derivation of the Multigroup P_1 and Simplified P_N Equations with Anisotropic Scattering," *Nucl. Sci. Eng.*, **123**, 328 (1996).

6. G. C. POMRANING, "Asymptotic and Variational Derivations of the Simplified P_N Equations," *Ann. Nucl. Energy*, **20**, 623 (1993).

7. P. S. BRANTLEY and E. W. LARSEN, "The Simplified P_3 Approximation," *Nucl. Sci. Eng.*, **134**, 1 (2000).

8. P. S. BRANTLEY and E. W. LARSEN, "Improved Iteration Strategy for the Simplified P_N Equations," *Trans. Am. Nucl. Soc.*, **75**, 129 (1996).

9. P. WESSELING, *An Introduction to Multigrid Methods*, Wiley, New York (1992).

10. C. GÁSPÁR and P. SIMBIEROWICZ, "Difference Schemes in Tree-Structured Multigrid Context," *Numerical Methods in Water Resources*, Vol. 1, p. 555, Elsevier Applied Science (1992).

11. J. H. CHENG, P. M. FINNIGAN, A. F. HATHAWAY, A. KELA, and W. J. SCHROEDER, "Quadtree/Octree Meshing with Adaptive Analysis," *Numerical Grid Generation in Computational Fluid Mechanics*, S. SENGUPTA, ed., Pineridge Press, Swansea, United Kingdom (1988).

12. W. A. RHOADES and R. L. CHILDS, "The DORT Two-Dimensional Discrete Ordinates Transport Code," *Nucl. Sci. Eng.*, **99**, 88 (1988).

PUBLICATION II

Application of the new MultiTrans SP_3 radiation transport code in BNCT dose planning

In: Medical Physics 2001. Vol. 28, pp. 1905–1910.

Application of the new MultiTrans SP_3 radiation transport code in BNCT dose planning

Petri Kotiluoto[a] and Pekka Hiismäki
VTT Chemical Technology, Industrial Physics, P.O. Box 1404, FIN-02044 VTT, Finland

Sauli Savolainen
Helsinki University Central Hospital, Departments of Laboratory Diagnostics and of Radiology, P.O. Box 380, FIN-00029 HUS, Finland

(Received 22 February 2001; accepted for publication 26 June 2001)

Dose planning in boron neutron capture therapy (BNCT) is a complex problem and requires sophisticated numerical methods. In the framework of the Finnish BNCT project, new deterministic three-dimensional radiation transport code MultiTrans SP_3 has been developed at VTT Chemical Technology, based on a novel application of the tree multigrid technique. To test the applicability of this new code in a realistic BNCT dose planning problem, cylindrical PMMA (polymethylmethacrylate) phantom was chosen as a benchmark case. It is a convenient benchmark, as it has been modeled by several different codes, including well-known DORT and MCNP. Extensive measured data also exist. In this paper, a comparison of the new MultiTrans SP_3 code with other methods is presented for the PMMA phantom case. Results show that the total neutron dose rate to ICRU adult brain calculated by the MultiTrans SP_3 code differs less than 4% in 2 cm depth in phantom (in thermal maximum) from the DORT calculation. Results also show that the calculated $^{197}Au(n,\gamma)$ and $^{55}Mn(n,\gamma)$ reaction rates in 2 cm depth in phantom differ less than 4% and 1% from the measured values, respectively. However, the photon dose calculated by the MultiTrans SP_3 code seems to be incorrect in this PMMA phantom case, which requires further studying. As expected, the deterministic MultiTrans SP_3 code is over an order of magnitude faster than stochastic Monte Carlo codes (with similar resolution), thus providing a very efficient tool for BNCT dose planning. [DOI: 10.1118/1.1397716]

Key words: BNCT, dose planning, radiation transport

I. INTRODUCTION

Boron neutron capture therapy (BNCT) has been mainly applied as a radiotherapy of malignant brain tumors,[1] such as glioblastoma multiforme (GBM). In recent years, clinical human trials utilizing epithermal neutron beams produced by nuclear reactors have been ongoing both in the USA and Europe. These ongoing trials can still be described as experimental, as recovering of patients from the GBM has not yet been achieved. At present the treatment response of the BNCT to the GBM seems to be as good (or insufficient) as with conventional radiotherapy, or with any other therapies under development, but in many aspects BNCT can be expected to be a useful treatment modality in the future.[2,3]

In BNCT the treatment effect is based on boron neutron capture phenomena in cancer cells. When epithermal neutrons in an energy range of 0.414-10 keV penetrate through the skull, they are moderated by the brain tissue to thermal energies below 0.414 keV. When a thermal neutron hits boron isotope ^{10}B, there is always a certain probability for a neutron capture. In the neutron capture the ^{10}B isotope splits in two smaller nuclei in a nuclear reaction, namely in ^{7}Li and an α-particle. These relatively heavy particles have a nominal distance of flight of about a few μm, in which they release all there kinetic energy of about 2.5 MeV. These high-LET particles cause very much biological damage in the range of one or two cells. By having some appropriate boron carrier that selectively accumulates into cancer cells, the radiation damage caused by boron neutron capture can thus in principle be chemically targeted almost entirely to the tumor cells.[2–4]

In practice the total dose in BNCT consists of several different dose components.[5–10] For instance, in the boron neutron capture reaction gamma radiation with 478 keV energy is also released. Also hydrogen and nitrogen, that are natural compounds both in soft and brain tissue, capture neutrons—hydrogen with 2.2 MeV gamma radiation release and nitrogen with 0.6 MeV proton release. It should also be noted that whenever a nuclear reactor is used as a neutron source, the energy spectrum of neutrons is not purely epithermal: some thermal and fast neutron radiation (inducing the proton recoil dose from hydrogen), and in fact also gamma radiation, always exist in the primary beam. The so called epithermal beams produced by nuclear reactors, like FiR 1 in Finland,[11,12] are actually mixed beams.

Radiation transport and dose distribution calculations in BNCT are much more complicated than in conventional radiotherapy, where rather simple convolution methods with measured pencil beam kernels can be utilized.[13] The calculation of neutron and photon flux in BNCT is a complex problem and requires sophisticated deterministic or stochastic simulation methods.

In BNCT treatment planning stochastic Monte Carlo

methods are most common. Monte Carlo methods can be considered to be very dependable, but are often also very time-consuming. In the framework of the Finnish BNCT project, a novel MultiTrans SP_3 radiation transport code has been developed at VTT Chemical Technology, based on the efficient deterministic tree multigrid technique.[14]

In this paper, a first comparison of the MultiTrans SP_3 code to other methods is reported for a realistic BNCT dose planning problem.

II. MATERIALS AND METHODS

Diffusion (P_1) theory is a well-known approximation for radiation transport, but is unsatisfactory in many cases. The so called Simplified P_3 (SP_3) approximation[14,15] produces much more transport-like solutions with only slightly higher computational costs over diffusion theory. Simplified P_3 approximation is based on expanding flux in spherical harmonics in one-dimensional planar geometry and then generalizing the resulting transport equations to higher-dimensions. The approximation was first proposed by Gelbard in the early 1960s.[16] The theoretical basis of the SP_N approximations (N being the order of the expansion in spherical harmonics) have been historically weak. Only recently it has been shown by Brantley and Larsen[15] that SP_3 equations with boundary conditions can be derived from the variational principle for an inhomogeneous medium with multi-group anisotropic scattering.

In the novel MultiTrans SP_3 code developed at VTT Chemical Technology, SP_3 transport approximation has been combined with the extremely efficient numerical tree multigrid technique.[14] This new method enables a high-speed iterative solution of complicated three-dimensional radiation transport problems with normal desktop computers.

Practical multigrid[17] methods were first introduced by Brandt[18] in the 1970s. These methods can solve partial differential equations discretized on N grid points in $O(N)$ operations. For example Gauss-elimination would require $O(N^2)$ operations, and even ''rapid'' direct elliptic solvers require $O(N \log N)$ operations for solving elliptic equations. Thus, the multigrid method is very efficient for large problems (the number of grid points N being large).

The efficiency of the multigrid methods is based on discretizing the original problem on coarser and finer grids, i.e., with different mesh sizes. The multigrid is formed by nested grids with a refined mesh size. On a coarse grid, much less iterations are required to obtain a converged solution. These coarse solutions can be interpolated into finer grids, and thus be used to accelerate the iteration process of the fine-grid solutions. In the multigrid methods data is transferred both from coarser grids to finer grids, and backwards, in so called multigrid cycles.[14,17]

In the traditional multigrid method, uniform mesh size is used on all grid levels. The number of grid points can become huge for large three-dimensional problems, and the amount of required computer work can still be very demanding. In the tree multigrid technique the iteration procedure is further accelerated by using self-adaptive features of the grid generating procedure. That is: the mesh is refined only when required from computational or geometric reasons, e.g., at the interface of different materials—otherwise a much coarser mesh is used. This approach leads to nonuniform, nonequidistant mesh and makes the discretizing of the problem more complicated. However, it enables the number of grid points to be modest even for large three-dimensional problems, and among the multigrid acceleration forms the basis for the extremely efficient solver of the SP_3 radiation transport equations.[14]

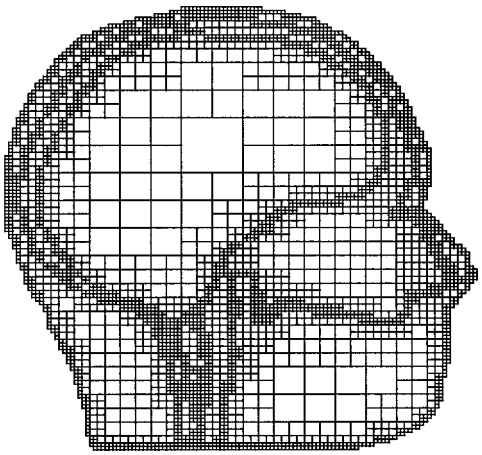

FIG. 1. Cross section of an octree grid representing a human head.

In the MultiTrans SP_3 code, the so called octree grid is generated by a recursive subdivision procedure with a conditional subdivision of each cell into eight children cells. The ratio of sizes of any adjacent cells is restricted to be at most 2, which makes the grid regular. The regular octree grid can be generated directly from stereolitography (STL) files, which can be exported from practically all CAD-systems. The geometry input is thus very easy. The octree-grid can also be easily generated from segmented CT or MRI images (Fig. 1). This enables the application of the tree multigrid technique to BNCT treatment planning.

The new MultiTrans SP_3 code requires naturally thorough testing. To test the applicability of the MultiTrans SP_3 code to BNCT dose planning, a cylindrical PMMA (polymethylmethacrylate) phantom with 20 cm diameter and 24 cm length was chosen as a benchmark. This phantom has served as a reference phantom in the dosimetric campaign for characterization of the FiR 1 epithermal beam.[19,20] The 14 cm beam aperture diameter (from 8, 11, 14, 17 and 20 cm options) was chosen for the source plane definition, as this aperture size has most often been utilized in patient irradiations at FiR 1.

The source plane used in treatment planning for the 14 cm beam aperture is situated 5 cm inwards the beam direction into FiR 1 collimator structures. The averaged group intensity and group angular dependency of the flux have been defined in 47 neutron and 20 gamma groups of the BUGLE broad energy group structure.[21,22] The source is homogenized and has an 11 cm radius. Source calculations have been performed by Tiina Seppälä[23,24] using the DORT[25] code with a

forward-biased quadrature set (D_{166}) and a BUGLE-80 cross section library.[21] Calculations include models of the FiR 1 reactor core, Fluental™ moderator ($Al+AlF_3$ composite), and the collimator structures with a water phantom situated into the beam (in order to consider back-scattering effects correctly).

For the MultiTrans SP_3 code, the first collision source method was used in source processing. In the first collision source method the intrinsic uncollided flux (the flux of neutrons that have undergone zero collisions) is solved from the incident boundary flux analytically. This uncollided flux is then used to generate the intrinsic source terms for the collided flux. The collided flux can be solved by the tree multigrid technique with vacuum boundary conditions. Total flux is then calculated as a sum of the collided and uncollided flux for each energy group. The reason for this procedure is that the collided flux is much more isotropic than the uncollided flux, and can thus be better approximated by a low-order spherical harmonics expansion.

It should be noted, however, that the source terms emerging from the intrinsic uncollided flux cannot be approximated by a simple isotropic source term: all moment terms of the spherical harmonics expansion of the source are needed instead. Normally these anisotropic source terms are not used,[14,15] which applies well for fission sources, for instance. Also isotropic group-to-group scattering is a common assumption in multi-group diffusion theory, but cannot be applied in the BNCT case where the beam has an obvious direction. Thus, the anisotropic source terms were added into SP_3 equations in order to take into account both the anisotropic first collision source and the anisotropic group-to-group scattering correctly.

The PMMA phantom is a very convenient benchmark, as it has been modeled by several different codes, including DORT,[25] MCNP4B[26] and the BNCT treatment planning system SERA (http://esus.cs.montana.edu/~bnct/manual/sec00.html).[27] In the PMMA phantom epithermal flux is thermalized, thermal maximum being about 2 cm depth in the phantom. This thermal flux has been characterized by using activation foil detectors, for instance. Gold and manganese have been the main activation elements in diluted aluminum foils (with 1 wt.% ^{197}Au or ^{55}Mn isotope) used for phantom measurements. After an irradiation the activated foils are measured with a spectrometer in order to count the gold and manganese saturation activities. The $^{197}Au(n,\gamma)$ and $^{55}Mn(n,\gamma)$ reaction rates can also be evaluated from the calculated group fluxes using corresponding response cross sections. This allows a direct comparison of the neutron transport calculations to the foil activation measurements.

A multiTrans SP_3 code can read both BUGLE-80 and BUGLE-96 cross section libraries.[21,22] In the calculations reported in this paper, the older BUGLE-80 library was used (though the newer version BUGLE-96 is recommended) in order to enable a pure computational comparison of the calculations by the MultiTrans SP_3 code with the former calculations by DORT. Thus the macroscopic transport cross sections for the PMMA were generated from the BUGLE-80 cross section library using corresponding material coefficients defined by ICRU.[28]

In MCNP4B calculations the standard ENDF/B-VI cross section library[29] (distributed along the MCNP4B code package) was used. SERA uses its own condensed cross section data library (with 94 neutron groups) based on Evaluated Nuclear Data Files (ENDF/B) and other sources.

III. NUMERICAL RESULTS

Group fluxes were calculated in the PMMA phantom with a MultiTrans SP_3 code. The first collision source was analytically calculated from the treatment planning source plane.[23,24] Transport cross sections were derived from the BUGLE-80 cross section library.[21] A calculation of the group fluxes in 47 neutron groups with a MultiTrans SP_3 code took 14 minutes with a normal desktop PC with 200 MHz Pentium processor and 128 Mb memory, with the minimum octree cell side length being 0.38 cm. MCNP4B and SERA calcu-

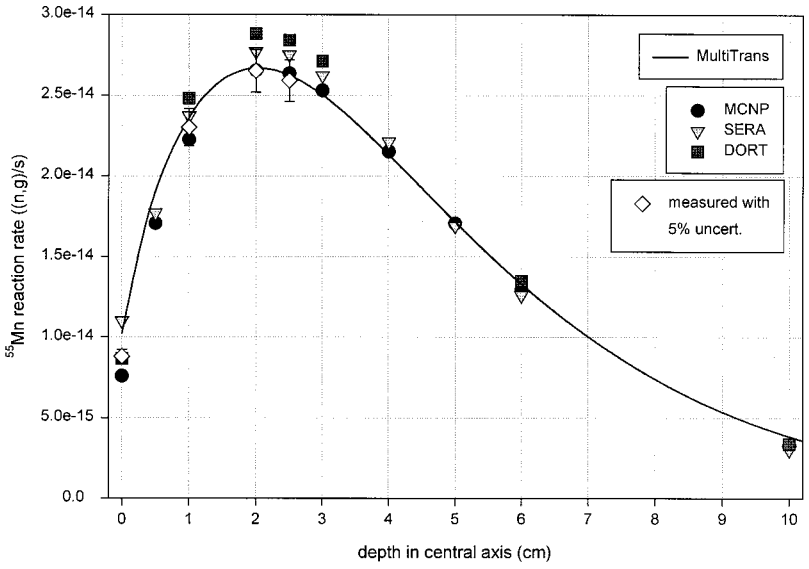

FIG. 2. Calculated and measured depth curves of the $^{55}Mn(n,\gamma)$ reaction rate in the central axis of the cylindrical PMMA phantom, with a 14 cm FiR 1 epithermal beam.

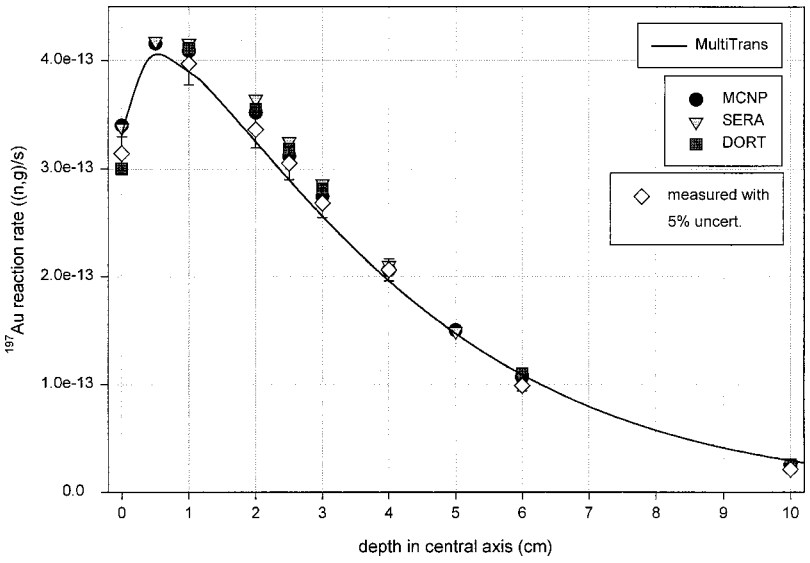

FIG. 3. Calculated and measured depth curves of the $^{197}\mathrm{Au}(n,\gamma)$ reaction rate in the central axis of the cylindrical PMMA phantom, with a 14 cm FiR 1 epithermal beam.

lations were performed on Sun Ultra60 SPARC station. MCNP4B was run for five days, resulting in over 150 million particle histories with reliable statistics. With SERA, 10 million particle histories were simulated in about one hour CPU time. Normally in treatment planning with SERA, 2 million particle histories are considered to produce sufficient statistics. The statistical uncertainty in Monte Carlo methods (including SERA) is directly proportional to tally size: SERA uses 1 cm^3 voxels for tallying. It should be noted that SERA calculations with resolution comparable to a minimum octree cell side length of 0.38 cm would require approximately 18 times longer running time to produce similar statistics than calculations with 1 cm^3 tally size.

The $^{55}\mathrm{Mn}(n,\gamma)$ and $^{197}\mathrm{Au}(n,\gamma)$ reaction rates were calculated from the group fluxes by using IRDF-90 dosimetry cross sections[30] condensed into the BUGLE group structure with the program FLXPRO from the LSL-M2 package.[31] The calculated $^{55}\mathrm{Mn}(n,\gamma)$ and $^{197}\mathrm{Au}(n,\gamma)$ reaction rates in the central axis of the PMMA phantom with a comparison to measurements and calculated results by MCNP4B, SERA and DORT are presented in Figs. 2 and 3. In the MCNP and the SERA calculations, as well as in the calculations by the MultiTrans SP_3 code, the same unscaled treatment planning source has been used, i.e., the source has been derived directly from the DORT calculations. It should be noted that for the treatment planning procedure, source intensity has been adjusted for SERA, based on activation foil measurements. An unscaled source has been used here only to enable a pure computational comparison, and the SERA results presented in this paper do not necessarily correlate to the final accuracy of the treatment planning procedure at the Finnish BNCT facility. This comparison shows, however, that the $^{197}\mathrm{Au}(n,\gamma)$ reaction rate calculated by the MultiTrans SP_3 code in 2 cm depth in phantom (in thermal maximum) differs from the measured value 3%, as the MCNP and SERA calculations differ 5% and 8% from the measured reaction rate, respectively. Correspondingly the $^{55}\mathrm{Mn}(n,\gamma)$ reaction rate in the thermal maximum calculated by the MultiTrans SP_3 code differs less than 1% from the measured value, as the MCNP and SERA calculations differ less than 1% and 5% from the measured $^{55}\mathrm{Mn}(n,\gamma)$ reaction rate, respectively. The measurement uncertainty for both $^{197}\mathrm{Au}(n,\gamma)$ and $^{55}\mathrm{Mn}(n,\gamma)$ reaction rates is approximated to be 5%.

From the comparison codes, MCNP can be considered most dependable as it is based on well-established and generally reliable stochastic simulation methods. When calculated results by MultiTrans SP_3 and MCNP are compared, it seems that MultiTrans SP_3 underestimates the calculated $^{197}\mathrm{Au}(n,\gamma)$ reaction rate at depths 1–3 cm up to 8%, but is in fairly good agreement within 1% with the $^{55}\mathrm{Mn}(n,\gamma)$ reaction rate at depths 2–3 cm calculated by MCNP. The results given by different comparison codes differ somewhat from each other, which is most likely due to different radiation transport methods.

It should be noted, that at the surface of the phantom (in 0 cm depth) a discrepancy between calculations and measurements exist. This is especially true for $^{55}\mathrm{Mn}(n,\gamma)$ reaction

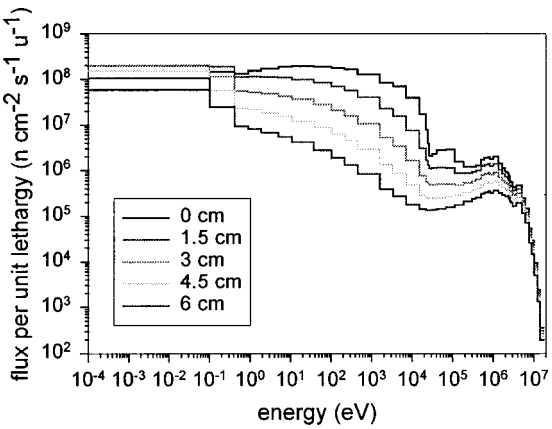

FIG. 4. Neutron spectra calculated with a MultiTrans SP_3 code at different depths in the central axis of the cylindrical PMMA phantom, with a 14 cm FiR 1 epithermal beam.

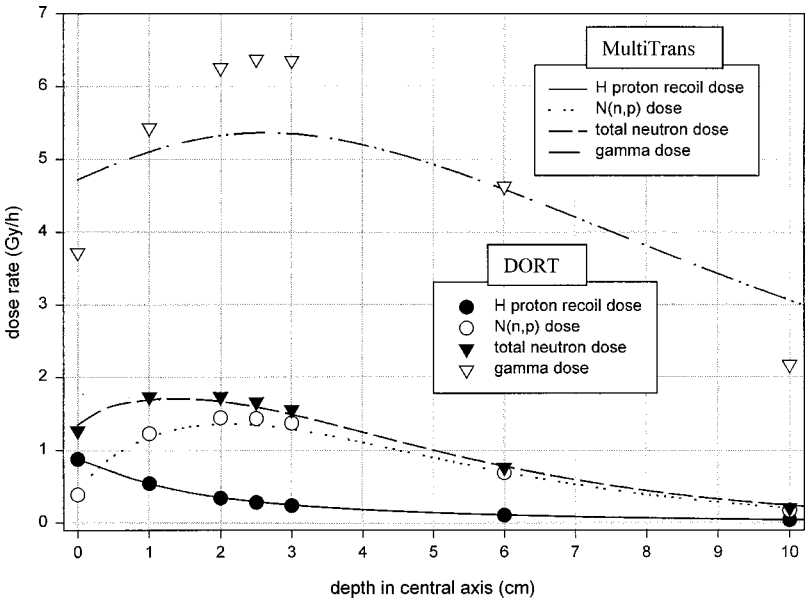

FIG. 5. Calculated dose rates to ICRU adult brain in central axis of the cylindrical PMMA phantom, with a 14 cm FiR 1 epithermal beam.

rate: a MultiTrans SP_3 calculation differs 16%, MCNP calculation 14%, and SERA calculation 25% compared to the measured $^{55}Mn(n,\gamma)$ reaction rate at the surface of the phantom.

One reason why SERA overestimate the reaction rate at the void interface might be in 1 cm^3 tally voxel size. Thus, the value is an average over the volume at the interface, not a value at a specific point. With MCNP, on the other hand, the first (0 cm depth) tally with actual dimensions of the activation foil has been defined into the void area (at the PMMA phantom surface). The reason why MCNP underestimates the reaction rate might be for instance in the source plane description, e.g., the incident thermal flux is somewhat higher in reality.

In the MultiTrans SP_3 calculation, no void area has been defined, and the surface (0 cm depth) value can only be interpolated from the values inside the phantom. This can cause the overestimation of the reaction rate at the surface, in a similar fashion with SERA. Another possible explanation for the overestimation of the reaction rate at the void surface is in the Marshak-like vacuum boundary condition used with a SP_3 approximation.[14,15] It is a well-known fact that with a spherical harmonics method in general, no exact free surface boundary condition can be determined.[32]

In Fig. 4 the neutron spectra calculated by the MultiTrans SP_3 code is presented at different depths in the PMMA phantom. Using corresponding conversion factors, the hydrogen proton recoil dose rate, nitrogen $N(n,p)$ dose rate and total neutron dose rate have been calculated from the spectra for the ICRU adult brain,[33] both with DORT and MultiTrans SP_3 codes. Also the gamma dose rate has been calculated by both codes. A comparison of the different dose rate components calculated by DORT and MultiTrans SP_3 codes in the central axis of the PMMA phantom is presented in Fig. 5. According to ICRU Report 24, an accuracy of $\pm 5\%$ in the delivery of an absorbed dose to a target volume is required.[34] The neutron dose rate calculated by DORT and MultiTrans SP_3 agree within 4% in 2 cm depth in thermal maximum, and differ less than 14% in 10 cm depth. However, the gamma dose rate calculated by the MultiTrans SP_3 code has a notable discrepancy compared to the DORT calculation. It should be noted that the gamma dose distribution calculated by DORT has been verified with ionization chamber measurements.[10] The MultiTrans SP_3 code seems to produce a much too flat gamma dose distribution, compared to the correct one.

The main component of the gamma dose arises from 2.2 MeV photons induced by hydrogen neutron capture. The mean free path of such photons is approximately 19 cm: for such photons the transport problem might not be optically thick enough for a valid SP_3 approximation, and this could cause the discrepancy. Another possible explanation might be some mistake in the code performance, for example with the photon cross sections, or some problem with the boundary conditions (with photons). However, as the gamma dose is the major component of the overall BNCT dose distribution, this problem definitely requires further studying.

IV. CONCLUSIONS

The results show that in the chosen BNCT phantom benchmark, the total neutron dose rate to the ICRU adult brain calculated by the MultiTrans SP_3 code differs less than 4% in 2 cm depth in phantom (in thermal maximum) from the DORT calculation. Results also show that the calculated $^{197}Au(n,\gamma)$ and $^{55}Mn(n,\gamma)$ reaction rates in thermal maximum differ less than 4% and 1% from the measured values, respectively, and are within the measurement uncertainty. As expected, the deterministic MultiTrans SP_3 code is over an order of magnitude faster than Monte Carlo codes (with similar resolution), thus providing a very efficient new tool for BNCT dose planning. At present, however, the gamma dose component calculated by the MultiTrans SP_3 code is not satisfactory, and requires further studying.

ACKNOWLEDGMENTS

Authors acknowledge the financial support from Tekes, the National Technology Agency of Finland (granted to Petri Kotiluoto and Pekka Hiismäki) and the financial support from Academy of Finland (granted to Sauli Savolainen).

[a]Electronic mail: petri.kotiluoto@vtt.fi

[1] B. Larsson, J. Grawford, and R. Weinreich, in *Advances in Neutron Capture Therapy*, Excerpta Medica, International Congress Series 1132 (Elsevier Science B.V., Amsterdam, 1998), Vols. 1 and 2.

[2] R. F. Barth, A. H. Soloway, J. H. Goodman, R. A. Gahbauer, N. Gupta, T. E. Blue, W. Yang, and W. Tjarks, ''Boron neutron capture therapy of brain tumors: an emerging therapeutic modality,'' Neurosurgery **44**, 433–451 (1999).

[3] R. F. Barth, A. H. Soloway, R. G. Fairchild, and R. M. Brugger, ''Boron neutron capture therapy for cancer. Realities and prospects,'' Cancer (N.Y.) **70**, 2995–3007 (1992).

[4] D. N. Slatkin, ''A history of boron neutron capture therapy of brain tumors,'' Brain **114**, 1609–1629 (1991).

[5] R. D. Rogus, O. K. Harling, and J. C. Yanch, ''Mixed field dosimetry of epithermal neutron beams for boron neutron capture therapy at the MITR-II research reactor,'' Med. Phys. **21**, 1611–1625 (1994).

[6] C. P. J. Raaijmakers and M. W. Konijnenberg, ''Determination of dose components in phantoms irradiated with an epithermal neutron beam for boron neutron capture therapy,'' Med. Phys. **22**, 321–329 (1995).

[7] C. Aschan, M. Toivonen, S. Savolainen, T. Seppälä, and I. Auterinen, ''Epithermal neutron beam dosimetry with thermoluminescence dosemeters for boron neutron capture therapy,'' Radiat. Prot. Dosim. **81**, 47–56 (1999).

[8] A. Kosunen, M. Kortesniemi, H. Ylä-Mella, T. Seppälä, J. Lampinen, T. Serén, I. Auterinen, H. Järvinen, and S. Savolainen, ''Twin ionisation chambers for dose determinations in phantom in an epithermal neutron beam,'' Radiat. Prot. Dosim. **81**, 187–194 (1999).

[9] S. Savolainen, I. Auterinen, C. Aschan, P. Hiismäki, M. Kortesniemi, A. Kosunen, P. Kotiluoto, J. Lampinen, T. Seppälä, T. Serén, V. Tanner, and M. Toivonen, ''Dosimetry chain for the treatments of glioma patients in the epithermal neutron beam at the Finnish BNCT facility (FiR 1),'' Med. Biol. Eng. Comput. **37**, 388–389 (1999).

[10] M. Kortesniemi, A. Kosunen, C. Aschan, T. Serén, P. Kotiluoto, M. Toivonen, P. Välimäki, T. Seppälä, I. Auterinen, and S. Savolainen, ''Measurements of phantom dose distributions at the Finnish BNCT facility,'' in *Frontiers in Neutron Capture Therapy*, edited by M. F. Hawthorne, K. Shelly, and R. J. Wiersema (Plenum, New York, 2000).

[11] I. Auterinen, C. Aschan, P. Hiismäki, M. Kortesniemi, A. Kosunen, P. Kotiluoto, J. Lampinen, R. Rosenberg, S. Salmenhaara, S. Savolainen, T. Seppälä, T. Serén, V. Tanner, M. Toivonen, and P. Välimäki, ''Metamorphosis of a 35 years old Triga reactor into a modern BNCT facility,'' in Ref. 10.

[12] I. Auterinen, P. Hiismäki, P. Kotiluoto, R. Rosenberg, S. Salmenhaara, T. Seppälä, T. Serén, C. Aschan, M. Kortesniemi, A. Kosunen, J. Lampinen, S. Savolainen, M. Toivonen, and P. Välimäki, ''The new boron neutron capture therapy facility at the Finnish nuclear research reactor (FiR 1),'' Med. Biol. Eng. Comput. **37**, 398–399 (1999).

[13] A. T. Redpath, J. R. Williams, and D. I. Thwaites, ''Treatment planning for external beam therapy,'' in *Radiotherapy Physics*, edited by J. R. Williams and D. I. Thwaites (Oxford University Press, Oxford, 1993), pp. 135–185.

[14] P. Kotiluoto, ''Fast tree multigrid transport application for the simplified P_3 approximation,'' Nucl. Sci. Eng. **138**, 269–278 (2001).

[15] P. S. Brantley and E. W. Larsen, ''The simplified P_N approximation,'' Nucl. Sci. Eng. **134**, 1–21 (2000).

[16] E. M. Gelbard, ''Application of spherical harmonics methods to reactor problems,'' WAPD-BT-20, Bettis Atomic Power Laboratory, 1960.

[17] P. Wesseling, *An Introduction to Multigrid Methods* (Wiley, New York, 1992).

[18] A. Brandt, ''Multi-level adaptive solutions to boundary-value problems,'' Math. Comput. **31**, 333–390 (1977).

[19] T. Serén, M. Kortesniemi, C. Aschan, T. Seppälä, J. Lampinen, I. Auterinen, and S. Savolainen, ''A tale of two beams—Comparison of the radiation fields at the BMRR and FiR 1 epithermal BNCT facilities,'' Med. Biol. Eng. Comput. **37**, 396–397 (1999).

[20] T. Serén, I. Auterinen, T. Seppälä, and P. Kotiluoto, ''Spectrum measurements and calculations in the epithermal neutron beam at the FiR 1 BNCT facility,'' *15th European TRIGA Conference*, Espoo, Finland, 15–17, June 1989, pp. 167–179.

[21] R. W. Roussin, ''BUGLE-80 coupled 47-neutron, 20 gamma-ray P3 cross section library,'' DLC-75, Radiation Shielding Information Center, 1980.

[22] J. E. White, D. T. Ingersoll, R. Q. Wright, H. T. Hunter, C. O. Slater, N. M. Greene, R. E. MacFarlane, and R. W. Roussin, ''Production and testing of the revised VITAMIN-B6 fine-group and the BUGLE-96 broad-group neutron/photon cross-section libraries derived from ENDF/B-VI.3 nuclear data,'' ORNL-6795, R1, NUREG/CR-6214, 1995.

[23] T. Seppälä, T. Serén, and I. Auterinen, ''Source characterisation for the rtt_MC treatment planning program at FiR 1,'' in Ref. 10.

[24] T. Seppälä, M. Kortesniemi, L. Kankaanranta, J. Perkiö, I. Auterinen, and S. Savolainen, ''Aspects of dose planning and patient positioning for BNC-treatment at FiR 1,'' Med. Biol. Eng. Comput. **37**, 402–403 (1999).

[25] W. A. Rhoades and R. L. Childs, ''The DORT two-dimensional discrete ordinates transport code,'' Nucl. Sci. Eng. **99**, 88 (1988).

[26] J. F. Briesmeister, in ''MCNP—A General Monte Carlo *N*-particle transport code, Version 4B,'' LA-12625-M, Los Alamos National Laboratory, 1997.

[27] F. J. Wheeler, ''Radiation transport in tissue by Monte Carlo,'' EGG-BNCT-11178, 1994.

[28] ICRU Report 44, ''Tissue substitutes in radiation dosimetry and measurement,'' International Commission on Radiation Units and Measurements, 1989.

[29] J. S. Hendricks, S. C. Frankle, and J. D. Court, ''ENDF/B-VI Data for MCNP,'' LA-12891, 1994.

[30] N. P. Kocherov and P. K. McLaughlin, ''The international reactor dosimetry file (IRDF-90),'' IAEA-NDS-141, Rev. 2, 1993.

[31] F. W. Stallmann, ''LSL-M2: A computer program for least-squares logarithmic adjustment of neutron spectra,'' NUREG/CR-4349, ORNL/TM-9933, 1986.

[32] B. Davison, *Neutron Transport Theory* (Oxford University Press, London, 1957).

[33] ICRU Report 46, ''Photon, electron, proton and neutron interaction data for body tissues,'' International Commission on Radiation Units and Measurements, 1992.

[34] ICRU Report 24, ''Determination of absorbed dose in a patient irradiated by beams of x or gamma rays in radiotherapy,'' International Commission on Radiation Units and Measurements, 1976.

PUBLICATION III

Application of the new MultiTrans SP_3 radiation transport code in criticality problems and potential use in dosimetry

In: Wagemans, J., Abderrahim, H. A., D'hondt, P. and De Raedt, C. (Eds.). Reactor Dosimetry in the 21st Century. 2003. Singapore: World Scientific. Pp. 580–587.

APPLICATION OF THE NEW MULTITRANS SP_3 RADIATION TRANSPORT CODE IN CRITICALITY PROBLEMS AND POTENTIAL USE IN DOSIMETRY

Petri Kotiluoto
VTT Processes, VTT Technical Research Centre of Finland, P.O.B 1608
Espoo, FIN-02044 VTT, Finland
E-mail: petri.kotiluoto@vtt.fi

ABSTRACT

In the novel MultiTrans SP_3 radiation transport code the advanced tree multigrid technique is applied to the simplified P_3 (SP_3) transport approximation. The tree multigrid is generated directly from stereolitography (STL) files exported by computer-aided design (CAD) systems, thus allowing an easy interface for construction and upgrading of the geometry. The deterministic MultiTrans code allows fast solution of complicated three-dimensional transport problems in detail, offering a new tool for calculation of quantities of dosimetric interest. In order to determine the feasibility of a new code, computational benchmarks need to be carried out. In this paper, an application of the MultiTrans code to criticality problem is for the first time reported.

1. Introduction

Computer simulated spectra and other calculated quantities are always required as a complement to various dosimetric methods. Measurements are often restricted to specific locations, whereas particular interest might be in an area that cannot be reached directly by the detector (e.g., inside a pressure vessel). Also, in order to estimate the neutron energy-spectrum, it is often necessary to combine measured data with calculations. Computer programs for radiation transport are based either on deterministic solution of the Boltzmann transport equation or on stochastic simulation (i.e., Monte Carlo method). The Monte Carlo method is extremely time consuming and often cannot present all radiation distribution details. Deterministic methods are more efficient for solving radiation transport problems, but in practice they often require approximations.

The spherical harmonics P_N approximation is well-established for the Boltzmann radiation transport equation [1]. However, the three-dimensional P_N equations are very complicated. Gelbard proposed in 1960 a simplification for the P_N equations [2]. These simplified P_N (SP_N) equations have historically been viewed with suspicion, as the original derivation of the equations by Gelbard was theoretically weak. Only recently have SP_N equations had asymptotic and variational derivations, thus giving them a solid theoretical base [3,4].

In order to solve elliptic differential equations (such as SP_N equations, which are composed of a coupled set of diffusion like equations) efficiently in three-dimensions, fast iterative methods are required. A new deterministic MultiTrans SP_3 radiation transport code has been developed at VTT [5,6]. It is based on a combination of the advanced tree multigrid technique and the simplified P_3 (SP_3) transport approximation.

The MultiTrans code has been applied, for instance, to a simplistic two-group PWR benchmark with a fixed source [5], and to phantom dose calculations in the Finnish boron neutron capture therapy (BNCT) project [6]. In the latter case, the BUGLE-96 cross section library [7] was used in the calculation of the neutron and photon flux in a phantom. Also gold and manganese activation reaction rates were calculated for direct comparison with dosimetric measurements, showing good agreement [6]. MultiTrans can also read coupled electron-photon cross sections created by the CEPXS code [8], and has a mixing capability for creating compound material cross sections from either the BUGLE-96 library or from the CEPXS generated cross sections.

Any new code requires thorough testing and benchmarking. Until now MultiTrans has been tested only on problems with fixed source. Implementation of an outer source iteration method for multiplication eigenvalue problems has been a distinct objective. Two test cases were chosen from the proposal of 3-D neutron transport benchmarks by the Osaka University to NEACRP [9,10]. The first one is a small LWR with a core model of Kyoto University Critical Assembly (KUCA), and the second one is a small FBR.

2. Materials and Methods

2.1. Theoretical background

In the MultiTrans code the SP_3 radiation transport approximation is used. SP_3 equations form a coupled set of two second-order elliptic differential equations [3,4]. If one defines the unknown

$$\hat{\Phi}_0(\vec{r}) \equiv \Phi_0(\vec{r}) + 2\Phi_2(\vec{r}) \tag{1}$$

where $\Phi_0(\vec{r})$ is the scalar flux and $\Phi_2(\vec{r})$ is the P_2 moment term, the SP_3 equations in matrix form (with superscript i as a material and superscript g as an energy group index) are

$$\begin{bmatrix} -D_0\nabla^2 + \sigma_{a0} & -2\sigma_{a0} \\ -\frac{2}{5}\sigma_{a0} & -D_2\nabla^2 + \sigma_{a2} + \frac{4}{5}\sigma_{a0} \end{bmatrix}^{i,g} \begin{bmatrix} \hat{\Phi}_0 \\ \Phi_2 \end{bmatrix}^{i,g} = S^{i,g} \begin{bmatrix} 1 \\ -\frac{2}{5} \end{bmatrix}, \tag{2}$$

where the transport cross sections are defined by subtraction of the corresponding Legendre component of the scattering cross section from the total cross section:

$$\sigma_{an}^{i,g} = \sigma_t^{i,g} - \sigma_{sn}^{i,g->g} \quad , \; n \geq 0 \quad . \tag{3}$$

The diffusion coefficients are defined by transport cross sections as

$$D_0^{i,g} = \frac{1}{3\sigma_{a1}^{i,g}} \quad , \tag{4}$$

and

$$D_2^{i,g} = \frac{9}{35\sigma_{a3}^{i,g}} \quad . \tag{5}$$

The group source in Eq. (2) is defined as

$$S^{i,g}(\vec{r}) = \sum_{g'=1, g' \neq g}^{G} \sigma_{s0}^{i,g'->g} \Phi_0^{g'}(\vec{r}) + \frac{\chi^g}{k} \sum_{g'=1}^{G} \nu^{g'} \sigma_f^{i,g'} \Phi_0^{g'}(\vec{r}) \tag{6}$$

using standard multi-group neutronics notation. The source includes group-to-group scattering terms and the fission source

$$S_f(\vec{r}) = \sum_{g'=1}^{G} \nu^{g'} \sigma_f^{i,g'} \Phi_0^{g'}(\vec{r}) \quad . \tag{7}$$

In the multigrid solution technique, the iteration procedure is accelerated by first solving the problem on a coarser grid and then transferring data to finer grids, and vice versa, in so-called multigrid cycles [11]. In the tree multigrid technique, an adaptive subdivision procedure enables refinement of the calculation grid on material surfaces (see Fig. 2 for example) or by computational demand. The tree-structure enables the modelling of complicated geometries and surfaces accurately with only a limited number of mesh cells.

The three-dimensional octree grid, utilised in the MultiTrans code, is generated directly from stereolitography (STL) files which can be exported from practically all computer-aided design (CAD) systems. The adaptive tree structure leads to non-equidistant meshes, and a proper difference scheme for estimating the derivatives has to be applied. In the MultiTrans code the tree multigrid technique has been used to solve the SP_3 approximation by estimating the Laplace operators in Eq. (2) by an integrated difference scheme [5,12].

The multiplication eigenvalue for criticality problems is solved by the MultiTrans code with an algorithm similar to the standard source iteration method for multigroup diffusion equations. First, some initial guess for the fission source and the multiplication eigenvalue is set. Next, all the moment terms of the multigroup SP_3 equations are solved iteratively with the tree multigrid technique, by starting from the highest energy group and proceeding towards the lowest. Having done so, a new fission source

$$S_f^{(1)}(\vec{r}) = \sum_{g'=1}^{G} \nu^{g'} \sigma_f^{i,g'} \Phi_0^{g'(1)}(\vec{r}) \tag{8}$$

and a new multiplication eigenvalue

$$k^{(1)} = \frac{\int S_f^{(1)}(\vec{r}) d^3 r}{\frac{1}{k^{(0)}} \int S_f^{(0)}(\vec{r}) d^3 r} \tag{9}$$

are calculated, and a new sweep for solving the multigroup SP_3 equations is started. The whole procedure is repeated until the multiplication eigenvalue or the fission source converge. It is assumed that there is no upscattering. The convergence criterion is defined as

$$\left| \frac{k^{(n)} - k^{(n-1)}}{k^{(n)}} \right| < \varepsilon_1 \qquad \text{and/or} \qquad \max \left| \frac{S_f^{(n)} - S_f^{(n-1)}}{S_f^{(n)}} \right| < \varepsilon_2 \quad . \tag{10}$$

After the group flux values have been solved, it is possible to calculate dosimetric quantities of interest by simply multiplying the group flux values by corresponding dosimetry cross sections, derived for instance from the IRDF-90 library [13]. The accuracy of the method depends on the broad energy group structure, the accuracy of the calculated group flux values, the weighting technique used for deriving broad energy group cross sections, and the uncertainty of the basic transport and dosimetry cross sections.

2.2. Numerical benchmarks

The first chosen benchmark (Fig. 1) is a small 2-group LWR, labelled as model 1. Two cases have been considered: control rod position empty (case 1) and control rod inserted (case 2). The second chosen benchmark (Fig. 3) is a small 4-group FBR, labelled as model 2. Two cases have been considered also in this second benchmark, with control rod position filled with Na (case 1) and with control rod half-inserted (case 2). The details of the problems are not repeated here: an interested reader can find e.g. the multigroup cross sections either in the proposal or in the compilation report of the NEACRP 3-D neutron transport benchmarks [9,10]. The three-dimensional tree multigrid (octree grid) used in MultiTrans calculations is generated directly from STL-files exported from a CAD-model. Horizontal and vertical cross sections of the octree grids of the models are shown in Figs. 2 and 4.

In numerical calculations by the MultiTrans code, a convergence criterion for the k_{eff} value Eq. (10) has been set to ε_1=1e-4.

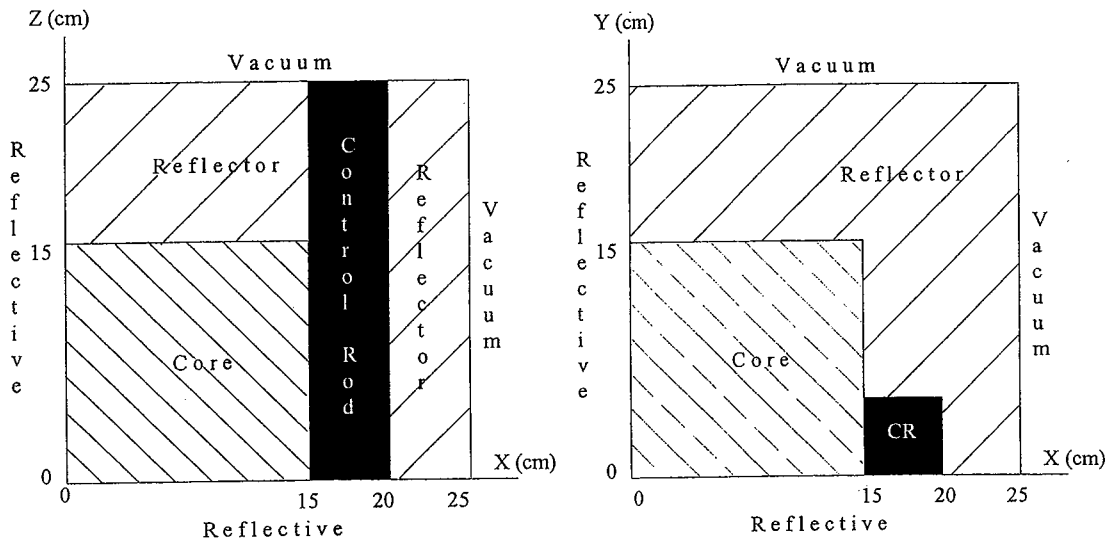

Fig. 1. Vertical and horizontal cross sections of small LWR benchmark.

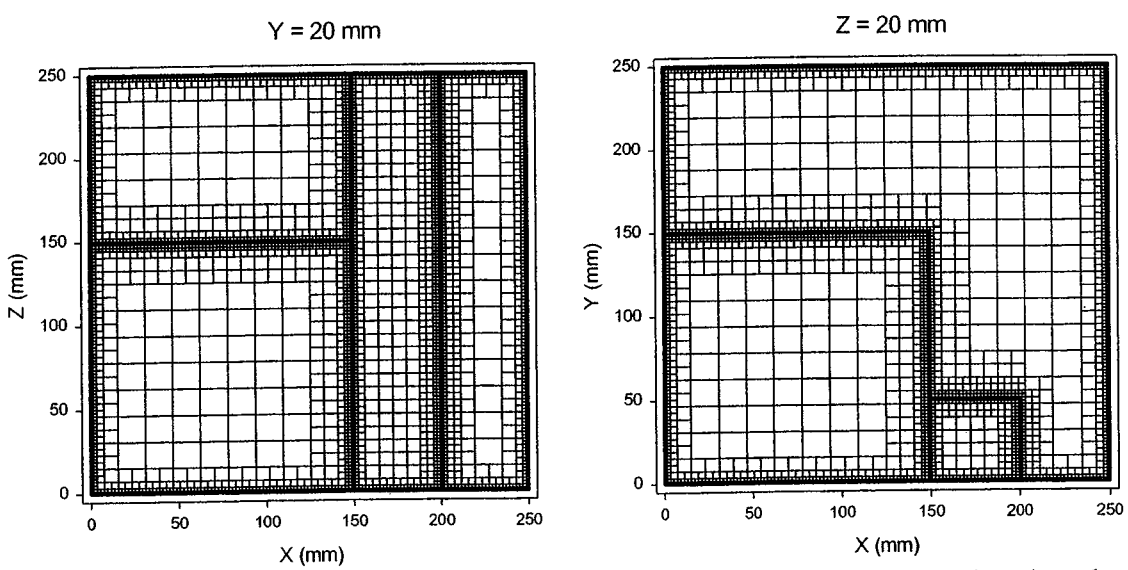

Fig. 2. Vertical and horizontal cross sections of an octree grid of small LWR benchmark.

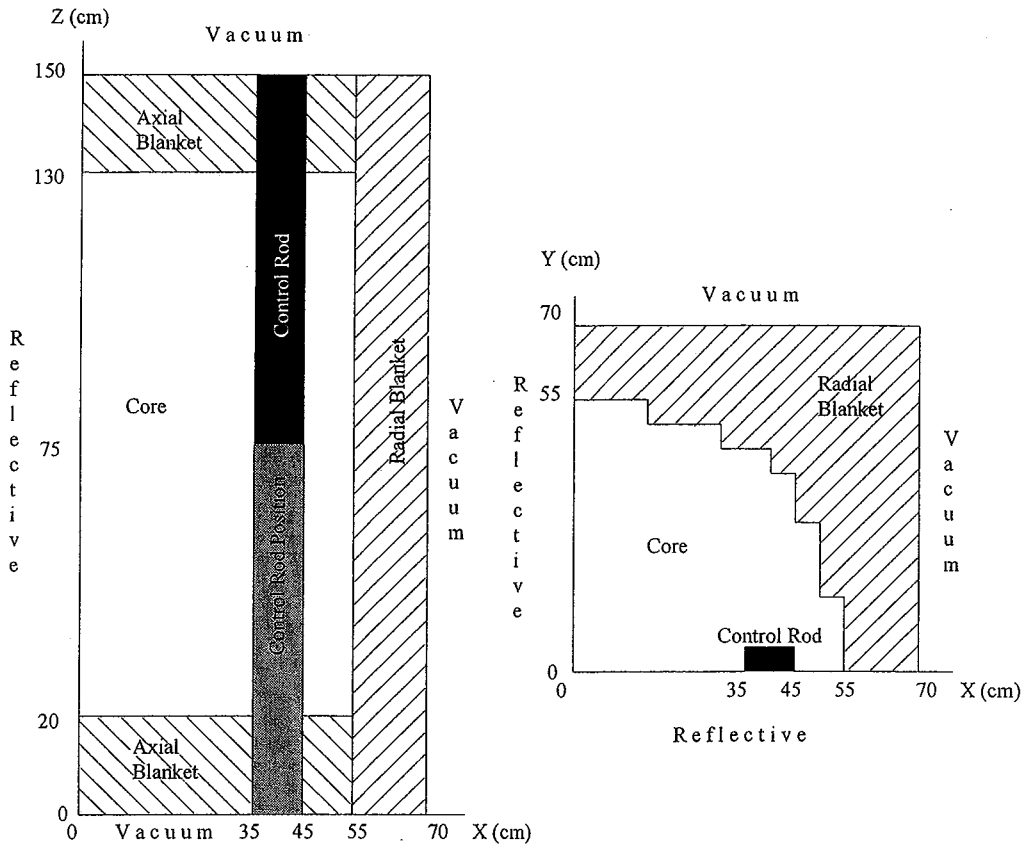

Fig. 3. Vertical and horizontal cross sections of small FBR benchmark.

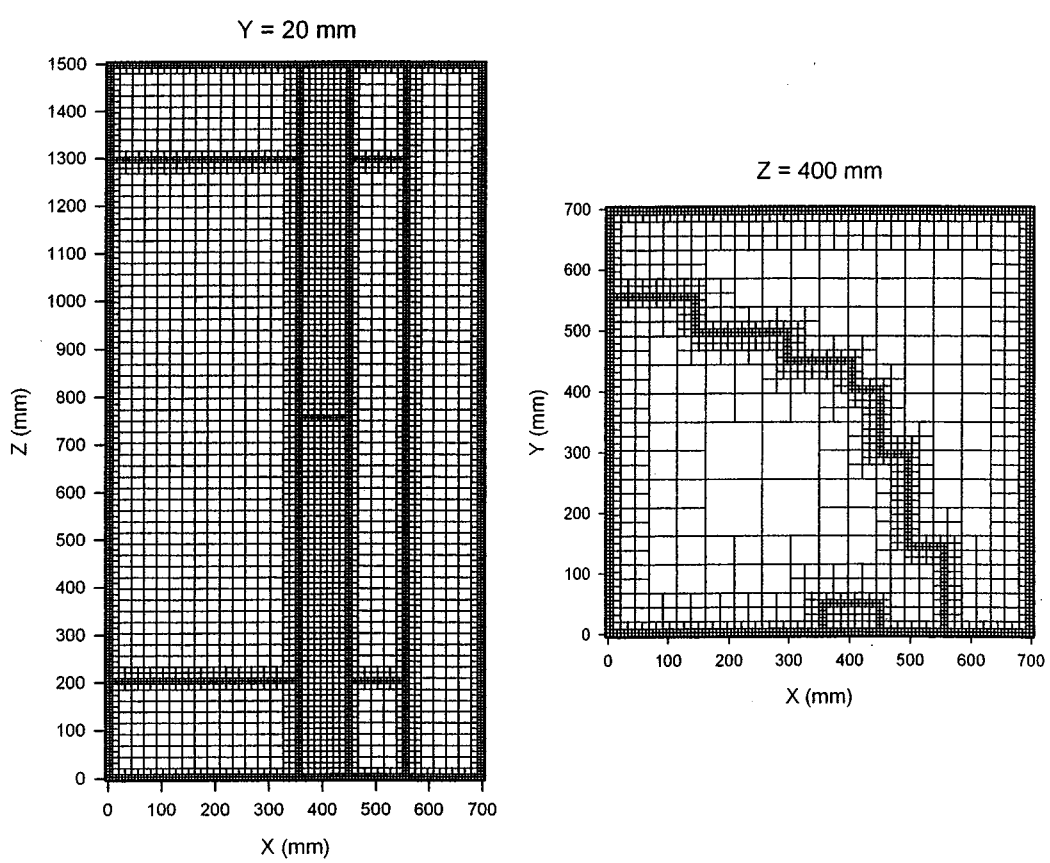

Fig. 4. Vertical and horizontal cross sections of an octree grid of small FBR benchmark.

For both calculated benchmarks, control rod worth is defined [9,10] to be the value

$$\left.\frac{1}{k_{eff}}\right|_{case2} - \left.\frac{1}{k_{eff}}\right|_{case1} . \tag{11}$$

In the calculation of the region-averaged fluxes, the total production of the whole reactor is normalised to unity [9,10],

$$\sum_{g=1}^{G} \int_V \nu^g \sigma_f^{i,g} \Phi_0^g(\vec{r}) d^3r \ . \tag{12}$$

3. Results

The multiplication eigenvalue k_{eff} calculated by MultiTrans is given for cases 1 and 2 of the small LWR benchmark in Table 1, and for the small FBR benchmark in Table 2. Also the calculated control rod worth from k_{eff} values is given for both benchmarks, as well as the Exact Monte Carlo results taken from the report of Takeda and Ikeda [10]. The k_{eff} eigenvalues calculated by MultiTrans agree well with the Exact Monte Carlo results (within 0.4%) except for the rod-out case (case 1) of the LWR benchmark with 2.6% difference, which leads to a negative control rod worth.

Table 1. Multiplication factor k_{eff} and control rod worth for LWR benchmark.

Method	Case1	Case2	Control Rod Worth
Exact Monte Carlo	0.9780	0.9624	1.66×10^{-2}
MultiTrans SP_3	0.9521	0.9647	-1.37×10^{-2}

Table 2. Multiplication factor k_{eff} and control rod worth for FBR benchmark.

Method	Case1	Case2	Control Rod Worth
Exact Monte Carlo	0.9732	0.9594	1.47×10^{-2}
MultiTrans SP_3	0.9768	0.9625	1.52×10^{-2}

The region-averaged group flux values calculated by MultiTrans for the FBR benchmark cases 1 and 2 are given in Tables 3 and 4, respectively. Comparing to the Exact Monte Carlo results reported by Takeda and Ikeda [10] (which are not repeated here), these region-

averaged group flux values can be seen to differ most in group number 4 in the region of the axial blanket (Fig. 3). The maximal difference between the MultiTrans and the Exact Monte Carlo results for the FBR benchmark is found to be 9% in case 1, and 8% in case 2. All the region-averaged flux values calculated by MultiTrans for this FBR benchmark are somewhat lower than the Exact Monte Carlo results. In the core region the difference in both cases is 2% in all groups.

Table 3. Region-averaged group flux values for FBR benchmark case 1.

Group	Core	Radial Blanket	Axial Blanket	Control Rod Position
1	4.1907×10^{-5}	3.2401×10^{-6}	5.0348×10^{-6}	2.5206×10^{-5}
2	2.3648×10^{-4}	2.9707×10^{-5}	4.4820×10^{-5}	1.6222×10^{-4}
3	1.6125×10^{-4}	3.1415×10^{-5}	4.4074×10^{-5}	1.2351×10^{-4}
4	6.0957×10^{-6}	1.9521×10^{-6}	3.4514×10^{-6}	6.8232×10^{-6}

Table 4. Region-averaged group flux values for FBR benchmark case 2.

Group	Core	Radial Blanket	Axial Blanket	Control Rod Position	Control Rod
1	4.2540×10^{-5}	3.2230×10^{-6}	5.0877×10^{-6}	2.5461×10^{-5}	1.6315×10^{-5}
2	2.3742×10^{-4}	2.9262×10^{-5}	4.4701×10^{-5}	1.6190×10^{-4}	8.8444×10^{-5}
3	1.5920×10^{-4}	3.0682×10^{-5}	4.3344×10^{-5}	1.2075×10^{-4}	4.9829×10^{-5}
4	5.9106×10^{-6}	1.8975×10^{-6}	3.3499×10^{-6}	6.5105×10^{-6}	1.0764×10^{-6}

4. Discussion and Conclusions

Benchmark model 1 (small LWR) is known to have a very strong transport effect: e.g. the diffusion solution gives a negative control rod worth for the problem [10]. It is worth noticing, that also the SP_3 approximation produces a negative control rod worth. This is due to the inaccurate result for the rod-out case. The same result can be seen in the paper by Larsen, Morel and McGhee [3]. They conclude that the reason of the inaccurate result for the rod-out case is the void region with long neutron streaming paths. However, the results obtained for the benchmark model 2 (small FBR) agree well with the Monte Carlo results. As the k_{eff} for the rod-in case in benchmark model 1 is also in good agreement with the Monte Carlo result, one can conclude that the MultiTrans SP_3 radiation transport code is suitable for multiplication eigenvalue problems. Nevertheless, in problems with void regions the SP_3 results are substantially incorrect.

So far only the standard source iteration method has been implemented for MultiTrans. It might be possible to accelerate the convergence rate of the outer iterations with a source extrapolation method. There is also an ongoing project to make the octree grid generating procedure in MultiTrans dynamic. The octree grid would be further refined during the calculation based on truncation error estimation. Such an automatic mesh refinement would ensure the desired level of accuracy in every part of the problem.

The calculated simple 3-D benchmark problems have demonstrated the applicability of the new MultiTrans code to criticality problems. After the group fluxes are solved, it is straightforward to calculate dosimetric quantities of interest by simply multiplying the group flux values by corresponding dosimetry cross sections. Thus, the new MultiTrans code is applicable to dosimetry problems also. The CAD-interface allows easy upgrading of the geometry, and makes MultiTrans a flexible design tool, e.g. for planning dosimetric experiments in complicated geometries. In the future, more relevant benchmarks such as VENUS-3 might be conducted.

5. Acknowledgements

I wish to acknowledge Pekka Hiismäki and Sauli Savolainen for their supervision, as well as Pawel Simbierowicz for his important role in development of the tree multigrid technique in general. I also wish to thank my colleagues Tom Serén and Iiro Auterinen for fertile discussion and useful advice.

6. References

[1]. B. Davison, *Neutron Transport Theory* (Oxford University Press, London, 1957).
[2]. E.M. Gelbard, *WAPD-BT-20* (1960).
[3]. E.W. Larsen, J.E. Morel, and J.M. McGhee, *Nucl. Sci. Eng.* **123** (1996) 328.
[4]. P.S. Brantley and E.W. Larsen, *Nucl. Sci. Eng.* **134** (2000) 1.
[5]. P. Kotiluoto, *Nucl. Sci. Eng.* **138** (2001) 269.
[6]. P. Kotiluoto, P. Hiismäki, and S. Savolainen, *Med. Phys.* **28** (2001) 1905.
[7]. J.E. White, D.T. Ingersoll, R.Q. Wright et al., *ORNL-6795* (1995).
[8]. L.J. Lorence Jr., J.E. Morel, and G.D. Valdez, *SAND89-1685* (1989).
[9]. T. Takeda, M. Tamitani, and H. Unesaki, *NEACRP A-953 REV. 1* (1988).
[10]. T. Takeda and H. Ikeda, *NEACRP-L-330* (1991).
[11]. P. Wesseling, *An Introduction to Multigrid Methods* (Wiley, New York, 1992).
[12]. C. Gáspár and P. Simbierowicz, *Num. Methods in Water Resources 1* (1992) 555.
[13]. N.P. Kocherov and P.K. McLaughlin, IAEA-NDS-141 (1993).

PUBLICATION IV

Verification of MultiTrans calculations by the VENUS-3 benchmark experiment

In: Journal of ASTM International 2006.
Vol. 3, Issue 3, 6 p.
Reprinted with permission from the publisher

Journal of ASTM International, March 2006, Vol. 3, No. 3
Paper ID JAI13433
Available online at www.astm.org

P. Kotiluoto[1]

Verification of MultiTrans Calculations by the VENUS-3 Benchmark Experiment

ABSTRACT: The MultiTrans software has been developed at VTT Technical Research Centre of Finland for 3D radiation transport problems. Adaptive tree multigrid technique is used as a deterministic solution method. This enables local refinement of the calculation grid combined with the use of effective multigrid acceleration on tree-structured nested grids: starting from a fast solution on coarse grid, successive solutions are obtained on finer and finer grids. In the MultiTrans code, simplified spherical harmonics (SP_3) radiation transport approximation is used. In order to test the applicability of the new MultiTrans code to reactor dosimetry problems, light water reactor pressure vessel steel (LWR-PVS) benchmark experiment VENUS-3 (with partial length shielded assemblies) was chosen. The results show good agreement to the experimental reaction rates of the VENUS-3 benchmark, demonstrating the applicability of the new MultiTrans code in reactor dosimetry.

KEYWORDS: MultiTrans, radiation transport, reactor dosimetry, tree multigrids, VENUS-3 benchmark

Introduction

Advanced 3D radiation transport methods allow detailed calculation of neutron flux distributions and related quantities for internal parts of nuclear reactors. For instance, DPA (displacement per atom) rates are important for estimation of embrittlement of reactor materials.

In reactor dosimetry, computational methods of radiation transport give important complementary information to measurements. For such positions where dosimeters simply cannot be placed, one is enforced to rely on calculated quantities. Furthermore, dosimeters usually respond to some reaction-specific neutron energies and therefore will not give complete information about the whole neutron spectrum. On the other hand, in deterministic solution of the radiation transport, some approximations usually have to be made—not only for the radiation transport equation, but also for the geometry and for the transport cross sections—before numerical solution of the problem becomes feasible. Measured values give valuable information about the accuracy of the computational (approximative) method and some estimate of the general uncertainty of the calculated values.

MultiTrans is a deterministic radiation transport software developed at VTT Technical Research Centre of Finland [1–3]. Multigroup simplified spherical harmonics (SP_3) approximation of the Boltzmann transport equation has been used to describe the transport process of neutrons through a host medium [4,5]. Adaptive tree multigrid technique has been utilized as an efficient numerical method to solve these SP_3 equations.

Obviously there is a strong need to verify that any new code is performing as expected and suitable for the intended scope of application. In order to test the applicability of the MultiTrans code to reactor dosimetry problems, light water reactor pressure vessel steel (LWR-PVS) benchmark experiment VENUS-3 (with partial length shielded assemblies) was chosen [6]. Comparison between the calculated and experimental $^{58}Ni(n,p)$, $^{115}In(n,n')$ and $^{27}Al(n,\alpha)$ reaction rates for all the measured detector positions of the 3D VENUS-3 benchmark is presented in this paper.

Manuscript received June 20, 2005; accepted for publication September 29, 2005; published December 2005. Presented at ASTM Symposium on Reactor Dosimetry, 12th Volume on 8–13 May 2005 in Gatlinburg, TN; D. W. Vehar, Guest Editor.
[1] Research Scientist, VTT Technical Research Centre of Finland, P.O. Box 1608, FI-02044 VTT, Finland.

Materials and Methods

Simplified P_3 Approximation

The spherical harmonics P_N approximation is well established for the Boltzmann radiation transport equation [7]. However, P_N equations are very complicated in 3D. In 1960 simplified P_N approximation was introduced by Gelbard ad hoc [8], but did not gain much popularity due to lack of solid theoretical background. At present, it has been shown that SP_N equations can have asymptotic and variational derivations [4,5], and therefore the SP_N approximation has attracted growing attention.

In the MultiTrans code SP_3 radiation transport approximation is used [1]. The angular flux in 1D Boltzmann equation is expanded as a series of Legendre polynomials up to order 3, and the orthogonality of the base functions (when integrating over the space) is used to get a coupled set of diffusion like equations for the expansion coefficients. The within-group equations for these coefficients are given in Eqs 1–4.

$$\frac{d}{dx}\Phi_1^g(x) + \sigma_{a0}^g\Phi_o^g(x) = S^g(x) \tag{1}$$

$$\frac{1}{3}\frac{d}{dx}\Phi_0^g(x) + \frac{2}{3}\frac{d}{dx}\Phi_2^g(x) + \sigma_{a1}^g\Phi_1^g(x) = 0 \tag{2}$$

$$\frac{2}{5}\frac{d}{dx}\Phi_1^g(x) + \frac{3}{5}\frac{d}{dx}\Phi_3^g(x) + \sigma_{a2}^g\Phi_2^g(x) = 0 \tag{3}$$

$$\frac{3}{7}\frac{d}{dx}\Phi_2^g(x) + \sigma_{a3}^g\Phi_3^g(x) = 0 \tag{4}$$

$S^g(x)$ in the above equations is scalar source term in energy group g, and $\Phi_n^g(x)$ are the Legendre expansion coefficients of the angular group flux. $S^g(x)$ and $\Phi_n^g(x)$ are components of $1 \times G$ vector functions, where G is the total number of energy groups in multigroup approximation. The group transport cross sections are defined by subtraction of the corresponding Legendre component of the group scattering cross section from the group total cross section: these group transport cross sections are given in Eq 5.

$$\sigma_{an}^g = \sigma_t^g - \sigma_{sn}^{g\to g} \tag{5}$$

Generalized 3D equations, with a formal substitution of the 1D derivative with ∇ operator, can be written in second order form by solving odd-moments from Eqs 2 and 4, and then by substituting these odd-moments into Eqs 1 and 3. If one defines the unknown by Eq 6

$$\hat{\Phi}_0^g(\vec{r}) \equiv \Phi_0^g(\vec{r}) + 2\Phi_2^g(\vec{r}) \tag{6}$$

where $\Phi_0^g(\vec{r})$ is the scalar flux and $\Phi_2^g(\vec{r})$ is the P_2 moment term of the group flux, the within-group SP_3 approximation in second-order matrix form (with superscript i as a material and superscript g as an energy group index) is given by Eq 7.

$$\begin{bmatrix} -D_0\nabla^2 + \sigma_{a0} & -2\sigma_{a0} \\ -\frac{2}{5}\sigma_{a0} & -D_2\nabla^2 + \sigma_{a2} + \frac{4}{5}\sigma_{a0} \end{bmatrix}^{i,g} \begin{bmatrix} \hat{\Phi}_0(\vec{r}) \\ \Phi_2(\vec{r}) \end{bmatrix}^{i,g} = S^{i,g}(\vec{r}) \begin{bmatrix} 1 \\ -\frac{2}{5} \end{bmatrix} \tag{7}$$

The diffusion coefficients depend on transport cross sections and are given in Eqs 8 and 9.

$$D_0^{i,g} = \frac{1}{3\sigma_{a1}^{i,g}} \tag{8}$$

$$D_2^{i,g} = \frac{9}{35\sigma_{a3}^{i,g}} \tag{9}$$

The scalar group source including fixed source, group-to-group scattering and fission source term is given by Eq 10.

$$S^{i,g}(\vec{r}) = Q^{i,g}(\vec{r}) + \sum_{g'=1,g'\neq g}^{G} \sigma_{s0}^{i,g'\rightarrow g}[\hat{\Phi}_0^{g'}(\vec{r}) - 2\Phi_2^{g'}(\vec{r})] + \frac{\chi^g}{k}\sum_{g'=1}^{G} \nu^{g'}\sigma_f^{i,g'}\Phi_0^{g'}(\vec{r}) \tag{10}$$

Standard multi-group neutronics notation has been used above.

Tree Multigrid Technique

In the adaptive tree multigrid technique used in MultiTrans software, tree structured nested grids of different coarseness are generated from the computer-aided design (CAD) model. The grid adapts to the surface triangulation of each solid part of the CAD model by recursive subdivision of cubic cells. Each cubic cell is conditionally divided into eight sub-cubes, which become the children cells of the parent cell. Every children cell can become a parent and have their own children cells. This procedure is continued until the desired accuracy in the geometry description is achieved. As a result, finest grid is obtained at material borders.

The resulting cell system has a tree structure, in which the subdivisions form the branches and the leaves are the children, which are not divided further. Two cells are said to be neighbors if their boundaries are not disjoint but none of them contains the other. Neighbor cells are called face neighbors if they share a common surface, side neighbors if they share a common line, and corner neighbors if they have a common corner only.

The created nested grid structure, which is called an octree grid, is nonuniform. Therefore it is important to construct a proper difference scheme that works on this nonuniform grid structure but is also as simple as possible for inexpensive numerical solution. In order to simplify the construction of the difference scheme, an additional constraint has been used in octree grid subdivision procedure: the ratio of the size of every face neighbor cells is restricted to be at most 2, which makes the grid regular. This adds up to the amount of cells to some extent, depending on the geometry, and therefore increases the problem size, but on the other hand might also reduce the truncation error farther away from the material borders.

For the SP_3 radiation transport approximation in MultiTrans, an integrated difference scheme is utilized [1]. In the integrated difference scheme the flux derivatives are approximated over each side of a cell C by applying the Green's first identity, Eq 11.

$$\int_C \nabla\Phi dV = \int_{\partial C} (\vec{n}\cdot\nabla)\Phi dA \tag{11}$$

In Eq 11 $\vec{n}$ is the normal vector of the cell surface. When the face neighbor cells are same size, flux over side of the cell can be approximated by using central difference, Eq 12.

$$(\vec{n}\cdot\nabla)\Phi \approx \frac{1}{h}(\Phi_N - \Phi_C) \tag{12}$$

In Eq 12 above, h is the mesh size and Φ_C and Φ_N are the flux values in cell and it's neighbor, respectively. Otherwise, parent of the smaller cell is used, and the difference is given by Eq 13.

$$(\vec{n}\cdot\nabla)\Phi \approx \begin{cases} \frac{1}{2h}(\Phi_N - \Phi_{P(C)}), & \textit{neighbor N is bigger than C} \\ \frac{1}{2h}(\Phi_{P(N)} - \Phi_C), & \textit{neighbor N is smaller than C} \end{cases} \tag{13}$$

In Eq 13 the value of the parent cells $\Phi_{P(C)}$ and $\Phi_{P(N)}$ is the average of their children's values. The discretized within-group SP_3 approximation solved by MultiTrans code in iterative diagonal form is then finally given by Eq 14.

$$\begin{bmatrix} -D_0h^2(\vec{n}\cdot\nabla) + h^3\sigma_{a0} & 0 \\ 0 & -D_2h^2(\vec{n}\cdot\nabla) + h^3\sigma_{a2} \end{bmatrix}_h^{i,g} \begin{bmatrix} \hat{\Phi}_0 \\ \Phi_2 \end{bmatrix}_h^{i,g,l+1} = h^3\sigma_{a0}\begin{bmatrix} 2\Phi_2 \\ \frac{2}{5}\hat{\Phi}_0 - \frac{4}{5}\Phi_2 \end{bmatrix}_h^{i,g,l} + h^3 S_h^{i,g}\begin{bmatrix} 1 \\ -\frac{2}{5} \end{bmatrix} \tag{14}$$

For a fixed source, multigroup flux solution is obtained by first solving the above equation by MultiTrans for the first energy group (with the highest energy), and then using the obtained solution to calculate

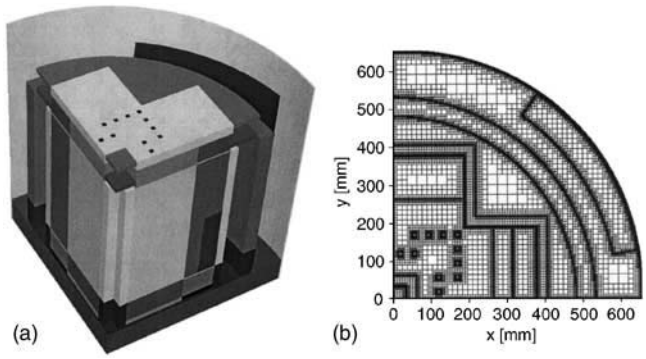

FIG. 1—*VENUS-3 benchmark geometry: (a) CAD model (water regions transparent), (b) horizontal cross section of the octree grid 10 cm below the core mid-plane (with PLSA).*

the source on next lower energy group. This procedure is continued in one sweep through all the groups from highest energy to the lowest, taking group-to-group down-scattering into account at every step. If up-scattering exist, however, several sweeps are required in order to get the correct converged solution. It is also possible to solve a problem with fissile material without defining any fixed source, but doing a criticality eigenvalue search instead. This procedure has been outlined in an earlier paper [3].

The octree algorithm automatically produces all the coarser grids. The sequence of nested fine and coarse grids enables the use of multigrid acceleration method [9]. In a multigrid cycle, the solution strategy recursively leads the discrete problem back to a similar one defined on the next coarser grid. On the coarser grid the solution requires less iteration. The coarse grid solution interpolated to the finer grid can then be used to accelerate the fine grid solution. In the MultiTrans code, all grid levels from coarsest (the root cube) to the finest (the leaf cell representation) are used in nested iteration, producing solution on all grid levels. The multigrid method in connection with the SP_3 equations is described in more detail elsewhere [1].

VENUS-3 Benchmark

The VENUS Critical Facility is a zero power reactor located at SCK●CEN, Mol, Belgium. It has been used to study LWR core designs and to provide experimental data for nuclear code validation. LWR-PVS benchmark experiment VENUS-3 (with partial length shielded assemblies) is a computational 3D radiation transport exercise of the OECD NEA based on the measured data in the experimental program conducted in 1988 [6]. Nuclear Science Committee (NSC) expert group launched the computational VENUS-3 benchmark in 1997: about 14 independent benchmark calculations were supplied by eight institutions. The results of this benchmark have been published by NEA [10]. The well-documented experimental and computational data with detailed material and geometry specifications offers a good resource to verify the calculations with any new transport code, such as MultiTrans.

In order to be able to generate the octree grid for the MultiTrans code, the VENUS-3 benchmark geometry was first constructed with commercially available CAD software based on benchmark specifications [6], see Fig. 1(*a*). All material regions were modeled in detail, except that fuel pin, fuel cladding, and water regions were homogenized over each fuel zone. The external regions outside the jacket inner wall (air, jacket outer wall, reactor vessel, water, and reactor room) were left away from the model, as they can be assumed to have no significant effect to the responses at the measurement points.

The geometry of each material region of the model was exported from the CAD software as a stereolitography (STL) file. A three-dimensional tree multigrid (octree grid) was generated directly from these STL-files, resulting in over 2.46 million cells. A horizontal cross section of the generated octree grid is illustrated in Fig. 1(*b*), showing also the partial length shielded assemblies (PLSA) fuel region below the core mid-plane.

The venus3.src file from NEA-1517/69 SINBAD-VENUS-3 distribution CD was used to generate a fixed-source for MultiTrans calculation. Fission spectrum for ^{235}U was taken from BUGLE-96 library [11]. BUGLE-96 library (version without up-scattering) was also used in generation of the material transport cross sections in 47 neutron groups by MultiTrans for 26 different elemental material compositions involved.

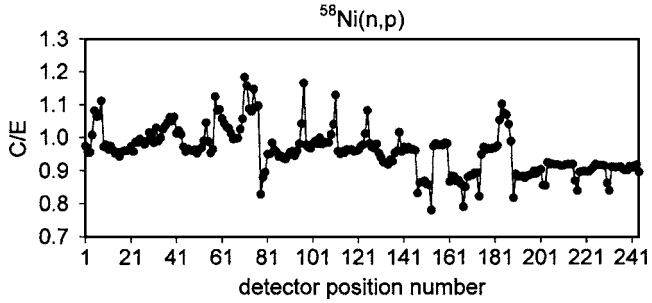

FIG. 2—*Ratio of calculated and experimental $^{58}Ni(n,p)$ reaction rate in 244 detector positions.*

For calculation of the reaction rates, $^{58}Ni(n,p)$, $^{115}In(n,n')$, and $^{27}Al(n,\alpha)$ cross sections were condensed into the 47 BUGLE groups from IRDF-90 version 2 dosimetry library in SAND II energy group structure by using X333 utility program from the neutron metrology file NMF-90 [12] with combined Maxwell, 1/E, and fission weighting spectrum. Resulting fission spectrum averaged dosimetry cross sections were 105.7, 186.3, and 0.726 mbarn for Ni, In, and Al, respectively.

Results

Comparison of calculated and experimental reaction rates for VENUS-3 detector positions is given in Figs. 2–4.

In general, reaction rates agree well with the experimental values: the majority of the values are within 5 % for Ni and Al and within 7 % for In. The deviation is larger than 20 % only in 2 detector positions of Ni in uppermost PLSA region, and in one detector position of In and Al in core barrel near the corner of the PLSA. According to the final NEA report of the VENUS-3 computational benchmark, a systematic overestimation of measurements (more than 5 %) occurs at the extreme top and bottom locations of the active core region [10]. This can partly explain the large deviation of the C/E values for the two Ni detector positions (−22 % for position 153 and −21 % for position 167). However, the overestimation of the calculated In and Al reaction rates near the corner of the PLSA is probably due to the SP_3 approximation, which does not produce accurate results when the solution behaves more transport-like.

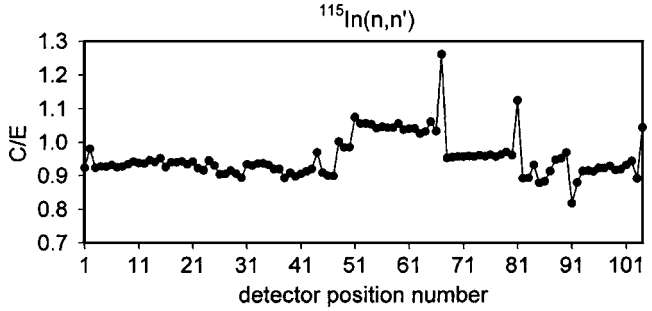

FIG. 3—*Ratio of calculated and experimental $^{115}In(n,n')$ reaction rate in 104 detector positions.*

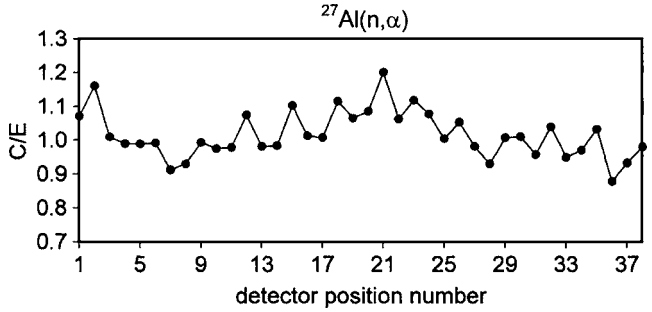

FIG. 4—*Ratio of calculated and experimental $^{27}Al(n,\alpha)$ reaction rate in 38 detector positions.*

The MultiTrans calculations were performed on desktop PC running Windows XP with 3.0 GHz P4 CPU and with 3.62 GB of RAM. Calculation time was 70 min for 47 BUGLE neutron groups.

Conclusions

The MultiTrans results show good agreement to the experimental reaction rates of the VENUS-3 benchmark, demonstrating the applicability of the new MultiTrans code in reactor dosimetry.

Acknowledgments

I wish to acknowledge my colleague, Tom Serén, for help with the dosimetry cross sections and related utility programs, as well as for other valuable guidance.

References

[1] Kotiluoto, P., "Fast Tree Multigrid Transport Application for the Simplified P_3 Approximation," *Nucl. Sci. Eng.* Vol. 138, 2001, pp. 269–278.
[2] Kotiluoto, P., Hiismäki, P., and Savolainen, S., "Application of the New MultiTrans SP_3 Radiation Transport Code in BNCT Dose Planning," *Med. Phys.* Vol. 28, 2001, pp. 1905–1910.
[3] Kotiluoto, P., "Application of the New MultiTrans SP_3 Radiation Transport Code in Criticality Problems and Potential Use in Dosimetry," in *Reactor Dosimetry in the 21st Century*, World Scientific, Singapore, 2003, pp. 580–587.
[4] Larsen, E. W., Morel, J. E., and McGhee, J. M., "Asymptotic Derivation of the Multigroup P_1 and Simplified P_N Equations with Anisotropic Scattering," *Nucl. Sci. Eng.* Vol. 123, 1996, pp. 328–342.
[5] Brantley, P. S. and Larsen, E. W., "The Simplified P_N Approximation," *Nucl. Sci. Eng.* Vol. 134, 2000, pp. 1–21.
[6] Leenders, L., "LWR-PVS Benchmark Experiment VENUS-3 (with Partial Length Shielded Assemblies)," FCP/VEN/01, SCK/CEN, September 1988.
[7] Davison, B., *Neutron Transport Theory*, Oxford University Press, London, 1957.
[8] Gelbard, E. M., "Application of Spherical Harmonics Methods to Reactor Problems," Bettis Atomic Power Laboratory, WAPD-BT-20, 1960.
[9] Wesseling, P., *An Introduction to Multigrid Methods*, Wiley, New York, 1992.
[10] Prediction of Neutron Embrittlement in the Reactor Pressure Vessel, OECD Nuclear Energy Agency, NEA/NSC>/DOC(2000) 5, 2000.
[11] White, J. E., Ingersoll, D. T., Wright, R. Q., et al., "Production and Testing of the Revised VITAMIN-B6 Fine-Group and the BUGLE-96 Broad-Group Neutron/Photon Cross-Section Libraries," Oak Ridge National Laboratory, ORNL-6795, NUREG/CR-6214, Rev. 1, 1995.
[12] Zsolnay, É. M., Szondi, E. J., and Nolthenius, H. J., "The Neutron Metrology File NMF-90," IAEA-NDS-171, Rev. 1, January 1999.

PUBLICATION V

MultiTrans SP_3 code in coupled photon-electron transport problems

In: Radiation Physics and Chemistry 2007.
Vol. 76, pp. 9–14.

Available online at www.sciencedirect.com
ScienceDirect
Radiation Physics and Chemistry 76 (2007) 9–14
Radiation Physics and Chemistry
www.elsevier.com/locate/radphyschem

MultiTrans SP_3 code in coupled photon–electron transport problems

Petri Kotiluoto[a,*], Joakim Pyyry[b], Hannu Helminen[b]

[a]*VTT Technical Research Centre of Finland, P.O. Box 1000, FI-02044 VTT, Finland*
[b]*Varian Medical Systems Finland Oy, Paciuksenkatu 21, FI-00270 Helsinki, Finland*

Received 26 January 2005; accepted 12 April 2006

Abstract

Detailed modeling of photon and electron transport is advantageous in radiotherapy and dosimetry. MultiTrans radiation transport code is based on tree multigrid technique and SP_3 approximation. The standard SP_3 approximation has been extended into a form that takes into account anisotropic group-to-group scattering. A first collision source method has been implemented. Applicability range of standard and extended SP_3 approximations in coupled photon–electron transport problems is examined by comparing calculated doses with deterministic MultiTrans and stochastic EGS4 radiation transport codes.

Keywords: MultiTrans; EGS4; Photon–electron transport

1. Introduction

Application of the traditional dose calculation methods in inhomogeneous medium may generate inaccurate results. Algorithms based on equivalent tissue–air ratio method or other purely analytic methods are often sufficient for the primary radiation field, but fail to treat higher order of scattered particles. Lateral electronic non-equilibrium conditions can cause errors greater than 5% for analytical systems (Wong and Purdy, 1990; Hunt et al., 1997). Better results can be achieved by more detailed modeling of photon and electron transport.

EGS4 Monte Carlo code has been applied to photon and electron radiation transport problems (Nelson et al., 1985; Luxton and Jozsef, 1999). However, stochastic Monte Carlo methods are very time consuming in getting sufficient statistics. Especially tracking of electrons is tedious, as electron transport is dominated by the long-range Coulomb force, resulting in large numbers of small interactions.

With deterministic methods it is possible to solve a detailed flux distribution considerably faster than with stochastic Monte Carlo methods. The price is that it is often necessary to do some approximations to deterministic transport equation: these simplifications affect the accuracy of the computational results.

A novel MultiTrans radiation transport code has been developed at VTT Technical Research Centre of Finland, based on efficient deterministic tree multigrid technique (Kotiluoto, 2001; Kotiluoto et al., 2001). In the tree multigrid technique, the calculation mesh is refined only when required from geometric or computational requirements, leading to tree structured nested grids with refined mesh size, see Fig. 1. In multigrid cycles, the data are transferred from coarser grids to finer grids and vice versa (Wesseling, 1992). The multigrid acceleration enables

*Corresponding author. Tel.: +358 20 722 6357; fax: +358 20 722 6390.
E-mail address: petri.kotiluoto@vtt.fi (P. Kotiluoto).

0969-806X/$ - see front matter © 2006 Elsevier Ltd. All rights reserved.
doi:10.1016/j.radphyschem.2006.04.004

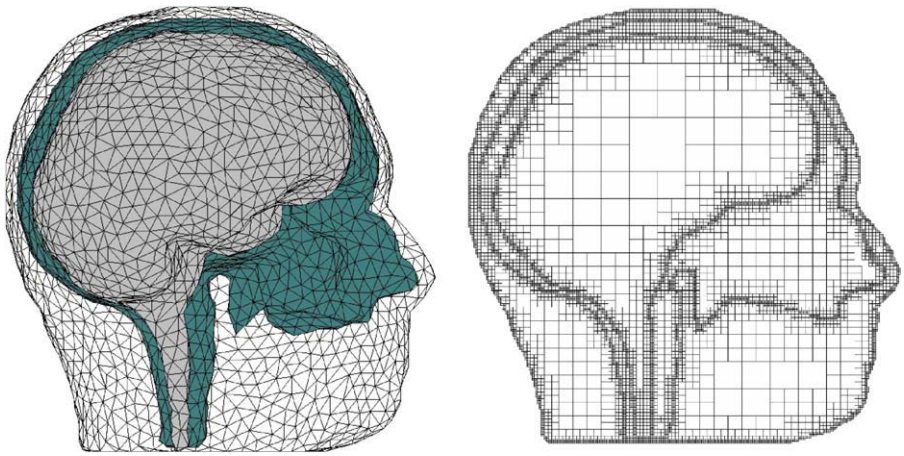

Fig. 1. Triangularized segmented CT image (left) and the cross section of the corresponding octree grid (right). Human head is just an example, the actual shape of the organs can be whatsoever.

high-speed solution of complicated three-dimensional radiation transport problems.

Boltzmann transport equation for photons can be approximated by a simplified low-order spherical harmonics SP_3 approximation (Brantley and Larsen, 2000; Kotiluoto, 2001). Electron transport, on the other hand, can be approximated by the Boltzmann-CSD (continuous-slowing-down) equation. The CSD-term can be further included into electron pseudo-cross sections and the pure Boltzmann equation and its SP_3 approximation applies (Josef and Morel, 1998).

The second-order form of the SP_3 approximation, which is normally used and which we call the "standard" approximation, has been mostly applied in the field of nuclear physics to model neutron transport. This standard approximation does take anisotropic scattering into account within each energy group, but does not involve any anisotropic source terms or anisotropic group-to-group scattering. Therefore, we have extended the standard formalism to also include these anisotropies to the model.

The SP_3 approximation is only valid for problems that are optically thick, are scattering dominated, and have a scattering process that is not extremely forward peaked (Larsen et al., 1996). If there are low-density material regions such as air cavities, the SP_3 approximation will not be adequate. In addition, a low-order spherical harmonics approximation is applicable only to problems in which the angular flux is a weak function of angle. In medical physics problems there is often a strong anisotropy in angular photon flux (with an incident photon beam for instance) which makes the direct application of the SP_3 approximation unjustified. However, by treating the uncollided flux with the first collision source method, the resulting collided flux will be (at least to some extent) weaker in angle and the SP_3 approximation might become justified.

Aim of the present study has been to test MultiTrans code in well-defined homogeneous and heterogeneous photon–electron transport problems, in order to determine more quantitatively the applicability range of the standard and the extended SP_3 approximations. The results will show that the SP_3 approximation has the expected limitations and that the accuracy of the method is not enough e.g., for clinical use in treatment planning. We will discuss possibilities to improve the accuracy or to combine this method in effective manner with Monte Carlo technique.

2. Materials and methods

2.1. The extended SP_3 transport approximation

The "standard" SP_3 approximation (Larsen et al., 1996; Brantley and Larsen, 2000) includes anisotropic within-group scattering (up to Legendre order 3), but can only deal with isotropic (scalar) sources and with isotropic group-to-group scattering. Therefore, an attempt is introduced herein to include anisotropic sources and anisotropic group-to-group scattering into the SP_3 approximation. This is done in a similar formal manner as the original derivation of the standard equations by Gelbard: the only difference is that also source terms are expanded as a Legendre series up to order 3. The second-order within-group SP_3 equations then becomes (with group index g):

$$\begin{bmatrix} -D_0\nabla^2+\sigma_{a0} & -2\sigma_{a0} \\ -\frac{2}{5}\sigma_{a0} & -D_2\nabla^2+\sigma_{a2}+\frac{4}{5}\sigma_{a0} \end{bmatrix}^{i,g} \begin{bmatrix} \hat{\Phi}_0(\vec{r}) \\ \Phi_2(\vec{r}) \end{bmatrix}^{i,g} = \begin{bmatrix} 1 & -3D_0\nabla & 0 & 0 \\ -\frac{2}{5} & 0 & 1 & -\frac{7}{3}D_2\nabla \end{bmatrix}^{i,g} \begin{bmatrix} S_0(\vec{r}) \\ S_1(\vec{r}) \\ S_2(\vec{r}) \\ S_3(\vec{r}) \end{bmatrix}^{i,g}. \quad (1)$$

The variable $\hat{\Phi}_0(\vec{r})$ is defined as

$$\hat{\Phi}_0(\vec{r}) \equiv \Phi_0(\vec{r}) + 2\Phi_2(\vec{r}), \tag{2}$$

where $\Phi_0(\vec{r})$ is the scalar flux and $\Phi_2(\vec{r})$ the second-order moment term of the angular flux Legendre expansion. The group transport cross sections are defined by subtraction of the corresponding Legendre component of the group scattering cross section from the group total cross section:

$$\sigma_{an}^{g} = \sigma_t^g - \sigma_{sn}^{g->g}, \quad n \geqslant 0. \tag{3}$$

The diffusion coefficients are defined by the transport cross sections as

$$D_0^{i,g} = \frac{1}{3\sigma_{a1}^{i,g}} \tag{4}$$

and

$$D_2^{i,g} = \frac{9}{35\sigma_{a3}^{i,g}}. \tag{5}$$

The source moment terms are

$$\begin{bmatrix} S_0(\vec{r}) \\ S_1(\vec{r}) \\ S_2(\vec{r}) \\ S_3(\vec{r}) \end{bmatrix}^{i,g} = \begin{bmatrix} Q_0(\vec{r}) \\ Q_1(\vec{r}) \\ Q_2(\vec{r}) \\ Q_3(\vec{r}) \end{bmatrix}^{i,g} + \sum_{g'=1,g'\neq g}^{G} \begin{bmatrix} \sigma_{s0}^{g'->g}\Phi_0^{g'}(\vec{r}) \\ \sigma_{s1}^{g'->g}\Phi_1^{g'}(\vec{r}) \\ \sigma_{s2}^{g'->g}\Phi_2^{g'}(\vec{r}) \\ \sigma_{s3}^{g'->g}\Phi_3^{g'}(\vec{r}) \end{bmatrix}^{i,g}, \tag{6}$$

where $Q_n(\vec{r})$ are the group source Legendre expansion terms, and anisotropic group-to-group scattering is taken into account through the sum terms.

The first-order derivatives on the right-hand side of Eq. (1) are in this form problematic for the numeric solution, as they distort the positively definite nature of the second-order SP_3 approximation. By using the first-order transport equations for the odd-moment terms, it is possible to transform Eq. (1) into form

$$\begin{bmatrix} -D_0\nabla^2 + \sigma_{a0} & -2\sigma_{a0} \\ -\frac{2}{5}\sigma_{a0} & -D_2\nabla^2 + \sigma_{a2} + \frac{4}{5}\sigma_{a0} \end{bmatrix}^{i,g} \begin{bmatrix} \hat{\Phi}_0(\vec{r}) \\ \Phi_2(\vec{r}) \end{bmatrix}^{i,g} = \begin{bmatrix} 1 & 3D_0 & 0 & 0 \\ -\frac{2}{5} & 0 & 1 & D_2 \end{bmatrix}^{i,g} \begin{bmatrix} S_0(\vec{r}) \\ \hat{S}_1(\vec{r}) \\ S_2(\vec{r}) \\ \hat{S}_3(\vec{r}) \end{bmatrix}^{i,g}. \tag{7}$$

This equation is called hereinafter as an extended SP_3 approximation. The group source terms $\hat{S}_1^{i,g}(\vec{r})$ and $\hat{S}_3^{i,g}(\vec{r})$ containing group-to-group scattering are now

$$\hat{S}_1^{i,g}(\vec{r}) = -\nabla Q_1^{i,g}(\vec{r}) + \sum_{g'=1,g'\neq g}^{G} \sigma_{s1}^{i,g'->g} D_0^{i,g'} [\nabla^2 \hat{\Phi}_0^{i,g}(\vec{r}) + 3\hat{S}_1^{i,g'}(\vec{r})] \tag{8}$$

and

$$\hat{S}_3^{i,g}(\vec{r}) = -\frac{7}{3}\nabla Q_3^{i,g}(\vec{r}) + \frac{35}{9}\sum_{g'=1,g'\neq g}^{G} \sigma_{s3}^{i,g'->g} D_2^{i,g'} [\nabla^2 \Phi_2^{i,g}(\vec{r}) + \hat{S}_3^{i,g'}(\vec{r})], \tag{9}$$

where these odd order source moment terms depend on the second-order derivatives of the even flux moment terms, and are much easier to solve numerically. The same material interface conditions as for the standard approximation apply (Brantley and Larsen, 2000).

For spatial discretization of the transport equations on the non-uniform but regular octree grid (see Fig. 1), an integrated difference scheme has been used, described in detail elsewhere (Kotiluoto, 2001).

2.2. The first collision source method

First collision source method has been used in source processing. In the first collision source method the uncollided flux (the flux of photons that have undergone zero collisions) is solved analytically. This uncollided flux is then used to generate the distributed fixed source terms for the collided flux. The collided flux can be solved by the SP_3 approximation with vacuum boundary conditions (Brantley and Larsen, 2000). Total flux is then calculated as a sum of the collided and uncollided flux for each energy group. The collided flux is more isotropic than the uncollided flux, and can thus be better approximated by a low-order spherical harmonics expansion.

For an isotropic point source the first collision source becomes

$$Q_0^{i,g}(\vec{r}) = \sigma_{s0}^{i,g} q^g(\vec{r}_s) \frac{e^{-\beta(\vec{r},\vec{r}_s)}}{4\pi|\vec{r}-\vec{r}_s|^2}, \tag{10}$$

where $q^g(\vec{r}_s)$ is the point source strength in energy group g and $\beta(\vec{r},\vec{r}_s)$ is the number of mean-free-paths between the source point $\vec{r}_s$ and point $\vec{r}$. In this case, the higher moment terms cannot be taken into account with the SP_3 approximation.

For a monodirectional incident boundary surface flux, the first collision source moment terms are

$$Q_n^{i,g}(\vec{r}) = \sigma_{sn}^{g} q^g(\vec{r}_s) e^{-\beta(\vec{r},\vec{r}_s)} \quad (\vec{r}-\vec{r}_s)||\vec{e}_z, \tag{11}$$

where $q^g(\vec{r}_s)$ is now the surface source strength in energy group g. The rotational symmetry of the SP_3 equations has been used to make the incident monodirectional beam oriented to z-direction.

2.3. Cross sections and energy deposition

The electron pseudo-cross sections used in MultiTrans calculations were created by CEPXS program (Lorence et al., 1989). Multigroup photon–electron cross sections in 35 photon groups and 35 electron groups were output for all elements with full coupling. The protons are treated as electrons for simplicity as protons have identical transport behavior (only the charge is not conserved in this manner). In full coupling, not only photons can create electrons and protons (down-scatter from photon groups to electron groups), but also electrons and protons can create photons (up-scatter from electron groups to photon groups). Energy groups ranged from 1 keV to 20 MeV. The dose was calculated by using group energy deposition cross section $\Sigma_{E,g}$ (MeV cm^{-1}) available from CEPXS library.

The models used in CEPXS are described in detail elsewhere (Lorence et al., 1989). However, it is worth noticing that CEPXS does take into account in electron and positron interactions: the emission of bremmstrahlung, positron annihilation, energy-loss straggling (for catastrophic collisions and radiative events), and knock-on production (i.e., of going beyond the CSD approximation). Also impact ionization and relaxation from K, L1, L2, L3, and average M shells is considered. For photon interactions, incoherent scattering, Compton electron production, photoelectric absorption and production, and pair absorption and production are taken into account.

3. Numerical results

3.1. MultiTrans and EGS4 in homogeneous test cases

As a first homogeneous test case, a water sphere with 50 cm radius and with internal monoenergetic photon point source in center of the sphere was chosen. Luxton and Jozsef (1999) have published updated comparison data for this case.

The dose to water was calculated by MultiTrans code for 25–1750 keV monoenergetic photon point sources using standard SP_3 approximation. The calculated dose is presented for different source energies up to 700 keV in Fig. 2, with an EGS4 comparison. The dose has been multiplied by a factor of distance from the point source squared, in order to make the general behavior visible. In EGS4 simulations the results of Luxton and Jozsef (1999) were reproduced.

The MultiTrans results show that the dose agrees rather well with 25, 35, 70 and 125 keV energies, which have the maximal difference of 6% compared to EGS4 results. However, with higher energies the results start to disagree more: the maximal difference between MultiTrans and EGS4 results is up to 18% with 1.75 MeV source energy, in about 10 cm distance from the point source.

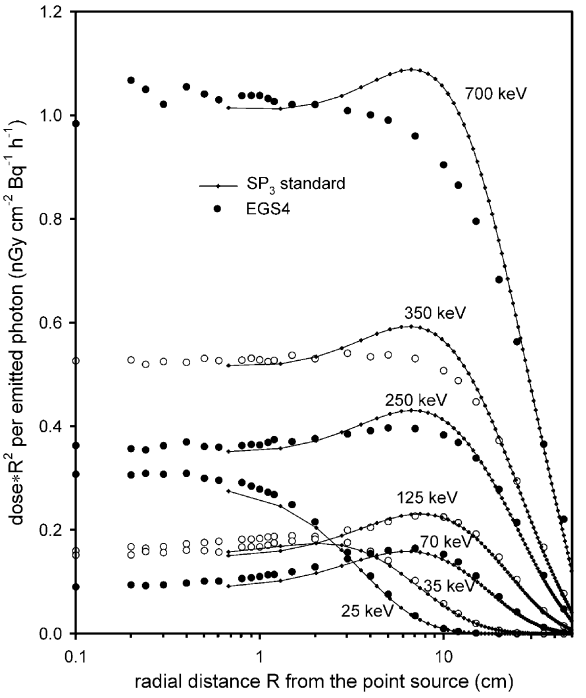

Fig. 2. Radial dose distribution to water from monoenergetic photon point sources.

As a second homogeneous test case, a water cylinder exposed to an external monoenergetic monodirectional photon beam (in $+z$-direction parallel to the cylinder axis) was chosen. The diameter of the cylinder was 80 cm and the length was 1 m. The external photon beam was square shaped and had side length of 125 mm. The used photon source energies were 0.25, 0.7, 2.5, 7, and 17.5 MeV. We performed EGS4 Monte Carlo simulations with a simple user code with the following parameters: ECUT = 1.0 MeV and PCUT = 0.1 MeV. The MultiTrans calculations were done with both the standard and the extended SP_3 approximations. Comparison with the results calculated by the MultiTrans and the EGS4 is presented in Fig. 3 for depth profiles along the beam center line for source energies 0.25, 0.7, 2.5, and 7 MeV. In Fig. 4 also off-axis ratios in 10 cm depth with photon source energy of 2.5 MeV are compared.

The results start to disagree more at higher energies, as expected. The extended SP_3 approximation seems to disagree slightly more than the standard approximation from the absolute value of EGS4 solution in greater

depths at higher energies, but on the other hand, seems to much better duplicate the shape of the depth–dose curve and the position of the dose build-up maximum. Also when comparing the off-axis ratios, the extended SP_3 approximation seems to better reproduce the correct profile shape and estimate the dose outside the beam.

3.2. MultiTrans and EGS4 in a heterogeneous test case

In order to study the computational effect of heterogeneity, a 2 cm thick lead disc with 13 cm radius was placed into a water cylinder in 5–7 cm depth. The diameter of the water cylinder was 40 cm and the length was 50 cm. The cylinder was exposed to monoenergetic monodirectional photon beam (in $+z$-direction parallel to the cylinder axis) with 5 cm radius.

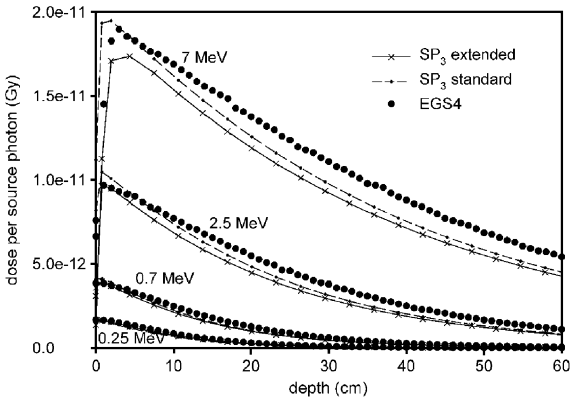

Fig. 3. Depth dose distribution to water along the beam center line ($x = y = 0$) from square shaped 0.25, 0.7, 2.5, and 7 MeV monoenergetic monodirectional photon beam sources with 125 mm length of side.

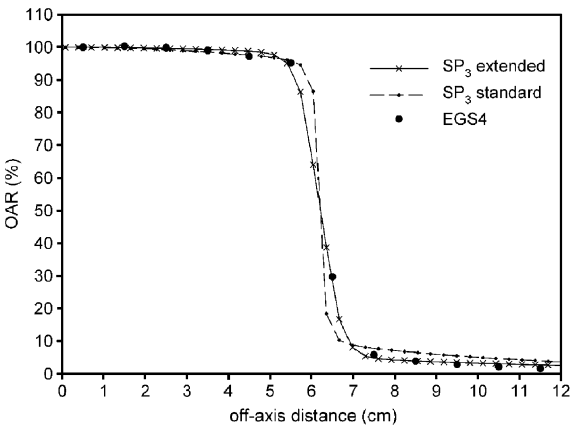

Fig. 4. Off-axis ratio (OAR) of dose distribution to water in 10 cm depth from square shaped 2.5 MeV monoenergetic monodirectional photon beam source with 125 mm length of side.

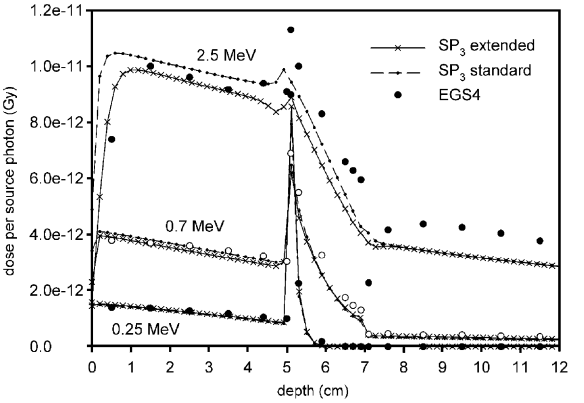

Fig. 5. Depth dose distribution from 0.25, 0.7, and 2.5 MeV monodirectional photon beam source with 5 cm radius. Lead disc as heterogeneity in 5–7 cm depth in water cylinder.

When performing the Monte Carlo calculations for this heterogeneous test case we used the DOSRZ user code which is included in the EGS4 distribution. The following transport parameters were used: ECUT = 0.521 MeV and PCUT = 0.001 MeV. The statistical uncertainty in the doses was less than 1.5% (1 SD) in all regions in the scoring geometry.

The results calculated by MultiTrans on symmetry axis of the cylinder for 0.25, 0.7, and 2.5 MeV circular photon beams with 5 cm radius are presented in Fig. 5 for the standard and the extended SP_3 approximations, with a comparison to results obtained by EGS4.

The results show good agreement at low energies. With 2.5 MeV energy and above, the standard SP_3 approximation seems to overestimate the dose near the vacuum surface. Also at higher energies, both the standard and the extended approximation seem to have too smooth dose curves at material interfaces, and especially miss the reduction of dose right after the lead disc.

4. Discussion and conclusions

The SP_3 approximation of the radiation transport has some well-known limitations, such as both the particle absorption probability and the particle escape probability from the system should be <0.5, and the mean scattering cosine should not be too close to unity (Larsen et al., 1996). Also, when the system is heterogeneous, the transport solution should have only weak tangential derivatives at material interfaces (Larsen et al., 1996). For problems that have strong multidimensional transport effects the SP_3 approximation is less accurate (Larsen et al., 1996). It is also well

known that with spherical harmonics method, in general, no exact vacuum boundary condition can be determined (Duderstadt and Martin, 1979).

In this paper we have extended the formulation of the SP_3 approximation to better take into account the anisotropic scattering and the first collision source terms. From the presented results we conclude, that to a certain degree, this extended SP_3 approximation seems to be advantageous when compared to the standard formulation. However, with high photon energies, the accuracy of both standard and extended approximations is rather poor, and the method is not applicable for treatment planning in conventional radiotherapy, where the uncertainty of the dose to the patient should not exceed 5% (ICRU, 1976).

One possibility to improve the accuracy of the MultiTrans code would be an implementation of a better radiation transport approximation, such as (non-simplified) P_N approximation. It should also be advantageous to use higher order SP_N approximations for the photon transport, such as SP_5 and SP_7 (on the other hand, for the electrons, a simple diffusion theory might be enough). Within the scope of this study we did not consider any of these higher (or lower) order approximations, but such an investigation should clearly be done. The extended formulation we have presented in this paper could be easily applied also to the higher order SP_N approximations. However, based on the SP_3 results and the limitations of the SP_N approximations, in general, the use of such approximations alone in clinical photon–electron treatment planning problems seems unrealistic.

One possibility would be to combine deterministic solution with the Monte Carlo method. Due to long-range Coulomb force, electron transport is characterized by large numbers of small interactions, which is the reason why electron tracking is handled very slowly by Monte Carlo method. However, the angular flux distribution of secondary electrons should be in most cases only smoothly dependent on angle, and could therefore be better approximated by low-order spherical harmonics expansion. Thus, Monte Carlo method could be used for accurate photon transport and the SP_3 approximation for the subsequent quick solution of electron transport in detail. This combination of two different methods could result in both fast and accurate approach to problems with electronic non-equilibrium conditions.

Acknowledgements

This work is partly based on methods developed in study of applicability of the tree multigrid technique to boron neutron capture therapy (BNCT) dose planning. We wish to thank the managing committee of this previous project for several useful advice and insight into the problem. Authors also acknowledge the financial support from Tekes, the National Technology Agency of Finland.

References

Brantley, P.S., Larsen, E.W., 2000. The simplified P_N approximation. Nucl. Sci. Eng. 134, 1–21.

Duderstadt, J.J., Martin, W.R., 1979. Transport Theory. Wiley, New York.

Hunt, M.A., Desobry, G.E., Fowble, B., Coia, L.R., 1997. Effect of low-density lateral interfaces on soft-tissue doses. Int. J. Radiat. Oncol. Biol. Phys. 37, 475–482.

ICRU Report 24, 1976. Determination of absorbed dose in a patient irradiated by beams of X or gamma rays in radiotherapy procedures.

Josef, J.A., Morel, J.E., 1998. Simplified spherical harmonic method for coupled electron–photon transport calculations. Phys. Rev. E 57, 6161–6171.

Kotiluoto, P., 2001. Fast tree multigrid transport application for the simplified P_3 approximation. Nucl. Sci. Eng. 138, 269–278.

Kotiluoto, P., Hiismäki, P., Savolainen, S., 2001. Application of the new MultiTrans SP_3 radiation transport code in BNCT dose planning. Med. Phys. 28, 1905–1910.

Larsen, E.W., Morel, J.E., McGhee, J.M., 1996. Asymptotic derivation of the multigroup P_1 and simplified P_N equations with anisotropic scattering. Nucl. Sci. Eng. 123, 328–342.

Lorence, L.J. Jr., Morel, J.E., Valdez, G.D., 1989. Physics guide to CEPXS: a multigroup coupled electron–photon cross-section generating code. SAND89-1685, Sandia National Laboratory.

Luxton, G., Jozsef, G., 1999. Radial dose distribution, dose to water and dose rate constant for monoenergetic photon point sources from 10 keV to 2 MeV: EGS4 Monte Carlo model calculation. Med. Phys. 26, 2531–2538.

Nelson, W.R., Hirayama, H., Rogers, D.W.O., 1985. The EGS4 code system. SLAC-265, Stanford Linear Accelerator Center.

Wesseling, P., 1992. An Introduction to Multigrid Methods. Wiley, New York.

Wong, J.W., Purdy, J.A., 1990. On methods of inhomogeneity corrections for photon transport. Med. Phys. 17, 807–814.

Series title, number and report code of publication

VTT Publications 639
VTT-PUBS-639

Author(s)
Kotiluoto, Petri

Title

Adaptive tree multigrids and simplified spherical harmonics approximation in deterministic neutral and charged particle transport

Abstract

A new deterministic three-dimensional neutral and charged particle transport code, MultiTrans, has been developed. In the novel approach, the adaptive tree multigrid technique is used in conjunction with simplified spherical harmonics approximation of the Boltzmann transport equation.

The development of the new radiation transport code started in the framework of the Finnish boron neutron capture therapy (BNCT) project. Since the application of the MultiTrans code to BNCT dose planning problems, the testing and development of the MultiTrans code has continued in conventional radiotherapy and reactor physics applications.

In this thesis, an overview of different numerical radiation transport methods is first given. Special features of the simplified spherical harmonics method and the adaptive tree multigrid technique are then reviewed. The usefulness of the new MultiTrans code has been indicated by verifying and validating the code performance for different types of neutral and charged particle transport problems, reported in separate publications.

ISBN
978-951-38-7016-4 (soft back ed.)
978-951-38-7017-1 (URL: http://www.vtt.fi/publications/index.jsp)

Series title and ISSN	Project number
VTT Publications 1235-0621 (soft back ed.) 1455-0849 (URL: http://www.vtt.fi/publications/index.jsp)	

Date	Language	Pages
May 2007	English	106 p. + app. 46 p.

Name of project	Commissioned by

Keywords	Publisher
MultiTrans, particle transport, tree multigrid, simplified spherical harmonics, boron neutron capture therapy, BNCT, radiotherapy, reactor physics, radiation transport	VTT P.O.Box 1000, FI-02044 VTT, Finland Phone internat. +358 20 722 4404 Fax +358 20 722 4374

In many areas dealing with ionising radiation, it is important to calculate the particle transport through matter. In radiotherapy applications the radiation dose to the patient has to be estimated in order to ensure the safety and success of the therapy. In reactor physics one is interested in criticality safety, radiation shielding issues, activity inventories, and radiation damage induced to materials and components important for safety. However, radiation transport is a complicated problem especially in three dimensions, and generally requires the use of sophisticated computer codes.

In this work, a new deterministic radiation transport code, MultiTrans, has been developed by using the adaptive tree multigrid technique and the simplified spherical harmonics approximation. The usefulness of the new code has been indicated by verifying and validating the code performance for different types of radiation transport problems.

Julkaisu on saatavana
VTT
PL 1000
02044 VTT
Puh. 020 722 4404
Faksi 020 722 4374

Publikationen distribueras av
VTT
PB 1000
02044 VTT
Tel. 020 722 4404
Fax 020 722 4374

This publication is available from
VTT
P.O. Box 1000
FI-02044 VTT, Finland
Phone internat. + 358 20 722 4404
Fax + 358 20 722 4374

ISBN 978-951-38-7016-4 (soft back ed.)
ISSN 1235-0621 (soft back ed.)
ISBN 978-951-38-7017-1 (URL: http://www.vtt.fi/publications/index.jsp)
ISSN 1455-0849 (URL: http://www.vtt.fi/publications/index.jsp)